A Mathematical Model for the Transpiration and Assimilation of Early Devonian Land Plants with Axially Symmetric Telomes

vorgelegt von

Wilfried Konrad aus Zaisenhausen bei Bretten

Tübingen März 2002

Ich versichere, daß ich bei der Anfertigung der vorliegenden Arbeit lediglich die angegebenen Hilfsmittel benutzt habe.

Tübingen, den 8. März 2002

Abstract

Early terrestrial ancestors of the land flora are characterized by a simple, axially symmetric habit and evolved in an atmosphere with much higher carbon dioxide concentrations than today.

In order to gain information about the ecophysiological interrelationships of these plants we introduce a model which encompasses gas diffusion within plants, photosynthesis and gaseous exchanges between plants and the atmosphere. Based on the mechanics of gas diffusion inside a porous medium and on a well-established quantitative description of photosynthesis, the model allows for the mathematical simulation of the local gas fluxes through the various tissue layers of a plant axis.

Parameters entering the model consist of, (i) kinetical properties of the assimilation process and other physiological parameters (which have to be taken from extant plants), (ii) physical constants of nature, and, (iii) anatomical parameters which can be obtained from well-preserved fossil specimens.

The model system is applied to two Early Devonian land plants, *Aglaophyton major* and *Rhynia gwynne-vaughanii*. The results demonstrate that, under an Early Devonian carbon dioxide concentration, both *Aglaophyton major* and *Rhynia gwynne-vaughanii* show extremely low transpiration rates and low, but probably sufficiently high assimilation rates. Variation of the atmospheric carbon dioxide concentration shows that the assimilation of *Aglaophyton major* and *Rhynia gwynne-vaughanii* is fully saturated even if the carbon dioxide content is decreased to about two thirds and one third of the initial value, respectively. This result indicates that both plants were probably able to exist under a wide range of atmospheric carbon dioxide concentrations.

Further applications of the model system to axially symmetric plants include the (sub-)systematic variation of the physiological and anatomical parameters "defining" these plants and the responses of the assimilation and transpiration rates to these variations. Examples are given, how such sensitivity studies can be used to identify ecophysiological optima and to understand functional morphological aspects of (extinct) land plants.

To the three therapsides
which came from beyond the palaeozoic borderline
and kept me good company during my studies.

Contents

The three therapsides are from Stanley, 1989. The raven, which hikes through the thesis, and the raven on the bridge are taken from Waechter, 1981.

1. Introduction

The origin and early diversification of land plants marks an interval of unparalleled innovation in the history of plant life. From a simple plant body consisting of only a few cells, land plants (liverworts, hornworts, mosses and vascular plants) evolved an elaborate two-phase life cycle and an extraordinary array of complex organs and tissue systems. Specialized sexual organs (gametangia), stems with an intricate fluid transport mechanism (vascular tissue), structural tissues (such as wood), epidermal structures for respiratory gas exchange (stomata), leaves and roots of various kinds, diverse spore-bearing organs (sporangia), seeds and the tree habit had all evolved by the end of the Devonian period. These and other innovations led to the initial assembly of plant-dominated terrestrial ecosystems, and had a great effect on the global environment (see Kenrick & Crane, 1997).

Early land plants with a "rhyniophytic" habit (see Figures 1, 2 and 3) represent the evolutive starting point of the extant terrestrial flora (Bateman et al., 1998). As documented by the fossil record, they existed through the Silurian and Lower Devonian (about 420 to 380 million years ago).

The members of this constructionally primitive group with still unsolved systematic interrelationships (Kenrick & Crane, 1997) such as *Rhynia gwynne-vaughanii* or *Aglaophyton major* existed in an atmosphere with a carbon dioxide concentration which was much higher than today (Berner, 1997). New data about the ecophysiological features of these plants do not only improve our knowledge of land plant evolution and ancient ecosystems. More informations concerning the physiological behaviour of plants under high carbon dioxide concentrations are also valuable in attempts to consider the consequences of the current increase of carbon dioxide concentration in the atmosphere.

It is thus of increasing interest (Raven, 1994) to understand in more detail the diffusional exchange processes of water vapour and carbon dioxide within these plants, between these plants and the surrounding atmosphere, and the coupling of these exchange processes to their "driving forces" transpiration and assimilation. For relevant literature consult, for instance, Raven, 1977, 1993, who estimated possible assimilation and transpiration rates of rhyniophytic plant axes and Beerling & Woodward, 1997, who calculated gaseous exchange of numerous fossil plants by treating the gas fluxes with the common approach of resistance models (analogous to electrical circuits, as explained, for example, in Nobel, 1999).

In this thesis, we[1] present an approach, which simulates the gas fluxes of rhyniophytic plants in detail. With *Aglaophyton major* and *Rhynia gwynne-vaughanii* serving as examples, we show how the local tracking of gas fluxes along the different tissues of the plant axis can be deduced from

(i) assumptions based on the mechanism of diffusion and physical constants that have obviously not changed since Devonian times,

(ii) anatomical and morphological properties of the plants available from well preserved fossil remains, and

(iii) assumptions concerning the mechanism of photosynthesis and the carbon dioxide conductance

---

[1] 'We' in the sense of 'I'.

within the cells of the assimilation tissue.

The kinetic properties of the assimilation process may have changed over the course of time. However, a radical difference between the kinetic properties of the key enzymes of extant C_3 plants and Devonian plants appear to be unlikely (Robinson, 1994). Thus, we may be confident that the characteristic ranges of assimilation parameters of extant C_3 plants overlap with those of Lower Devonian plants.

Our approach is in two respects superior to the widely used concept of describing molecular fluxes in analogy to networks of electric currents:

— the latter method works only, if such a high degree of symmetry is valid, that the pathways of the molecules reduce to straight, parallel lines. (An example which fulfills this condition is provided by a typical leaf: molecular currents diffuse in or out of its stomata in directions perpendicular to the leaf's principal plane.)

— the electric network analogy breaks down if mechanisms like carbon assimilation extract molecules from the carbon dioxide flux along its path.

Our mathematical approach is an analytical one: we perform the solution of the diffusion equation and subsequent manipulations of the mathematical structures of the model in an analytic way, by using closed functions, and not by numerical techniques. By emphasizing the functional interdependencies of the perhaps 35 variables which define the morphology of the plant, the photosynthetic mechanisms and the atmospheric boundary conditions, we keep the model very flexible. Thus the behaviour of any parameter can be studied by systematic variation of any other parameter and sensitivity studies can be performed very easily.

The organisation of the paper is as follows: First we sketch the morphologies of *Aglaophyton major* and of *Rhynia gwynne-vaughanii*, two typical rhyniophytic plants, which will serve as examples throughout the paper. Then we give a discussion of the physics behind diffusion and explain how the mathematical complexity of the resulting differential equation is reduced by exploiting symmetries and approximations. Subsequently, we describe the assimilation model which will be used and the mathematical proceedings. Then the model is applied to the tissue organization of *Aglaophyton major* and *Rhynia gwynne-vaughanii*. Finally we present the results and discuss possible further applications of the method.

2. Characteristic Features of Rhyniophytic Plants

Early ideas on the origin of land plants were based on living groups, but since the discovery of exceptionally well-preserved fossil plants in the Early Devonian Rhynie Cherts (408 Ma – 380 Ma), research has focussed almost exclusively on the fossil record of vascular plants. Evidence on the origin and diversification of land plants has come mainly from dispersed spores and megafossils like those which have been found in the Rhynie Cherts. (Rhynie is the name of a scottish village about 60 kilometers northwest of Aberdeen, chert is a finely crystalline silica that commonly forms in association with hot springs). Exactly how the Rhynie Cherts of Scotland formed is still questionable, but it clearly represents an autochthonous deposition of plants in a swampy setting. Because of apparent rapid preservation by pulses of silica-bearing water, the Rhynie Chert preserves Early Devonian land plants in exquisite detail.
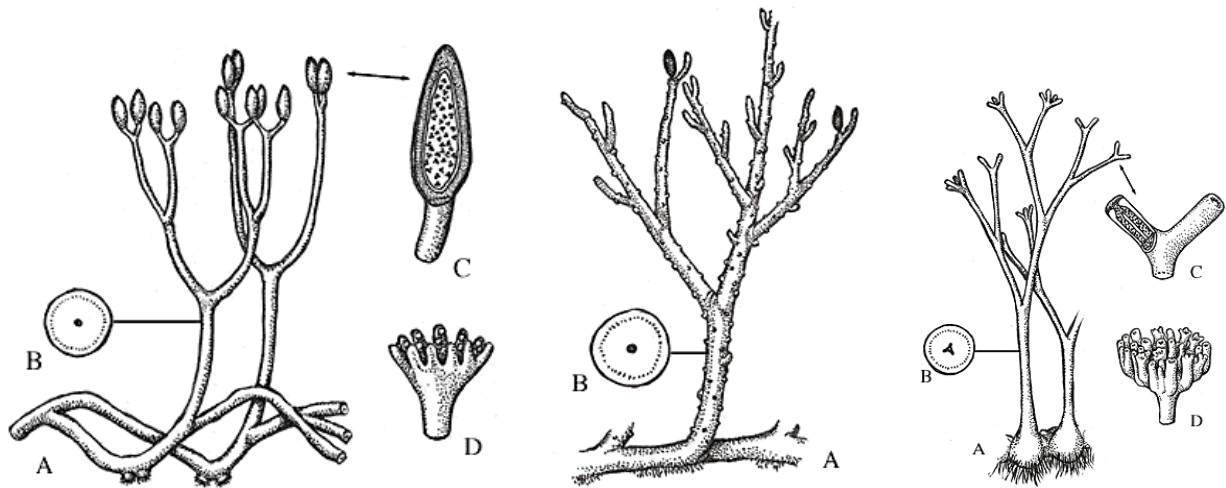
Figures 1, 2 and 3: Reconstructions of *Aglaophyton major* (left), *Rhynia gwynne-vaughanii* (centre) and *Horneophyton lignieri* (right) show that all three species consisted of axially symmetric telomes — a design element common to many early land plants. *Aglaophyton* and *Rhynia* reached a height of about 18 cm, *Horneophyton* of approximately 6 cm. (Drawings after Löffler, 1999.)
Left: *Aglaophyton major.* (A) Whole plant reconstruction showing rhizome and vertical axes. (B) Cross section showing "protostele", (C) sporangium in longitudinal section with spores inside. (D) *Lyonophyton rhyniensis*, the suggested gametophyte of *Aglaophyton*.
Centre: *Rhynia gwynne-vaughanii.* (A) Whole plant reconstruction, and (B) schematic protostele in transverse section.
Right: *Horneophyton lignieri.* (A) Whole plant reconstruction, (B) schematic protostele. (C) sporangia. (D) *Langiophyton mackiei*, the suggested gametophyte of *Horneophyton*.

Phylogenetic studies favour a single origin of land plants from charophycean algae. Based on the ecology of living species, a freshwater origin of land plants seems likely, but direct evidence from the fossil record is inconclusive as mid-Palaeozoic charophytes are found in both freshwater and, more commonly, marine facies. Living charophycean algae posses several biosynthetic attributes that are expressed more fully among land plants, including the capacity to produce sporopollenin, cutin, phenolic compounds and the glycolate oxidase pathway. However, the absence of well-developed sporophytes, gametophytes with sexual organs of land plant type, cuticle and non-motile, airborne,

sporopollenin-walled spores suggests that these innovations evolved during the transition to the land. In contrast to animal groups, the entire multicellular diploid phase of the plant life cycle probably evolved in a terrestrial setting.

The transition from an aqueous to a gaseous medium exposed plants to new physical conditions that resulted in key physiological and structural changes. Phylogenetic studies predict that early land plants were small and morphologically simple, and this hypothesis is borne out by fossil evidence (see Figures 1, 2 and 3). Early fossils bear a strong resemblance to the simple spore-producing phase of living mosses and liverworts, and these similarities extend to the anatomical details of the spore-bearing organs and the vascular system. The fossil record also documents significant differences from living groups, particularly in life cycles and the early evolution of the sexual phase.
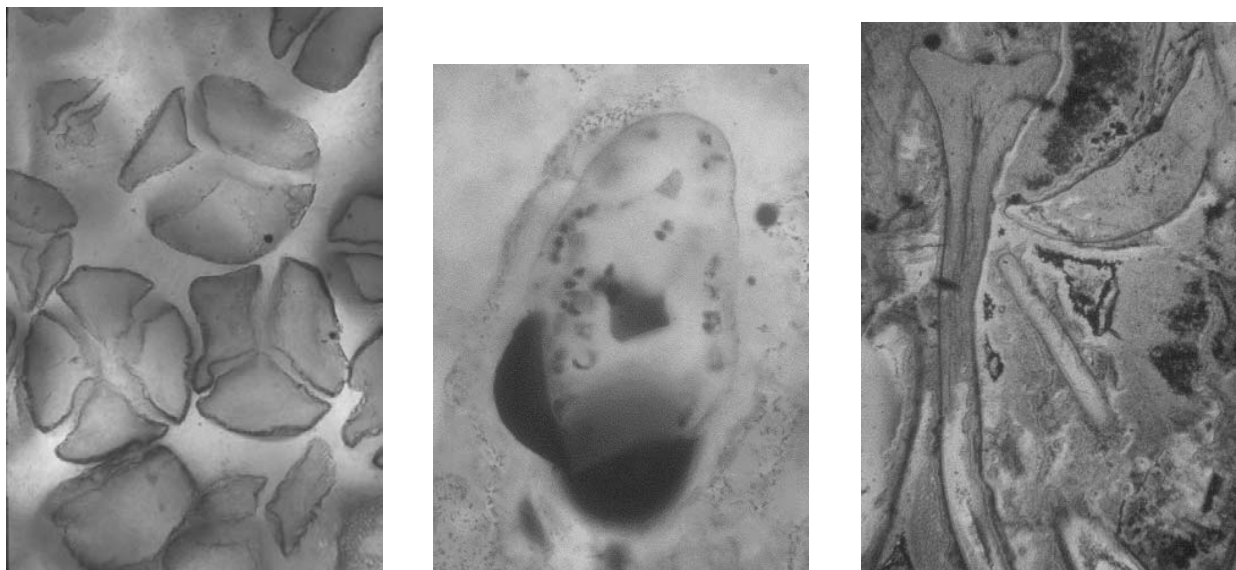
Figures 4, 5 and 6: Left: Several spore tetrades inside a sporangium of *Aglaophyton major*. Centre: Germinating spore of *Aglaophyton major* with tongue-shaped young gametophytes. Right: *Lyonophyton rhyniensis*, the suggested gametophyte of *Aglaophyton*. Section through the longitudinal axes of two gametangiophores. (Photographies from Kerp & Hass, 1999.)

Land-plant life cycles are characterized by alternating multicellular sexual (haploid gametophyte, n) and asexual phases (diploid sporophyte, 2n)(see Figures 4, 5 and 6). Phylogenetic studies indicate that land plants inherited a multicellular gametophyte from their algal ancestors but that the sporophyte evolved during the transition to the land. Most megafossils are sporophytes, and until recently there was no direct early fossil evidence for the gametophyte phase. Recent discoveries of gametophytes in the Rhynie Chert have shed new light on the evolution of land-plant life cycles.

Early gametophytes are more complex than in extant land plants and have branched stems bearing sexual organs on terminal cup- or shield-like structures. Archegonia (female gametangia) are flask-shaped with a neck canal and egg chamber, and are sunken as in hornworts and most vascular plants. Antheridia (male gametangia) are roughly spherical, sessile or with a poorly-defined stalk, and superficial. Gametophytes are very similar to associated sporophytes, and shared anatomical features (water-conducting tissues, epidermal patterns, and stomates) have been used to link

corresponding elements of the life cycle. Provisional reconstructions of the life cycle of an early vascular plant are based on information from anatomically preserved plants and contemporaneous compression fossils (see Kenrick & Crane, 1997).
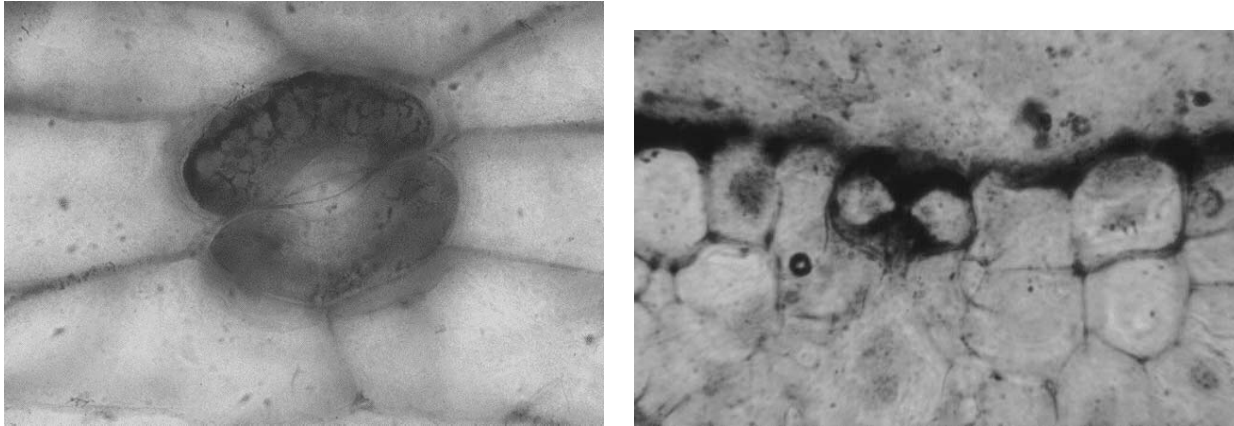
Figures 7 and 8: Left: A stoma of *Aglaophyton major* as seen from above the plant surface. The length of the stomatal pore is approximately 0.04 mm.
Right: Section through a stoma of *Rhynia gwynne-vaughanii*. Note the two guard-cells. (Photographies from Kerp & Hass, 1999.)

In common with some animal groups, internalization of vital functions and organs (such as gas exchange surfaces and sexual organs), combined with the development of impermeable exterior surfaces, seem to have been primary adaptions to life on land. Together, these changes resulted in more highly differentiated plants with stomata, multicellular sexual and spore-bearing organs, water-conducting and other tissue systems. Morphological differentiation ocurred in both phases of the life cycle (gametophyte and sporophyte), but there was subsequently a dramatic reduction in the gametophyte and a great increase in sporophyte complexity among vascular plants. Apical growth and branching coupled with delayed initiation of spore-bearing organs were important innovations of vascular plants that led to a more complex architectural framework on which subsequent morphological diversification was based. The fossil record clearly shows that many vascular-plant organs can be interpreted in terms of modification (especially duplication and sterilization) of basic structural units such as the spore-bearing tissues and the stem.

We give now a more detailed description of *Aglaophyton major* and *Rhynia gwynne-vaughanii*. It may be helpful to consult the habit reconstructions shown in Figures 1 and 2, the stomata in Figures 7 and 8, and the cross-section through *Rhynia gwynne-vaughanii* given in Figure 9 as well as the schematic cross-section in Figure 10.

Aglaophyton major and *Rhynia gwynne-vaughanii* were small plants, lacking leaves and true roots and bearing terminal sporangia on dichotomous branching axes (termed as telomes after Zimmermann, 1959).

The axes of *Aglaophyton major* and *Rhynia gwynne-vaughanii* were approximately 20 cm high with radii of about 2 mm to 2.5 mm and 1 mm, respectively (Edwards, 1986). The one-layered
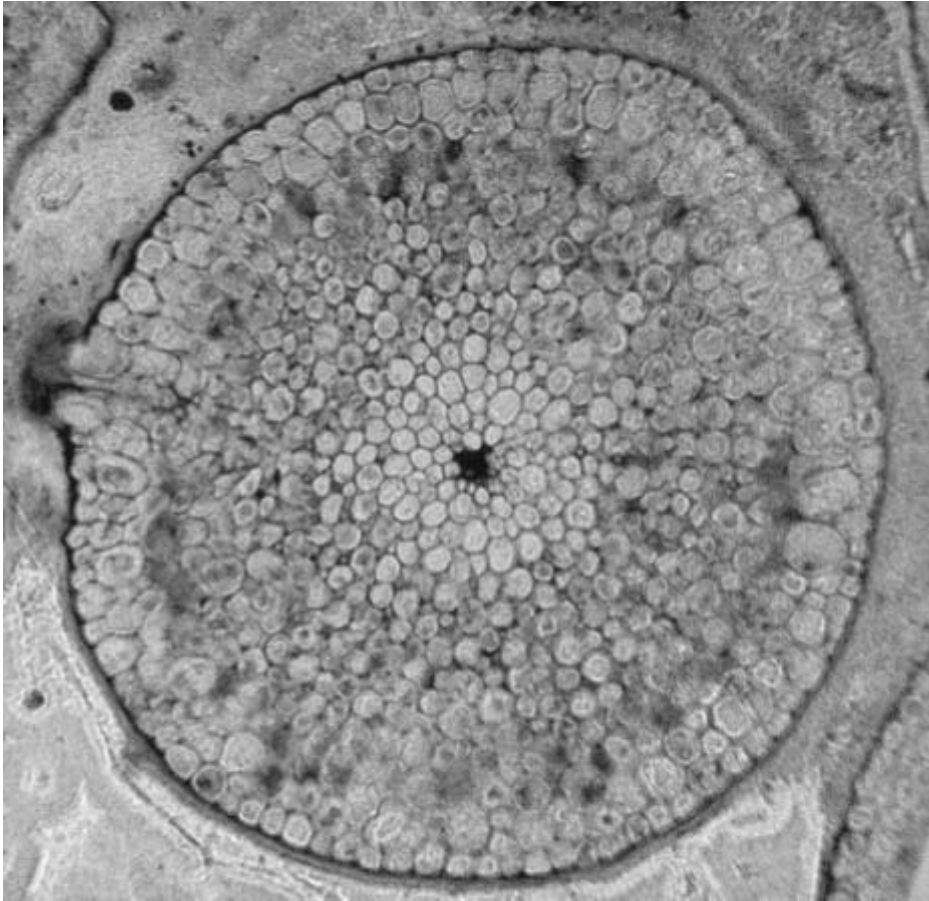
Figure 9: A cross-section through an axis of *Rhynia gwynne-vaughanii.* The radius of the axis amounts to about 1 mm. (Photograph taken from Kerp & Hass, 1999.)
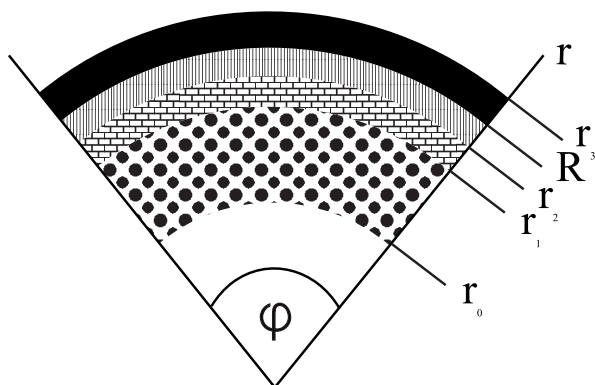
Boundary layer

Stomatal layer

Hypodermal layer

Assimilation Layer

Figure 10: Schematic representation of a sector from the axis slice which represents the tissue model for *Rhynia gwynne-vaughanii* and *Aglaophyton major.* Only the tissue layers which are relevant for the model are shown, other structures, such as the inner cortex or conducting tissues, are not included. The z-axis is orientated perpendicularly to the plane of the illustration. Note that the radial dimensions indicated do not reflect the layers' real thickness values. These are given in Section 3.2. (Drawing from Konrad et al., 2000.)

epidermis covered by a cuticle and equipped with stomata lies on an approximately two- to three-layered hypodermis. A narrow channel formed by hypodermal cells is located directly under the stomatal pore. (Not all Lower Devonian species known so far show such a channel.) The channel terminates in a small substomatal chamber leading to the system of intercellular air spaces. This system is extensive in the outer cortex which is approximately two to four cell layers thick. The inner cortex extends to the central vascular bundle which surrounds the plant's symmetry axis.

The intercellular air spaces decrease considerably in size towards the axis centre. Their spatial structure and anatomical details of cells of the subhypodermal layer provide evidence that the assimilating cortex cells were located subhypodermally at the most peripheral region of the outer cortex (Edwards et al., 1998). Assimilation took thus place in the peripheral regions of the plant axis.

More detailed descriptions of the anatomy of early Devonian plants can be found in Remy and Hass, 1996 or in Edwards et al., 1998.

3. The Mathematical Model

3.1 The Process of Diffusion

The movement of water vapour and carbon dioxide in plants is governed by the process of diffusion, i.e. the tendency of gases and fluids to equalize differences in molecular concentration by establishing a molecular current from areas of high to areas of low concentration. Fick's first law

$$\vec{j} = -S \, \mathrm{grad} \, C \tag{3.1}$$

($[\vec{j}] = \mathrm{mol/m^2/s}$, $[S] = \mathrm{m^2/s}$, $[C] = \mathrm{mol/m^3}$) states that the current density $\vec{j}$ (number of molecules diffusing in time through area normal to the direction of movement) should be proportional to (i) the concentration gradient and (ii) an effective conductance S which depends on the properties of the diffusing molecules and on the medium through which they propagate[2].

The derivation of Fick's first law uses the basic idea of kinetic theory: the molecules of a gas (or a fluid) collide with one another and with the walls of their container. At room temperature ($T \approx 300\,°\mathrm{K}$) and atmospheric pressure ($p = 1$ atm) the collision frequency of a molecule is about 2×10^9 times per second. Energy and momentum among the molecules are hereby transferred and the molecular current of (3.1) results. Detailed calculations (see, for instance, Reif, 1974) show that the validity of equation (3.1) rests on two assumptions:

(i) not more than two molecules interact at the same time, which is equivalent to the statement that the diameter d of a molecule is much smaller than its mean free path length l_p (the mean free path length is the average distance a molecule travels between two collisions),

$$d \ll l_p \tag{3.2}$$

(ii) the molecules collide predominantly with other molecules rather than with the walls of their container, i.e. the mean free path length l_p should be much smaller than a typical linear dimension L of the container, that is

$$l_p \ll L \tag{3.3}$$

For "air molecules" moving at room temperature and atmospheric pressure through a stoma of *Aglaophyton major* or *Rhynia gwynne-vaughanii* with a diameter L of the stomatal pore we have $d \approx 2 \times 10^{-10}\mathrm{m}$, $l_p \approx 3 \times 10^{-7}\mathrm{m}$ and $L \approx 2 \times 10^{-5}\mathrm{m}$. (3.2) and (3.3) are thus fulfilled.

In order to derive the Diffusion Equation (also known as Fick's second law) we need a second component besides (3.1), the principle of mass conservation. It states the intuitively evident fact, that a temporal change in the number of molecules within a given volume $\partial C / \partial t$ is due to (at most)

---

[2] The gradient of a function is defined in the appendix.

two reasons: (i) molecules enter or leave the volume via the flux $\vec{j}$ and/or (ii) molecules within the volume disintegrate into or are built up from their constituents. These processes are summarized in the source strength Q. In mathematical language, this reads

$$\frac{\partial C}{\partial t} = \operatorname{div} \vec{j} + Q \tag{3.4}$$

Insertion of (3.1) into (3.4) leads to[3]

$$\frac{\partial C}{\partial t} = Q - \operatorname{div}\,(S\,\operatorname{grad}\,C) = Q - S\,\Delta C - \operatorname{grad}\,S\,\operatorname{grad}\,C \tag{3.5}$$

In polar coordinates (r, φ, z), defined by

$$\begin{aligned} x &= r\cos\varphi \\ y &= r\sin\varphi \\ z &= z \end{aligned} \tag{3.6}$$

and

$$0 \leq r < \infty \qquad 0 \leq \varphi < 2\pi \qquad -\infty < z < \infty$$

equation (3.5) becomes

$$S\frac{1}{r}\frac{\partial}{\partial r}\left(r\frac{\partial C}{\partial r}\right) + \frac{1}{r^2}\frac{\partial}{\partial \varphi}\left(S\frac{\partial C}{\partial \varphi}\right) + \frac{\partial}{\partial z}\left(S\frac{\partial C}{\partial z}\right) - \frac{\partial C}{\partial t} + \frac{\partial S}{\partial r}\frac{\partial C}{\partial r} = -Q \tag{3.7}$$

If the source (or sink) term $Q = Q(r, \varphi, z, t, C)$ ($[Q] = \mathrm{mol/m^3/s}$) is a linear function of C and if the effective conductance $S = S(r, \varphi, z)$ ($[S] = \mathrm{m^2/s}$) and appropriate boundary conditions are prescribed, the diffusion equation (3.7) has exactly one solution for the concentration $C = C(r, \varphi, z, t)$ of water vapour or carbon dioxide. $C(r, \varphi, z, t)$ represents a function of space and time and it is valid for the whole plant or plant parts[4]. Once $C = C(r, \varphi, z, t)$ is calculated the current density $\vec{j}(r, \varphi, z, t)$ follows from (3.1). This reads in polar coordinates

$$\vec{j} = -\,S(r, \varphi, z)\left(\frac{\partial C}{\partial r}\,\vec{e_r} + \frac{1}{r}\frac{\partial C}{\partial \varphi}\,\vec{e_\varphi} + \frac{\partial C}{\partial z}\,\vec{e_z}\right) \tag{3.8}$$

where $\vec{e_r}$, $\vec{e_\varphi}$ and $\vec{e_z}$ are the system of orthonormal unit vectors in the directions r, φ and z, respectively.

---

[3] Definitions of the operators grad, div and Δ can be found in the appendix.

[4] If $Q(C)$ is a non-linear function, the boundary value problem may or may not have a well-defined solution. This depends on the details of $Q(C)$.

3.2 Diffusion in Rhyniophytic Plants — Problems and Further Proceeding

It is impossible to solve (3.7) in all generality for realistic conditions, because the complex network of voids and channels which form the intercellular air space (see Figure 9), the principal gateway for carbon dioxide and water vapour, implies very complex boundary conditions for (3.7) (as long as we insist on solutions that are valid down to the mean free path length l_p of a molecule). If, however, we claim that C and $\vec{j}$ shall be correct only down to dimensions of a few diameters of a typical cell, we can employ approximations which lead to symmetries that allow for drastic simplifications in (3.7) and (3.8).

If we choose the second option, we can apply the porous medium approach, assume translatorial symmetry along the plants symmetry axis and stationary conditions. Moreover, we can assume that the effective conductance S remains constant within the functionally different tissue layers of rhyniophytic plants. These approximations and some estimations of the possible errors caused by their application will be discussed in the next section.

All terms with the exception of first on the left side of equation (3.7) disappear due to the aforementioned assumptions and (3.7) transformes into the ordinary differential equation

$$\frac{1}{r}\frac{d}{dr}\left(r\frac{dC}{dr}\right) = -\frac{Q}{S} \qquad S = const. \qquad C = C(r) \qquad Q = Q(r, C(r)) \tag{3.9}$$

which will be central to our approach. (3.8) reduces to

$$j(r) = -S\frac{dC(r)}{dr} \tag{3.10}$$

where j is defined by $\vec{j} = j\,\vec{e_r}$.

The solution procedure will be as follows: After assigning appropriate values to S and specifying $Q(C)$ — after applying a quantitative model of photosynthesis — equation (3.9) must be solved separately for each tissue layer. Because (3.9) is an ordinary differential equation of the second order, each of the layer specific solutions contains two arbitrary constants. These constants will be fixed in a second step by combining the layerspecific solutions in such a way that (i) $C(r)$ and $j(r)$ become continuous functions of r, and, (ii) certain boundary conditions (which are explained below) are satisfied.

3.3 Approximations

3.3.1 The porous medium approach

The overall structure of rhyniophytic plants with their concentric layers suggests axial symmetry. If this would be true down to the dimensions of a cell, the orientation of the coordinate systems z-axis along the plant's symmetry axis would eliminate the φ-dependance of C and S (compare

Figure 11). As a consequence, the second term on the right hand side of (3.7) would disappear. A closer look at Figure 9 reveals, however, that the internal structures of the concentric layers consist of cells and voids which do not fit the mathematically favourable axial symmetry of the overall structure.
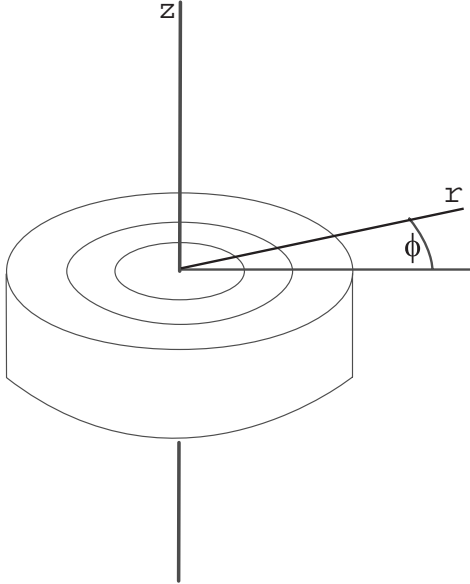
Figure 11: The coordinate system is oriented in such a way that its z-axis coincides with the plant's symmetry axis. The coordinate r measures the (orthogonal) distance from the symmetry axis and φ revolves around the symmetry axis in a plane $z=const.$, attaining values between 0 and 2π.

In order to establish axial symmetry despite this difficulty, we apply the porous medium approximation.

The porous medium approach is widely used (but seldom stated explicitly) as a tool in Applied Geology in order to describe the flow of water (via Darcy's law) or the transport processes of contaminants in soils and aquifers (via Fick's laws) (see, for instance, Grathwohl, 1998). It was developed by engineers who deal with industrial processes which take place in porous media (Aris, 1975). It was was applied to plant leaf tissue by Parkhurst & Mott (1990) in order to study the gradients of intercellular carbon dioxide concentrations inside angiosperm leaves (see also the review by Parkhurst, 1994 and literature cited therein).

The central idea of the porous medium approach is the replacement of the discontinuous arrangement of cells and voids inside the real plant by a fictitious tissue whose continuous material properties are partly attributable to the cells and partly to the voids of the real plant. This is achieved by an averaging process which reduces the complex geometrical details of the cell and void architecture to just two quantities, the porosity n and the tortuosity τ, defined by

$$n := \frac{V_p}{V} \tag{3.11}$$

with V_p the pore volume and V the total volume of a volume element, and

$$\tau := \frac{l_e}{l} \tag{3.12}$$

with l_e denoting the length of the actual path which a molecule has to follow in order to move from one given point to another and l the (geometrically) shortest distance between these same points. The effective conductance S is defined in terms of n, τ and the free air conductance D via

$$S := D \frac{n}{\tau^2} \tag{3.13}$$

The price of this simplification is obvious: *Some* information about the geometry of the cells and voids of the plant tissue gets irrecoverably lost due to the averaging process. Other parts of the knowledge on the plant geometry are condensed and shifted into the quantity S. S will turn out later on to be a piecewise constant factor (and not even a non-trivial scalar function) in the differential equation (3.7) itself. This simplifies the solution process considerably. Moreover, we gain *very* simple boundary conditions for (3.7) in the geometrical shape of a circle, which are much easier to handle than boundary conditions specified on the irregular boundaries between voids and cells in Figure 9.

The porous medium approximation raises the lower limit of the validity of equation (3.7) and of its solutions from the mean free path length l_p of the carbon dioxide or water vapour molecules to a few diameters of a typical plant cell.

The independence of C and S from the coordinate φ is now established: once the differences between cells and voids have been eliminated by the averaging approach, the axial symmetry of the "macroscopic" scale is no longer disturbed and the second term in equation (3.7) disappears.
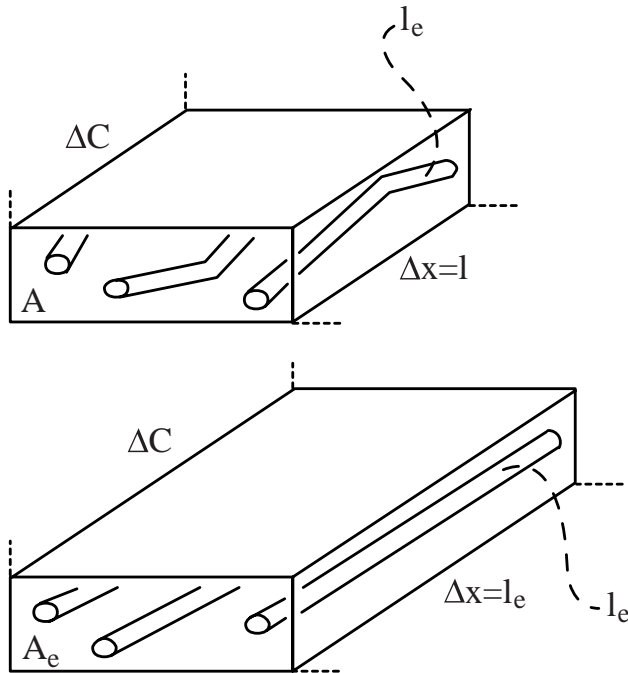
Figure 12: The upper parallelepiped (Figure 12a) is supposed to be realistic in that the tubes inside are tortuous, i.e. $\tau = l_e/l > 1$.
The lower parallelepiped (Figure 12b) is derived from the upper one by the process of continuous deformation. Its tubes are no more tortuous, i.e. $\tau = 1$.
The concentration difference $\triangle C$ along the direction $\triangle x$ is in both cases the same, as is the total cross section A_t. The cross sections A and A_e of the parallelepipeds' faces are *not* identical.

In the following we present a derivation of equation (3.13). Consider the parallelepiped of Figure 12a with length $\triangle x = l$ and cross section A. The tubes inside are tortuous and of the length l_e.

They point essentially into the x-direction. We denote the sum of the cross sections of all tubes by A_t and the concentration difference along $\triangle x$ by $\triangle C$.

The parallelepiped of Figure 12b has straight tubes, the length $\triangle x = l_e$ and the cross section A_e. It is derived from the one in Figure 12a by continuous deformation, subject to the following constraints:

(i) the deformation process affects neither the tube length $\triangle x = l_e$ nor the tubes' total cross section A_t ,

(ii) the volume V remains constant, i.e.

$$V = A\,l = A_e\,l_e \tag{3.14}$$

(iii) the porosity n remains constant, i.e.

$$n = \frac{A_t\,l_e}{A\,l} = \frac{A_t\,l_e}{A_e\,l_e} = \frac{A_t}{A_e} \tag{3.15}$$

(iv) the concentration difference along $\triangle x$ varies in both cases by the amount $\triangle C$,

(v) the deformation process does not affect the total current I, i.e.

$$I = -S_t\,A_t\frac{\triangle C}{l} = -D\,A_t\frac{\triangle C}{l_e} \tag{3.16}$$

Application of the "free air version" $\vec{j} = -D\,\mathrm{grad}\,C$ of equation (3.1) to the interior of the straight tubes of Figure 12b and subsequent multiplication with A_t (under the assumption that the tubes are much longer than their diameters) yields the last term of equation (3.16). Solving (3.16) for the effective conductance S_t (which takes into account the tortuous nature of the tubes in Figure 12a) results in

$$S_t = D\,\frac{l}{l_e} = \frac{D}{\tau} \tag{3.17}$$

where (3.12) has been used.

In order to arrive at the version of Fick's first law which is appropriate within the framework of the porous medium approximation, we must "average out" the distinction between tubes and impermeable parts of the parallelepiped. This is done by dividing the total current I by the cross section A, thus giving rise to the (fictitious) current density

$$j = \frac{I}{A} \tag{3.18}$$

Insertion of (3.16) into (3.18), (3.17), (3.15) and (3.12) leads to

$$j = -\frac{D}{\tau}\,\frac{A_t}{A}\,\frac{\triangle C}{l} = -D\,\frac{n}{\tau^2}\,\frac{\triangle C}{\triangle x} = -D\,\frac{n}{\tau^2}\,\mathrm{grad}\,C \tag{3.19}$$

Comparison with (3.1) yields the desired result

$$S = D\,\frac{n}{\tau^2} \tag{3.20}$$

We emphasize that fluxes (i.e current *densities* in mol/m^2/s) calculated by using the porous medium approximation via (3.19) show other numerical values than real fluxes measured within the plant's voids (e.g. the intercellular airspace). Measured values of concentrations (in mol/m^3), however, should attain the same values as those calculated in the framework of the porous medium approximation.

3.3.2 Translatorial symmetry

As the height of a rhyniophytic plant exceeds the plant radius considerably, we can assume that the fluxes of carbon dioxide and water vapour are oriented mainly radially, i.e. perpendicular to the plant's symmetry axis. If we orientate the coordinate system in such a way that the z-axis coincides with the plant's symmetry axis, C and S do not depend on z and the third term in equation (3.7) becomes zero.

This is not quite true near the top and the bottom of the plant. There the molecules do not move strictly radially. To estimate the error caused by ignoring this fact we assume that the flux through a given area of the plant's surface is proportional to this area:

$$\text{error} \approx \frac{\text{flux through tips}}{\text{total flux}} \approx \frac{\text{area of tips}}{\text{total area}} = \frac{2\pi R^2}{2\pi R^2 + 2\pi Rh} = \frac{R}{R+h} \approx \frac{R}{h} - \left(\frac{R}{h}\right)^2 \tag{3.21}$$

where we have used the assumption $R \ll h$. Typical values for *Aglaophyton major* ($h \approx 20$ cm, $R \approx 2$ mm) and *Rhynia gwynne-vaughanii* ($h \approx 20$ cm, $R \approx 0.5$ mm) result in errors of approximately 1 % and 0.25 %, respectively. This appears to be in an acceptable range.

3.3.3 Stationarity

We focus on situations which do not change with time, i.e. C and S do not depend on t and the term $\partial C/\partial t$ in (3.7) disappears.

This condition is not as restrictive as it appears at first sight: a concentration front of, for example, water vapour needs a time $t \approx s^2/4D_{H_2O}^{air} = 0.01\,$s to diffuse a distance $s = 1\,$mm through free air. The information that a change of humidity outside a plant (as caused by a sudden shower) has taken place needs roughly the same time to propagate to the plant's center. Stationary conditions — on a perhaps different level than before — should therefore reestablish very quickly.

Since carbon dioxide molecules are heavier than water molecules, they move slightly slower in air than water vapour molecules, but at the same order of magnitude. For the distance $s = 1\,$mm they would need a time $t \approx s^2/4D_{CO_2}^{air} = 0.017\,$s. (The diffusion constant of carbon dioxide in air is $D_{CO_2}^{air} = 1.51 \times 10^{-5}\text{m}^2/\text{s}$, that of water vapour in air is $D_{H_2O}^{air} = 2.42 \times 10^{-5}\text{m}^2/\text{s}$.)

As a rule of thumb, the diffusion constant for a substance diffusing through water is about 10^{-4} times its value in air. The carbon dioxide molecules travel the greater part of their journey from the free atmosphere through the intercellular airspace to the chloroplasts in airfilled voids, but once they have entered a cortex cell, they must diffuse for a distance of roughly $s = 5 \times 10^{-6}$m through an aqueous solution. With $D_{\mathrm{CO_2}}^{water} = 1.7 \times 10^{-9}$m^2/s this takes a time $t \approx 0.004$ s. It is therefore still justified, to assume stationary conditions.

It should be noted, that the "transport velocity"[5] of diffusion decreases with increasing distance: a water vapour front diffusing through air would require a time span $t \approx (100)^2 \times 0.01$ s $= 100$ s in order to cover a distance of $s = 100$ mm. This result is contrary to our intuition which — according to our experince with bicycles and cars — expects proportionality between time and distance. In the case of diffusion, however, time is proportional to the *square* of distance and velocity is proportional to the reciprocal of distance.

3.3.4 Constancy of effective conductance S

The axis of a rhyniophytic plant consists of various tissue layers (e.g. stomatal, hypodermal, assimilation layers, see Section 2 and Figures 9 and 10). The geometric properties porosity n and tortuosity τ which influence the effective conductance $S = D\,n/\tau^2$ change more or less abruptly between adjacent layers, but vary only slightly within the individual layers. As we shall calculate later on, the effective conductance S may increase abruptly between neighbouring layers by a factor of 10^4. Small variations of S *within* the layers appear thus negligible and we can assume $S = const.$ within the layers. As a result, the last term on the left hand side of (3.7) becomes zero.

In order to refine this somewhat crude argument in a more quantitative way, we shall now solve the differential equation (3.7) for $C(r)$ on a layer bounded by $r = r_a$ and $r = r_b > r_a$ outside the assimilation region (i.e. $Q = 0$ is valid). Using the approximations introduced in Sections 3.3.1, 3.3.2 and 3.3.3 and $Q = 0$, we rewrite equation (3.7) in the form

$$S\frac{1}{r}\frac{\partial}{\partial r}\left(r\frac{\partial C}{\partial r}\right) + \frac{\partial S}{\partial r}\frac{\partial C}{\partial r} = \frac{1}{r}\frac{\partial}{\partial r}\left(S\,r\frac{\partial C}{\partial r}\right) \tag{3.22}$$

Integration of (3.22) leads to

$$C(r) = A + B\int\frac{dr}{r\,S(r)} \tag{3.23}$$

where A and B are constants of integration. The integration in (3.23) cannot be performed unless the r-dependance of $S(r)$ is explicitly given, which is impossible, because we do not know it. A way out of this dilemma consists in expanding $S(r)$ into a Taylor series in r and to throw away all terms of higher than linear order. This is certainly justified, since we assume from the outset, that

---

[5] With diffusion the notion of transport velocity is not as clear-cut as for a point particle, because there is no unequivocal way to define something tangible like a "diffusion front" for a cloud of statistically independently moving molecules.

within the layer $r_a < r < r_b$ the function $S(r)$ varies only slowly (if at all). The ansatz for $S(r)$ is thus

$$S(r) = S_0 + S_1 \frac{r - r_s}{\triangle r} \qquad (3.24)$$

with the proviso

$$\frac{S_1}{S_0} \ll 1 \qquad (3.25)$$

and the definitions

$$r_s := \frac{r_a + r_b}{2} \qquad \text{and} \qquad \triangle r := r_b - r_a \qquad (3.26)$$

Insertion of (3.24) into (3.23), integration, application of the boundary conditions

$$C(r_a) = C_a \qquad \text{and} \qquad C(r_b) = C_b \qquad (3.27)$$

and expansion of the result according to (3.25) leads to

$$C(r) = \frac{C_b \ln \frac{r}{r_a} - C_a \ln \frac{r}{r_b}}{\ln \frac{r_b}{r_a}} + \frac{S_1}{S_0} \frac{\triangle C}{\triangle r \left(\ln \frac{r_b}{r_a} \right)^2} \left(\triangle r \ln r - r \ln \frac{r_b}{r_a} + r_a \ln r_b - r_b \ln r_a \right) \qquad (3.28)$$

with $\triangle C := C_b - C_a$

The first term in equation (3.28) stems from the constant term in equation (3.24), the second term in (3.28) — we abbreviate it henceforth by δC —, is produced by the term proportional to S_1 in (3.24), which represents the slowly varying part in $S(r)$ (that is, if there is any variation at all). This can be seen by putting $S_1 = 0$ in both equations.

Using $\ln r \leq \ln r_b$, $-r \ln (r_b/r_a) \leq -r_a \ln (r_b/r_a)$ and $\ln (r_b/r_a) \geq 1$ (all of which follow from $r_a \leq r_b$ and the isotony of the logarithm) we conclude the following chain of inequalities for the relative error $\delta C / \triangle C$

$$\frac{\delta C}{\triangle C} = \frac{S_1}{S_0} \frac{\left(\triangle r \ln r - r \ln \frac{r_b}{r_a} + r_a \ln r_b - r_b \ln r_a \right)}{\triangle r \left(\ln \frac{r_b}{r_a} \right)^2} \leq \frac{S_1}{S_0} \frac{1}{\ln \frac{r_b}{r_a}} \leq \frac{S_1}{S_0} \ll 1 \qquad (3.29)$$

The result is an agreeable one: The relative error $\delta C / \triangle C$ caused in $C(r)$ by neglecting a (possibly existing) linear term S_1 in $S(r)$ is always smaller than the relative error S_1/S_0 in the function $S(r) = S_0 + S_1 (r - r_s)/\triangle r$. In other words: small errors in S (as produced, for instance, whilst

measuring the porosity of a layer from thin sections like the one depicted in Figure 9) are not "amplified" by the mathematics of our model, they rather tend to be averaged out in the result for $C(r)$.

In parentheses we remark, that S_0 can be interpreted as the mean value $\overline{S}$ of the function $S(r)$

$$\overline{S} := \frac{\int_{r_a}^{r_b} S(r)dr}{\int_{r_a}^{r_b} dr} = S_0 \tag{3.30}$$

and S_1 is proportional to the standard deviation ΔS of $S(r)$

$$\Delta S := \sqrt{\overline{\left(S(r) - \overline{S}\right)^2}} = \frac{S_1}{2\sqrt{3}} \tag{3.31}$$

Since mean value and standard deviation are the basic ingredients of linear regression analyses, it is possible to analyze plots of the effective conductance S (or of the porosity n and/or the tortuosity τ) against the variable r, in order to establish tight upper bounds on the relative error via (3.29)

$$\frac{\delta C}{\triangle C} \leq \frac{S_1}{S_0} \frac{1}{\ln \frac{r_b}{r_a}} \leq \frac{S_1}{S_0} \tag{3.32}$$

The reduction of the equations (3.7) and (3.8) to equations (3.9) and (3.10), respectively, is thus completed.

3.4 Photosynthesis

Before solving (3.9) for the assimilation layer we have to

— specify the model of photosynthesis which will be used to construct an explicit expression for the carbon dioxide sink $Q = Q(C)$ in equation (3.9), generated by assimilation and

— connect it to (3.9).

3.4.1 The Model of Photosynthesis — General Remarks

The mechanism of photosynthesis provides plants (and the animals feeding upon them) with structural materials and with the energy required for vital functions. Photosynthesis converts the energy of electromagnetic radiation originating from the sun into chemical binding energy. First, the radiation energy is absorbed and splits water into oxygen and hydrogen. Then, the hydrogen is transferred along a long and complex chain of redox reactions to the carbon dioxide to form energy-rich sugars that serve both as structural material and as energy store for metabolistic demands of a plant[6].

---

[6] This is of course not the whole truth: The role of photosynthesis is also important for getting rid of the entropy which is invariably produced when plants (and animals) build up and rebuild their structures and when they transform chemical energy in order to sustain their life processes. If electromagnetic radiation from the sun would not import negentropy into the food chains on earth (which means exporting entropy), things would soon stand still.

As assimilation consumes (i) water, (ii) carbon dioxide and (iii) light, the assimilation rate (i.e the release rate of assimilation products, like sugar or oxygen) should depend on the supply of these three components. Plants, however, are able to close their stomata in order to minimize water loss by transpiration. They also cut hereby their carbon dioxide supply which results in — at least as far as C_3-plants are concerned — more severe consequences for the assimilation process than water shortage itself[7]. Therefore, with respect to photosynthesis, water shortage is always "dominated" by carbon dioxide shortage and water supply as an independent variable can be ignored in assimilation models.

Quantitative models of photosynthesis use the carbon dioxide consumption of chloroplasts per time and chloroplast area A^{chl} as a measure for the assimilation rate and describe it as a function of two independent variables: (i) the carbon dioxide concentration (or, equivalently, the carbon dioxide partial pressure q) and (ii) the irradiance I (i.e. the influx of photons per time and area of the plant surface). Additional parameters describe either the physical environment of the chloroplasts (e.g. temperature T, partial pressure of oxygen p_o), are derived from biochemistry (e.g. specificity factor τ for Rubisco) or serve as fitting parameters (e.g. the Michaelis-Menten constants K_c and K_o for carboxylation and oxygenation resp.). The parameters may vary from model to model.

We employ here the photosynthetic model of Harley & Sharkey, 1991 and Kirschbaum & Farquhar, 1984 (both based on an older model of Farquhar et al., 1980). The core of the model consists of the equation

$$A^{chl}(q, I) = \left(1 - \frac{p_o}{2\tau\, q}\right) \min\{W_c(q), W_j(q, I)\} \tag{3.33}$$

with

$$W_c(q) := V_{max} \frac{q}{q + K_c \left(1 + \frac{p_o}{K_o}\right)} \tag{3.34}$$

$$W_j(q, I) := J(I) \times \frac{q}{4\left(q + \frac{p_o}{\tau}\right)} \tag{3.35}$$

and

$$J(I) := \frac{\alpha\, I}{\sqrt{1 + \left(\frac{\alpha\, I}{J_{max}}\right)^2}} \tag{3.36}$$

The expression $\min\{W_c(q), W_j(q, I)\}$ denotes the smaller of $W_c(q)$ and $W_j(q, I)$ for given q and I.

The variables and parameters in (3.33) are defined as follows:

— A^{chl}: carbon dioxide consumption per time and chloroplast area
— $W_c(q)$: rate of carboxylation if limited by Rubisco activity

---

[7] The amount of water consumed by photosynthesis is negligible compared with the water loss caused by transpiration.

— $W_j(q, I)$: rate of carboxylation if limited by electron transport

— p_o: partial pressure of oxygen in the chloroplasts

— $\tau := K_o V_{c,max} / (K_c V_{o,max})$: specificity factor of Rubisco

— K_o: Michaelis-Menten constant of oxygenation

— K_c: Michaelis-Menten constant of carboxylation

— $V_{max} \equiv V_{c,max}$: maximum rate of carboxylation

— $V_{o,max}$: maximum rate of oxygenation

— J: potential rate of electron transport

— I: irradiance

— J_{max}: light-saturated rate of electron transport

— α: efficiency of light conversion

The functional form of $A^{chl}(q, I)$ does not represent the outcome of a conclusive biochemical theory of photosynthesis that has been derived from first principles of biochemistry and reaction kinetics. It is rather an attempt to describe certain qualitative aspects of C_3-plant specific photosynthesis in a heuristic way (Parkhurst, 1994).

We shall now discuss the structure of (3.33) in terms of its biochemical and kinetic background. As stated above, the goal of photosynthesis is to produce energy-rich carbonhydrates which can be used by the plant's metabolism. An important intermediate step is the fixation of carbon dioxide in the pentose (sugar) molecule ribulose-1,5-biphosphate (RuBP). This reaction is very sensitive with respect to

(i)   the supply with carbon dioxide, i.e. the carbon dioxide partial pressure q,

(ii) the supply with RuBP, whose regeneration within the Calvin cycle depends on a sufficient number of electrons being transported along the redox chain from water to carbon dioxide, a process which consumes necessarily radiation energy and thus depends ultimately on the irradiance I, and

(iii) the supply with and the catalytic activity of the enzyme ribulose-1,5-biphosphate-carboxylase/oxygenase (Rubisco), which performs the actual binding between carbon dioxide and RuBP.

The situation is considerably complicated by a feature of Rubisco: Rubisco is a bifunctional enzyme, it catalyses not only the reaction of carbon dioxide with RuBP ("carboxylation") but also the reaction of molecular oxygen with RuBP ("oxygenation") at the same catalytic site. Oxygen and carbon dioxide are thus mutually competitive inhibitors with respect to the activity of Rubisco.

The assimilation model (3.33) incorporates the features (i), (ii) and (iii) in the following way.

(i)   The min-operation in (3.33) reflects the fact that the assimilation rate is limited by either the rate of the ribulose-1,5-biphosphate (RuBP) regeneration via electron transport, described by $W_j(q, I)$, equation (3.35), or the amount, activity and kinetic properties of the enzyme ribulose-1,5-biphosphate-carboxylase/oxygenase (Rubisco), quantitatively described by the function $W_c(q)$, equation (3.34). For given values of q and I, only the smaller of $W_c(q)$ and $W_j(q, I)$ is

therefore to be used in (3.33).

(ii) The factor $1 - p_o/2\tau q$ in (3.33) becomes negative for $q < p_o/2\tau$ (because the parameters in equations (3.33) to (3.36) can attain only positive values, the functions $W_c(q)$ and $W_j(q, I)$ are always positive). This expresses the fact that the chloroplasts produce more carbon dioxide by photorespiration than they consume by photosynthesis, whenever the partial pressure q of carbon dioxide in the chloroplasts drops below the carbon dioxide compensation point $\Gamma_* := p_o/2\tau$. The chloroplasts' carbon dioxide net consumption per time and area A^{chl} attains accordingly negative values.

This behaviour is a direct consequence of Rubisco's nature as a bifunctional enzyme. Whether Rubisco processes carbon dioxide or rather oxygen depends on the quantity

$$\varphi := \frac{p_o}{q} \frac{K_c \, V_{o,max}}{K_o \, V_{c,max}} = \frac{p_o}{q} \frac{1}{\tau} \tag{3.37}$$

i.e. on the partial pressures q and p_o of both gases, on Rubisco's maximum rates of carboxylation $V_{c,max}$ and oxygenation $V_{o,max}$, and on the Michaelis-Menten constants K_c and K_o for both processes.

The specificity factor

$$\tau := \frac{K_o \, V_{c,max}}{K_c \, V_{o,max}} \tag{3.38}$$

can be understood as follows: Imagine some volume which contains as many oxygen as carbon dioxide molecules together with a large amount of Rubisco. If after some time Rubisco has catalyzed the binding between N oxygen and RuBP molecules, the number of carbon dioxide molecules appended to RuBP will be τN. As τ attains (depending on temperature) some value between $\tau = 6,741$ (for $T = 0\,^{\circ}C$) and $\tau = 1,906$ (for $T = 30\,^{\circ}C$), Rubisco's oxygenation function may appear to be negligible. However, as stated above in equation (3.37), the ratio φ of oxygenation to carboxylation is not given by τ alone. It is weighted with the ratio of the partial pressures of oxygen and carbon dioxide. Today's atmosphere is composed of about 20.95 % (volume %) oxygen and 0.03 % carbon dioxide. With $\tau = 2,822$ at $T = 20\,^{\circ}C$ this amounts to a $\varphi = 0.2474$. That is, if the oxygen/carbon dioxide ratio at an assimilating site would be the same as in the free atmosphere, while carboxylating 100 RuBP-molecules Rubisco would also oxygenate about 25 RuBP-molecules. In other words, about 20 % of Rubisco's catalyzing power would be involved in oxygenation.

(iii) We will now discuss how the dualistic activity of Rubisco affects $W_c(q)$ and $W_j(q, I)$ (equations (3.34) and (3.35)). We begin with $W_c(q)$.

Whether Rubisco processes carbon dioxide or rather oxygen depends on the quantity $\varphi = p_o/q\tau = p_o K_c V_{o,max}/q K_o V_{c,max}$ (i.e. on the partial pressures q and p_o of both gases), on Rubisco's maximum rates of carboxylation $V_{c,max}$ and oxygenation $V_{o,max}$, and on the Michaelis-Menten constants K_c and K_o for both processes.

The hyperbola

$$\widehat{W}_c(q) := V_{max} \frac{q}{q + K_c} \tag{3.39}$$

would be a good choice for a function which shall describe carboxylation if Rubisco would not process oxygen. For large q values it approaches V_{max} asymptotically, i.e. it shows "saturation behaviour" and, for a given q, smaller values of the Michaelis-Menten constant K_c imply steeper gradients in $\widehat{W}_c(q)$. By choosing appropriate values for V_{max} and K_c, the function $\widehat{W}_c(q)$ can thus be adjusted to experimentally obtained data. The introduction of fitting parameters like a Michaelis-Menten constant indicates the heuristic nature of a theory: the behaviour of a quantity as a function of the parameters that define a system cannot (yet) be calculated from first principles but is obtained by adjusting arbitrary parameters like V_{max} and K_c in a qualitatively plausible relation such as the hyperbola $\widehat{W}_c(q)$ in such a way that measured data are reproduced.

Considering competitive inhibition, the rate of the carboxylation of RuBP in the presence of competitive inhibition by oxygen with saturating RuBP is modelled by

$$W_c(q) = V_{max} \frac{q}{q + K_c \left(1 + \dfrac{p_o}{K_o}\right)} \tag{3.40}$$

Equation (3.40) is also a hyperbola. It

(a) approaches zero for $q \to 0$,

(b) approaches asymptotically the maximum carboxylation rate V_{max} for $q \to \infty$ (the Calvin cycle shows saturation behaviour with respect to carbon dioxide also in the presence of oxygen), and

(c) takes into account the competitive inhibition by oxygen via the term $K_c \left(1 + p_o/K_o\right)$ in the denominator, which can be considered as an effective Michaelis-Menten "constant" for carbon dioxide. (Here, effective means that it is rather a function of the oxygen partial pressure p_o than a true constant. As before, higher values for p_o result in smaller gradients of the function $W_c(q)$. For $p_o \to 0$ the term reduces to the "pure" Michaelis-Menten constant K_c and $W_c(q)$ reduces to $\widehat{W}_c(q)$ from equation (3.40).)

We note that the structure of $W_c(q)$ is by no means fixed by the conditions (a) to (c). There exists an infinite variety of functions which satisfy (a) to (c), for instance

$$\widetilde{W}_c(q) := V_{max} \tanh\left(\frac{q\,K_o}{K_c\,(K_o + p_o)}\right) \qquad \text{or} \qquad \widetilde{\widetilde{W}}_c(q) := \frac{q}{\sqrt{q^2 + \left(\dfrac{K_o\,V_{max}}{K_c\,(K_o + p_o)}\right)^2}} \tag{3.41}$$

would behave similarly as $W_c(q)$[8].

---

[8] Stated more explicitly, $W_c(q)$, $\widetilde{W}_c(q)$ and $\widetilde{\widetilde{W}}_c(q)$ behave for very large and for small values of q in

(iv) We will now reconsider Rubisco's bifunctional nature. In order to describe the rate of oxygenation of RuBP in the presence of competitive inhibition by carbon dioxide we can use the same mathematical structure as in the case of carboxylation. This is possible because in the biochemical mechanism responsible for inhibition, the roles of carbon dioxide and oxygen are equivalent — with the consequence that within the mathematical structure the respective variables are interchangeable. In more mathematical terms, this means that we perform the substitutions

$$q \leftrightarrow p_o \qquad K_c \leftrightarrow K_o \qquad V_{max} \leftrightarrow V_{o,max} \tag{3.42}$$

The application on the function $W_c(q)$ (equation (3.40)) results in

$$\frac{q\,V_{max}}{q + K_c\left(1 + \dfrac{p_o}{K_o}\right)} \qquad \leftrightarrow \qquad \frac{p_o\,V_{o,max}}{p_o + K_o\left(1 + \dfrac{q}{K_c}\right)} \tag{3.43}$$

The term $K_o\left(1 + q/K_c\right)$ in the denominator can again be viewed as an effective Michaelis-Menten "constant", but now for oxygen, taking into account the competitive inhibition by carbon dioxide.

If we use the definition of τ (see (3.38)) in order to eliminate $V_{o,max}$ in favour of V_{max} from (3.43), we obtain

$$\frac{p_o\,V_{o,max}}{p_o + K_o\left(1 + \dfrac{q}{K_c}\right)} = \frac{p_o}{\tau\,q} \times \frac{q\,V_{max}}{q + K_c\left(1 + \dfrac{p_o}{K_o}\right)} = \frac{p_o}{\tau\,q} \times W_c(q) \tag{3.44}$$

where the final step follows from the definition of $W_c(q)$, equation (3.34).

The net effect of this twofold Rubisco activity is given by

$$W_c(q) - \frac{1}{2}\frac{p_o}{\tau\,q} \times W_c(q) = \left(1 - \frac{p_o}{2\tau\,q}\right) \times W_c(q) = A^{chl}(q, I) \tag{3.45}$$

which describes the carboxylation rate (3.34) minus half of the oxygenation rate (3.44) of RuBP. The factor $1/2$ that is inserted before (3.44) reflects the fact that for each two oxygenations performed by Rubisco one molecule of carbon dioxide is released in photorespiration. The result

the same way:

(a) $\lim_{q\to\infty} W_c(q) = \lim_{q\to\infty} \widetilde{W}_c(q) = \lim_{q\to\infty} \widetilde{\widetilde{W}}_c(q) = V_{max}$

(b) $W_c(0) = \widetilde{W}_c(0) = \widetilde{\widetilde{W}}_c(0) = 0$

(c) $dW_c/dq(0) = d\widetilde{W}_c/dq(0) = d\widetilde{\widetilde{W}}_c/dq(0) = V_{max}/K_c(1 + p_o/K_o)$

(d) (b) and (c) imply for small values of q: $W_c(q) = \widetilde{W}_c(q) = \widetilde{\widetilde{W}}_c(q) \approx q\,V_{max}/K_c(1 + p_o/K_o)$

is the net carbon dioxide consumption (per time and area) A^{chl} (3.33) of the assimilating plant tissue in the case $W_j(q, I) > W_c(q)$.

(v)   We discuss now the function $W_j(q, I)$, which dominates $A^{chl}(q, I)$ for $W_j(q, I) < W_c(q)$. Again, it will appear twice, first as representing carboxylation and then as a description of its competitive process, oxygenation. As stated above, for $W_j(q, I) < W_c(q)$, the carboxylation rate is given by the rate of the ribulose-1,5-biphosphate (RuBP) regeneration via electron transport, equation (3.35)

$$W_j(q, I) = J(I) \frac{q}{4\left(q + \dfrac{p_o}{\tau}\right)} \tag{3.46}$$

If we interpret $W_j(q, I)$ merely as a function of the variable q (and treat I as a constant) it behaves — similarly as $W_c(q)$ — as a hyperbola which

(a)   becomes zero for $q \to 0$ and

(b)   approaches for $q \to \infty$ asymptotically $J/4$, which is one fourth of the potential rate of electron transport. The factor $1/4$ appears because the regeneration of one molecule RuBP in the Calvin cycle requires four electrons.

(c)   The second term in the denominator, p_o/τ, is also involved in competitive inhibition of carboxylation by oxygen. Although the RuBP regeneration by electron transport is not directly affected by Rubisco's bifunctional behaviour, the RuBP molecules, which are oxygenated by Rubisco instead of being carboxylated, are lost for assimilation. Therefore the term p_o/τ is included in the denominator. Again, higher values for p_o/τ result in smaller gradients of the function $W_j(q, I)$. For $p_o \to 0$, however, the function reduces to $W_j(q, I) = J/4$.

(vi)   In order to calculate the rate of oxygenation performed on RuBP molecules we follow the same ideas as we did above for $W_c(q)$: We retain the mathematical structure of $W_j(q, I)$ and submit it to the transformation (3.42). As the specificity factor τ is defined in terms of K_o, $V_{c,max}$, K_c and $V_{o,max}$ it transforms under (3.42) as

$$\frac{K_o V_{c,max}}{K_c V_{o,max}} = \tau \to \frac{1}{\tau} = \frac{K_c V_{o,max}}{K_o V_{c,max}} \tag{3.47}$$

and the oxygenation rate becomes

$$J(I)\frac{p_o}{4\,(p_o + q\tau)} = J(I)\frac{\dfrac{p_o}{\tau}}{4\left(\dfrac{p_o}{\tau} + q\right)} = \frac{p_o}{\tau q} \times J(I)\frac{q}{4\left(\dfrac{p_o}{\tau} + q\right)} = \frac{p_o}{\tau q} \times W_j(q, I) \tag{3.48}$$

The net effect is — as above — given by the carboxylation rate (3.35) minus half of the oxygenation rate (3.48) of RuBP.

$$W_j(q, I) - \frac{1}{2}\frac{p_o}{\tau\,q} \times W_j(q, I) = \left(1 - \frac{p_o}{2\tau\,q}\right) \times W_j(q, I) = A^{chl}(q, I) \tag{3.49}$$

provided $W_j(q, I) < W_c(q)$ is valid.

(vii) The rate of carboxylation, if limited by electron transport, $W_j(q, I)$, has the asymptotic value $J/4$ (for $q \to \infty$), where J is the *potential* rate of electron transport. That is, the potential for electron transport of $W_j(q, I)$ is exhausted only if the supply with carbon dioxide is plentiful.

J is not a constant but depends via equation (3.36) on the irradiance I (the number of photons arriving per time and surface(!) area of the plant), and on the efficiency of light conversion α. As the source of energy gained by the process of photosynthesis is electromagnetic radiation with a wavelength shorter than about 700 nm, it is of no surprise that the intensity I of this radiation is of importance.

The majority of the photons — typically around 80 % — is absorbed by photosynthetically inactive tissue (Wullschleger, 1993). They do thus not reach the acceptors of the photosystems, because they are "lost" during their way through the plant tissue. The fraction of the remaining photons is denoted by α. αI is thus the number of photosynthetically active photons reaching the chloroplasts. Obviously, rising numbers of photons I will raise the potential rate of electron transport J, but experimental evidence indicates a saturation relation for $J(I)$ as given in equation (3.36)

$$J(I) = \frac{\alpha\,I}{\sqrt{1 + \left(\frac{\alpha\,I}{J_{max}}\right)^2}} \tag{3.36}$$

J_{max}, the light-saturated rate of electron transport, denotes the asymptotic value.

In other words: If the supply with light and carbon dioxide is unrestricted, the function $W_j(q, I)$ is still bounded, attaining the value

$$\lim_{I\to\infty}\lim_{q\to\infty} W_j(q, I) = \lim_{I\to\infty}\lim_{q\to\infty}\left(\frac{\alpha\,I}{\sqrt{1 + \left(\frac{\alpha\,I}{J_{max}}\right)^2}} \times \frac{q}{4\left(q + \frac{p_o}{\tau}\right)}\right) = \frac{J_{max}}{4} \tag{3.50}$$

(viii) The assimilation model (3.33) does *not* provide for a light compensation point. This follows because (i) $W_j(q, I) > 0$ for $I > 0$, and (ii) the only factor in $A^{chl}(q, I)$ which can become negative, $1 - p_o/2\tau$, does not depend on I.

In preparation of constructing a linearized version of (3.33) we get rid of the $\min\{\,.\,,\,.\,\}$-operation in (3.33).

$W_c(q)$ and $W_j(q, I)$ are hyperbolas with asymptotes and poles $W_c(\infty) = V_{max}$, $q_{pole} = -K_c\,(1 + p_o/K_o)$ and $W_j(\infty, I) = J(I)/4$, $q_{pole} = p_o/\tau$ respectively. Therefore $W_c(q)$ and $W_j(q, I)$ intersect at at

most two points. For positive values of K_c, p_o, τ and K_o — which is guaranteed in view of their physical interpretation as pressures — the first intersection is invariably tied to the origin of the coordinate system at $q = 0$. The q-value of the second intersection

$$q_s := \frac{\tau K_c J(K_o + p_o) - 4V_{max}K_o p_o}{\tau K_o(4V_{max} - J)} \tag{3.51}$$

however depends on the specifics of photosynthesis and can attain positive or negative values.

The relation between $W_c(q)$ and $W_j(q, I)$ can be characterized as follows: If $q_s \leq 0$ is valid, $W_c(q)$ and $W_j(q, I)$ intersect nowhere along the (strict) positive part of the q-axis. Consequently, $W_j(\infty, I) > W_c(\infty)$ implies $W_j(q, I) > W_c(q)$ for all $q > 0$, and vice versa. If, on the other hand, $q_s > 0$ is true, $W_j(\infty, I) > W_c(\infty)$ implies $W_j(q, I) > W_c(q)$ only for q-values greater than q_s. Because $W_c(q)$ and $W_j(q, I)$ intersect at q_s they exchange their roles of dominating one another and for q-values between 0 and q_s follows $W_j(q, I) < W_c(q)$. We can therefore write (3.33) in the form

$$A^{chl}(q, I) := \begin{cases} V_{max} \dfrac{q - \dfrac{p_o}{2\tau}}{q + K_c\left(1 + \dfrac{p_o}{K_o}\right)} & \begin{cases} \text{if } q_s \leq 0 \text{ and } J/4 > V_{max} \\ \text{if } q_s > 0 \text{ and } J/4 > V_{max} \text{ and } q_s < q \\ \text{if } q_s > 0 \text{ and } J/4 < V_{max} \text{ and } 0 < q < q_s \end{cases} \\[4em] \dfrac{J(I)}{4} \times \dfrac{q - \dfrac{p_o}{2\tau}}{q + \dfrac{p_o}{\tau}} & \begin{cases} \text{if } q_s \leq 0 \text{ and } J/4 < V_{max} \\ \text{if } q_s > 0 \text{ and } J/4 < V_{max} \text{ and } q_s < q \\ \text{if } q_s > 0 \text{ and } J/4 > V_{max} \text{ and } 0 < q < q_s \end{cases} \end{cases} \tag{3.52}$$

with

$$J(I) = \frac{\alpha I}{\sqrt{1 + \left(\dfrac{\alpha I}{J_{max}}\right)^2}} \tag{3.36}$$

It appears that (3.52) is more complex than (3.33). Its benefits, however, will become visible later on.

3.4.2 Connection between Diffusion and Photosynthesis

The implementation of the photosynthesis model (3.33) into the diffusion equation (3.9) requires the following tasks:

(i) $A^{chl}(q, I)$ is to be connected to Q by bookkeeping considerations which involve

— the porosity n_{as} of the plant's outer cortex,
— the surface a_{as} of a typical cortex cell,
— the volume v_{as} of a typical cortex cell and
— the sum of the surfaces of all chloroplasts within one cortex cell a_{chl}.

These parameters have to be considered, because photosynthesis takes place in the chloroplasts located at the peripherie of an assimilating cell and the carbon dioxide flux depends on geometrical relations (see equation (3.54)).

Consider a volume V which encompasses several cortex cells and the intercellular air spaces between them. The left hand side of the equation

$$-Q\,V = \left\{ \frac{V}{v_{as}}\,(1 - n_{as}) \right\} \left[a_{chl}\,A^{chl}(q, I) \right] \qquad (3.53)$$

regards the number of molecules which are extracted per time from the diffusion current which flows through the volume V according to equation (3.10). It should be balanced by the right hand side, which consists of two factors: The entity in brackets is the product of the flux $A^{chl}(q, I)$ and the area a_{chl}. It describes therefore the number of molecules flowing per time into one cortex cell. As n_{as} stands for the porosity, $V\,(1 - n_{as})$ is the volume within V occupied by assimilating cells. v_{as} denotes the volume of *one* cortex cell. The entity in braces gives thus just the number of cortex cells within V. The product of bracket and brace indicates the number of molecules disappearing per time from the volume V and being processed in the biochemical assimilation machine represented by $A^{chl}(q, I)$.

Division by V and rearrangement of the factors lead to

$$-Q = \left(\frac{a_{chl}}{a_{as}} \right) \left(\frac{a_{as}}{v_{as}} \right) (1 - n_{as})\,A^{chl}(q, I) \qquad (3.54)$$

The ratio (a_{chl}/a_{as}) between the sum of the surfaces of all chloroplasts a_{chl} within one cortex cell and the surface a_{as} of this cell and the surface to volume ratio (a_{as}/v_{as}) of a typical cortex cell have been introduced in the last step, because these ratios are easier to calculate than the individual factors from which they are built up.

Insertion of (3.54) into equation (3.9) and the relation $S = D\,n/\tau^2$ lead to the following (intermediate) form of the diffusion equation in the assimilation layer:

$$\frac{d^2C}{dr^2} + \frac{1}{r}\frac{dC}{dr} = \frac{1}{D_{\mathrm{CO}_2}} \times \tau_{as}{}^2 \left(\frac{a_{chl}}{a_{as}} \right) \left(\frac{a_{as}}{v_{as}} \right) \frac{1 - n_{as}}{n_{as}} \times A^{chl}(q, I) \qquad (3.55)$$

(ii) There remain two problems — a minor one and a more serious one — in (3.55): the left hand side is an expression in $C(r)$, the carbon dioxide concentration in the intercellular airspaces of the assimilation layer, whereas its right hand side depends on the carbon dioxide partial pressure q inside the chloroplasts. That means comparing different quantities which are — still more important — defined at different places.

The minor problem is solved with the help of the equation of state of an ideal gas (carbon dioxide at atmospheric pressure and temperature is a quite ideal gas). It connects the (partial) pressure p of ν moles of an ideal gas at temperature T inside a volume V via the well-known

relation $pV = \nu R_{gas}T$. Using the definition $C := \nu/V$ of (molar) concentration, $p = R_{gas}T \times C$ follows immediately.

The more serious problem will now be considered. In order to turn (3.55) into a meaningful equation, we have to quantify how the carbon dioxide pathway from the intercellular airspace to the chloroplasts influences the diffusion rate. Cortex cells of rhyniophytic plants, like their modern counterparts, consisted presumably of cell walls, plasmalemmata, cytosols, chloroplast limiting membranes, and chloroplast stroma. As the anatomical knowledge of the assimilation region of fossilized specimen is restricted due to taphonomic reasons and only size and number density of cortex cells are known, it is impossible to calculate effective conductances for the diffusional pathway of carbon dioxide molecules by using anatomical parameters.

Instead, we follow Parkhurst & Mott, 1990, Parkhurst, 1994 and Nobel, 1999, and use the ansatz

$$A^{chl} = g_{liq}\left(R_{gas}T\,C(r) - q\right) \tag{3.56}$$

which is a spatially averaged analogue to Fick's first law (3.1). The quantity $R_{gas}T\,C - q$, the difference between the carbon dioxide partial pressure in the intercellular airspace and in the chloroplasts, plays the role of the "driving force" of diffusion (similar to $\mathrm{grad}\,C$ in equation (3.1)). The quantity g_{liq} ($[g_{liq}] = \mathrm{mol/m^2/s/Pa}$) is the analogue of the effective conductance $S = D\,n/\tau^2$ in (3.1). It contains in compressed form all information on the interior structures of the cortex cells which is relevant for the diffusion of the carbon dioxide molecules. Due to taphonomic reasons the value of g_{liq} must be estimated from extant plants (see Parkhurst & Mott, 1990). Note that the diffusion inside the cortex cells — described by g_{liq} — takes place not in air but in an aqueous solution.

After connecnting C and q by (3.56) we equate (3.56) with (3.33) and solve for q as a function of C, obtaining the result

$$
q = \begin{cases}
\begin{aligned}
&\frac{1}{2}\Bigg(R_{gas}T\,C - \frac{J}{4g_{liq}} - \frac{p_o}{\tau} \\
&\quad + \sqrt{\left(R_{gas}T\,C - \frac{J}{4g_{liq}} + \frac{p_o}{4}\right)^2 + \frac{3}{2}\frac{p_o}{\tau}}\,\Bigg) \qquad \text{if } W_j(q,I) < W_c(q)
\end{aligned} \\[2em]
\begin{aligned}
&\frac{1}{2}\Bigg(R_{gas}T\,C - \left[K_c\left(1 + \frac{p_o}{K_o}\right) + \frac{V_{max}}{g_{liq}}\right] \\
&\quad + \sqrt{\left(R_{gas}T\,C + \left[K_c\left(1 + \frac{p_o}{K_o}\right) + \frac{V_{max}}{g_{liq}}\right]\right)^2 + 4V_{max}R_{gas}T\left(\frac{p_o}{2\tau R_{gas}T} - C\right)}\,\Bigg) \\
&\hspace{10em} \text{if } W_j(q,I) > W_c(q)
\end{aligned}
\end{cases}
\tag{3.57}
$$

Insertion of this result back into (3.56) leads to an expression for A^{chl} in terms of C, so that via (3.55) the differential equation (3.9) for the carbon dioxide concentration in the assimilating region attains the form

$$\frac{d^2 C}{dr^2} + \frac{1}{r}\frac{dC}{dr} = a\,C + b + \sqrt{\alpha\,C^2 + \beta\,C + \gamma} \tag{3.58}$$

which causes problems, because

— a, b, α, β and γ are involved combinations of the photosynthetic and morphological parameters in equations (3.33) and (3.55), and

— (3.58) is a highly non-linear differential equation.

3.4.3 Linear Approximation of the Model of Photosynthesis

As equation (3.58) is a nonlinear differential equation in $C(r)$, it cannot be solved in closed form[9]. In order to circumvent this problem, we make use of the freedom granted by the fact that $A^{chl}(q, I)$ is only of qualitative nature. That is, we shall replace $A^{chl}(q, I)$ as given by (3.33) by a linear approximation $A_{lin}^{chl}(q, I)$, which retains the crucial features of (3.33) and casts (3.58) into a linear differential equation in C. The features of (3.33) which we want the linear approximation to retain are:

(i) $A_{lin}^{chl}(q, I)$ shall show saturation behaviour and approach the smaller of $W_c(\infty) = V_{max}$ and $W_j(\infty, I) = J(I)/4$ for large values of q asymptotically.

(ii) If q, the partial pressure of carbon dioxide at the assimilating site, drops below the carbon dioxide compensation point $\Gamma_* = p_o/2\tau$, photorespiration will outweigh photosynthesis and the chloroplasts' net consumption (per time and area) of carbon dioxide $A_{lin}^{chl}(q, I)$ becomes negative.

In other words: we want $A_{lin}^{chl}(q, I)$ to behave like $A^{chl}(q, I)$ (i) for very large values of q, and, (ii) for small values of q, i.e. in the neighbourhood of $q = 0$ and $q = \Gamma_*$. (Γ_* was defined as $\Gamma_* := p_o/2\tau$.) To this end we define the linear approximation $A_{lin}^{chl}(q, I)$ to (3.52) by

(i) the straight line through the points $(q, A^{chl}) = (0, A^{chl}(0, I))$ and $(q, A^{chl}) = (\Gamma_*, 0)$, and,

(ii) the straight line parallel to the q-axis with the asymptotic value $A^{chl} = \min\{V_{max}, J/4\}$.

that is,

---

[9] To be more precise: There *do* exist closed solutions for special numerical values of the parameters a, b, α, β and γ or, if certain relations between them are valid (For a trivial example try $\beta = 2\sqrt{\alpha\gamma}$.) Closed solutions may exist under even less restrictive conditions, but then they are beyond our knowledge. The crucial point, however, is not the information as such. Due to the non-linearity of (3.58), solutions cannot be calculated in a systematic, or semi-systematic fashion. This is quite different with linear differential equations. As they obey the principle of linear superposition, it is always possible to gain an at least qualitative understanding of the behaviour of their solutions.

$$A_{lin}^{chl}(q,I) := \begin{cases} V_{max} & \begin{cases} \text{if } q_s \leq 0 \text{ and } J/4 > V_{max} \text{ and } q_c < q \\ \text{if } q_s > 0 \text{ and } J/4 > V_{max} \text{ and } q_c < q \end{cases} \\[2em] \dfrac{J}{4} & \begin{cases} \text{if } q_s \leq 0 \text{ and } J/4 < V_{max} \text{ and } q_c < q \\ \text{if } q_s > 0 \text{ and } J/4 < V_{max} \text{ and } q_c < q \end{cases} \\[2em] \dfrac{J(2\tau q - p_o)}{8p_o} & \begin{cases} \text{if } q_s \leq 0 \text{ and } J/4 < V_{max} \text{ and } 0 \leq q \leq q_c \\ \text{if } q_s > 0 \text{ and } J/4 > V_{max} \text{ and } 0 \leq q \leq q_c \end{cases} \\[2em] \dfrac{K_o V_{max}(2\tau q - p_o)}{2\tau K_c(K_o + p_o)} & \begin{cases} \text{if } q_s \leq 0 \text{ and } J/4 > V_{max} \text{ and } 0 \leq q \leq q_c \\ \text{if } q_s > 0 \text{ and } J/4 < V_{max} \text{ and } 0 \leq q \leq q_c \end{cases} \end{cases} \tag{3.59}$$

with

$$q_c := \begin{cases} \dfrac{(J + 8V_{max})p_o}{2\tau J} & \text{if } q_s > 0 \text{ and } J/4 > V_{max} \\[1.5em] \dfrac{\tau K_c J(K_o + p_o) + 2V_{max}K_o p_o}{4V_{max}\tau K_o} & \text{if } q_s > 0 \text{ and } J/4 < V_{max} \\[1.5em] \dfrac{2\tau K_c(K_o + p_o) + K_o p_o}{2\tau K_o} & \text{if } q_s \leq 0 \text{ and } J/4 > V_{max} \\[1.5em] \dfrac{3p_o}{2\tau} & \text{if } q_s \leq 0 \text{ and } J/4 < V_{max} \end{cases} \tag{3.60}$$
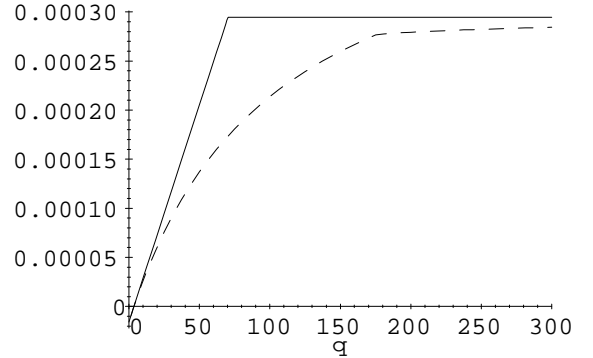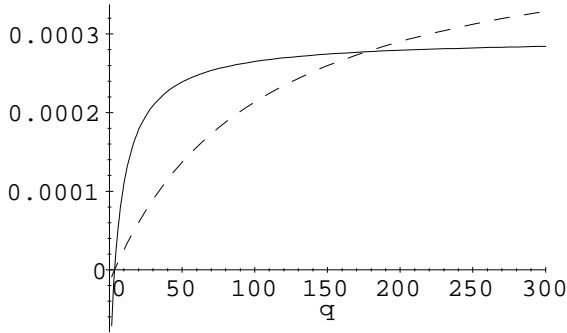
Figures 13 and 14: Left: Plots of the functions $(1 - q/\Gamma)\,W_c(q)$ and $(1 - q/\Gamma)\,W_j(q,I)$ in the case $q_s > 0$. For $W_c(\infty) > W_j(\infty, I)$ the solid line denotes $W_j(q,I)$ and the broken one $W_c(q)$. The function $A^{chl}(q,I)$ is a combination of both lines: for $q > q_s$ it is represented by the solid line, for $0 < q < q_s$ by the broken line.

Right: $A^{chl}(q,I)$ (broken line) and its linear approximation $A_{lin}^{chl}(q,I)$ (solid line). The latter one is constructed by

(i) the straight line through the points $(q, A^{chl}) = (0, A^{chl}(0,I))$ and $(q, A^{chl}) = (\Gamma_*, 0)$, and,

(ii) the straight line parallel to the q-axis with the asymptotic value $A^{chl} = \min\{V_{max}, J/4\}$.

q_c denotes the q-value of the intersection of (i) and (ii)

where

$$q_s = \frac{\tau K_c J(K_o + p_o) - 4V_{max}K_o p_o}{\tau K_o(4V_{max} - J)} \tag{3.51}$$

and

$$J(I) = \frac{\alpha I}{\sqrt{1 + \left(\dfrac{\alpha I}{J_{max}}\right)^2}} \tag{3.36}$$

q_c denotes the q-value of the intersection of (i) and (ii), q_s was defined above as the q-value of the second intersection point of $W_c(q)$ and $W_j(q, I)$ (the first one lies at $q = 0$). Figures 13 and 14 show plots of $A^{chl}(q, I)$ and $A_{lin}^{chl}(q, I)$ for the parameter values given in the appendix.

Next we repeat some steps from the non-linear case above, but now for $A_{lin}^{chl}(q, I)$ instead of $A^{chl}(q, I)$: we equate (3.59) with

$$A_{lin}^{chl} = g_{liq}\left(R_{gas}T\,C - q\right) \tag{3.61}$$

and solve for q as a function of C. Instead of (3.57) we get

$$q = \begin{cases} R_{gas}T\,C - \dfrac{V_{max}}{g_{liq}} & \begin{cases} \text{if } q_s \leq 0 \text{ and } J/4 > V_{max} \text{ and } q_c < q \\ \text{if } q_s > 0 \text{ and } J/4 > V_{max} \text{ and } q_c \leq q \end{cases} \\[3ex] R_{gas}T\,C - \dfrac{J}{4\,g_{liq}} & \begin{cases} \text{if } q_s \leq 0 \text{ and } J/4 < V_{max} \text{ and } q_c < q \\ \text{if } q_s > 0 \text{ and } J/4 < V_{max} \text{ and } q_c < q \end{cases} \\[3ex] \dfrac{8\,g_{liq}R_{gas}Tp_o\,C + p_o J}{2\,(4\,g_{liq}p_o + \tau J)} & \begin{cases} \text{if } q_s \leq 0 \text{ and } J/4 < V_{max} \text{ and } 0 \leq q \leq q_c \\ \text{if } q_s > 0 \text{ and } J/4 > V_{max} \text{ and } 0 \leq q \leq q_c \end{cases} \\[3ex] \dfrac{2\tau g_{liq}R_{gas}TK_c(K_o + p_o)\,C + K_o V_{max}p_o}{2\tau\,(g_{liq}K_c(K_o + p_o) + K_o V_{max})} & \begin{cases} \text{if } q_s \leq 0 \text{ and } J/4 > V_{max} \text{ and } 0 \leq q \leq q_c \\ \text{if } q_s > 0 \text{ and } J/4 < V_{max} \text{ and } 0 \leq q \leq q_c \end{cases} \end{cases} \tag{3.62}$$

We insert (3.62) back into (3.61) and obtain an expression for $A_{lin}^{chl}(C)$ which substitutes (3.52) (or (3.33)):

$$A_{lin}^{chl}(C) := \begin{cases} V_{max} & \begin{cases} \text{if } q_s \leq 0 \text{ and } J/4 > V_{max} \text{ and } C_{q_c} \leq C \\ \text{if } q_s > 0 \text{ and } J/4 > V_{max} \text{ and } C_{q_c} \leq C \end{cases} \\[3ex] \dfrac{J}{4} & \begin{cases} \text{if } q_s \leq 0 \text{ and } J/4 < V_{max} \text{ and } C_{q_c} \leq C \\ \text{if } q_s > 0 \text{ and } J/4 < V_{max} \text{ and } C_{q_c} < C \end{cases} \\[3ex] \dfrac{J\,g_{liq}\,(2\tau\,R_{gas}T\,C - p_o)}{2(4g_{liq}p_o + \tau J)} & \begin{cases} \text{if } q_s \leq 0 \text{ and } J/4 < V_{max} \text{ and } 0 \leq C \leq C_{q_c} \\ \text{if } q_s > 0 \text{ and } J/4 > V_{max} \text{ and } 0 \leq C \leq C_{q_c} \end{cases} \\[3ex] \dfrac{g_{liq}\,K_o V_{max}(2\tau\,R_{gas}T\,C - p_o)}{2\tau\,[g_{liq}K_c(K_o + p_o) + K_o\,V_{max}]} & \begin{cases} \text{if } q_s \leq 0 \text{ and } J/4 > V_{max} \text{ and } 0 \leq C \leq C_{q_c} \\ \text{if } q_s > 0 \text{ and } J/4 < V_{max} \text{ and } 0 \leq C \leq C_{q_c} \end{cases} \end{cases} \tag{3.63}$$

The concentration C_{q_c} in the intercellular airspace is the equivalent of the pressure q_c in the chloroplasts. It is obtained by setting $q = q_c$ and $C = C_{q_c}$ in (3.62) and solving for C_{q_c}. The result is

$$
C_{q_c} := \begin{cases}
\dfrac{(J + 8V_{max})p_o g_{liq} + 2V_{max}\tau J}{2\tau J R_{gas} T g_{liq}} & \text{if } q_s > 0 \text{ and } J/4 > V_{max} \\[3ex]
\dfrac{g_{liq}\tau K_c J(K_o + p_o) + V_{max}K_o(2g_{liq}p_o + \tau J)}{4\tau V_{max}K_o R_{gas} T g_{liq}} & \text{if } q_s > 0 \text{ and } J/4 < V_{max} \\[3ex]
\dfrac{2g_{liq}\tau K_c(K_o + p_o) + K_o(g_{liq}p_o + 2\tau V_{max})}{2\tau K_o R_{gas} T g_{liq}} & \text{if } q_s \leq 0 \text{ and } J/4 > V_{max} \\[3ex]
\dfrac{6g_{liq}p_o + \tau J}{4\tau R_{gas} T g_{liq}} & \text{if } q_s \leq 0 \text{ and } J/4 < V_{max}
\end{cases}
\tag{3.64}
$$

By replacing $A^{chl}(q, I)$ in (3.55) by $A^{chl}_{lin}(C)$ (as given in (3.59)) we arrive at the linearized version of the diffusion equation (3.9), valid for the assimilation layer:

$$
\frac{d^2 C}{dr^2} + \frac{1}{r}\frac{dC}{dr} = \begin{cases}
\chi & \text{if } r_c \leq r \leq r_1 \\[2ex]
k^2 C - \kappa & \text{if } r_0 \leq r \leq r_c
\end{cases}
\tag{3.65}
$$

χ, κ and k are defined by

$$
\chi := \frac{1}{D_{CO_2}} \times \tau_{as}^2 \left(\frac{a_{chl}}{a_{as}}\right)\left(\frac{a_{as}}{v_{as}}\right)\frac{1 - n_{as}}{n_{as}} \times \begin{cases}
V_{max} & \text{if } J/4 > V_{max} \\[2ex]
\dfrac{J}{4} & \text{if } J/4 < V_{max}
\end{cases}
\tag{3.66}
$$

$$
\kappa := \frac{1}{D_{CO_2}} \times \tau_{as}^2 \left(\frac{a_{chl}}{a_{as}}\right)\left(\frac{a_{as}}{v_{as}}\right)\frac{1 - n_{as}}{n_{as}} \times \begin{cases}
\dfrac{-J g_{liq} p_o}{(8\, g_{liq} p_o + 2\tau J)} & \begin{cases} \text{if } q_s \leq 0 \text{ and } J/4 < V_{max} \\ \text{if } q_s > 0 \text{ and } J/4 > V_{max} \end{cases} \\[3ex]
\dfrac{-g_{liq} V_{max} K_o p_o}{2\tau\left[g_{liq}K_c(K_o + p_o) + K_o V_{max}\right]} & \begin{cases} \text{if } q_s \leq 0 \text{ and } J/4 > V_{max} \\ \text{if } q_s > 0 \text{ and } J/4 < V_{max} \end{cases}
\end{cases}
\tag{3.67}
$$

$$
k^2 := \frac{1}{D_{CO_2}} \times \tau_{as}^2 \left(\frac{a_{chl}}{a_{as}}\right)\left(\frac{a_{as}}{v_{as}}\right)\frac{1 - n_{as}}{n_{as}} \times \begin{cases}
\dfrac{-J\tau g_{liq} R_{gas} T}{(4\, g_{liq} p_o + \tau J)} & \begin{cases} \text{if } q_s \leq 0 \text{ and } J/4 < V_{max} \\ \text{if } q_s > 0 \text{ and } J/4 > V_{max} \end{cases} \\[3ex]
\dfrac{-g_{liq} V_{max} K_o R_{gas} T}{g_{liq}K_c(K_o + p_o) + K_o V_{max}} & \begin{cases} \text{if } q_s \leq 0 \text{ and } J/4 > V_{max} \\ \text{if } q_s > 0 \text{ and } J/4 < V_{max} \end{cases}
\end{cases}
\tag{3.68}
$$

The parameter r_c, which has been introduced into (3.65), is defined by

$$r_c := \begin{cases} r_0 & \text{if } C(r = r_0, r_c = r_0) > C_{q_c} \\ r_1 & \text{if } C(r = r_1, r_c = r_1) < C_{q_c} \\ r_c^* & \text{if } C(r = r_0, r_c = r_0) < C_{q_c} \text{ and } C(r = r_1, r_c = r_1) > C_{q_c} \end{cases} \tag{3.69}$$

where r_c^* is solution of the equation

$$C(r = r_c^*, r_c = r_c^*) = C_{q_c} \tag{3.70}$$

r_c divides the assimilation area into two layers defined by $r_0 \le r \le r_c$ and $r_c \le r \le r_1$, resp.. In the outer part of the assimilation layer, photosynthesis then works in the "saturated mode" (i.e. the case $q_c \le q$ in (3.59) or $C_{q_c} \le C$ in (3.63)), and in the inner part of the layer in the "linear mode" (i.e. $0 \le q \le q_c$ in (3.59) or $0 \le C \le C_{q_c}$ in (3.63)). Thus, the model allows the net production of carbon dioxide only in the inner part of the assimilation layer. This is no real restriction, however, because the extreme cases $r_c = r_0$ or $r_c = r_1$ — meaning that the complete layer assimilates either in the saturated or in the linear mode, resp. — are covered by the mathematics of the model.

The splitting up of the assimilation layer into two sublayers deserves some justification. This will be given in the next section, in which we will discuss details of the calculation of r_c. Meanwhile, we affirm sceptical readers, that (3.69) (with (3.70)) is *not* a definition in circles.

We note that the information contained in the right hand side of equation (3.65) divides into the three categories of assumptions (and reliability) (according to (3.66), (3.67) and (3.68)) discussed in Section 1: the first factor, $1/D_{CO_2}$, is a time independent constant of nature, the second factor contains — apart from (a_{chl}/a_{as}) — measurable quantities obtained from the fossil record, and the third factor reflects photosynthetic considerations for extant C_3-plants. In contrast, the water vapour flux depends only on the first two categories and is therefore not affected by evolutionary changes of biochemical mechanisms which may have ocurred since the Lower Devonian.

3.5 The solution procedure

Before presenting explicit solutions of the Diffusion Equation we recapitulate in more mathematical terms what alterations it experienced in the last few sections.

— We started with the most general form of the Diffusion Equation, (3.5). It was a second order partial differential equation in the variable C, linear or non-linear, depending on the form of the source strength $Q(C)$. The introduction of polar coordinates transformed the outer appearance of the equation into (3.7) but left its mathematical nature untouched.

— The symmetries and approximations of Section 3.3 turned (3.7) into an *ordinary* differential equation of second order, given as equation (3.9). It is linear in the boundary, the stomatal and the hypodermal layer, because these layers provide no sources for water vapour or carbon dioxide, whereupon the term Q vanishes.

— In the assimilation area of the outer cortex equation (3.9) attains the nonlinear form (3.58), because the mechanism of photosynthesis (see (3.33) or (3.52), Section 3.4.1) shows saturation behaviour, which turns the source strength $Q(C)$ into a non-linear function of the carbon dioxide concentration C.

— In order to cope with the considerable mathematical difficulties caused by the non-linearities in (3.58) we linearized the model of photosynthesis with the result represented by equation (3.63) (Section 3.4.3), turning (3.58) into the linear ordinary second order differential equation of (3.65).

Putting the layer specific versions together, we arrive at the following piecewise defined, linear ordinary differential equation of second order:

$$
\frac{d^2 C_i}{dr^2} + \frac{1}{r} \frac{dC_i}{dr} =
\begin{cases}
0 & \text{if } r_1 \leq r \leq r_3 \quad \text{(i.e. } i = bl, st, hy) \\[2mm]
\chi & \text{if } r_c \leq r \leq r_1 \quad \text{(i.e. } i = as, \\
& \quad \text{``saturated mode'' of photosynthesis)} \\[2mm]
k^2\, C_i - \kappa & \text{if } r_0 \leq r \leq r_c \quad \text{(i.e. } i = as, \\
& \quad \text{``linear mode'' of photosynthesis)}
\end{cases}
$$

$$(3.71)$$

with bl = boundary layer, st = stomata layer, hy = hypodermal layer, as = assimilation layer.

In the case of water vapour diffusion only the first line of (3.71) applies, because we assume that the intercellular airspace of the outer cortex is constantly saturated with water vapour. The concentration of water vapour in this layer is therefore obtained from the Kelvin-Equation (see (3.76) below).

In the case of carbon dioxide diffusion, the whole system of equations (3.71) is appropriate. χ, k, and κ (equations (3.66) through (3.68)) are combinations of natural constants and of parameters that characterize the model of photosynthesis and the plant's morphology. r_c (defined in equations (3.69) and (3.70)) results from the application of the linear approximation to the photosynthesis model. It divides the assimilation layer into two areas: an inner zone ($r_0 \leq r \leq r_c$), where photosynthesis works in "linear mode" and carbon dioxide net production is allowed to take place, and a peripheral zone ($r_c \leq r \leq r_1$), where photosynthesis is in "saturated mode" and carbon dioxide is only consumed at a constant rate (constant in the sense of being independent from r).

In mathematical terms, (3.71) represents a boundary value problem for both gases. In order to solve it, we have to match the layer specific solutions of (3.71) in such a way that the overall solution $C(r)$ becomes a continuously differentiable function of r such that $C(r)$ (and — depending on the circumstances — perhaps $j(r)$) assume arbitrarily prescribed values at the boundaries of the region considered.

The standard procedure of solving second order differential equations which are piecewise defined,

such as (3.71) consists of the following steps:

(i) **General solution of the diffusion equation.**

General solutions of (3.71) can either be calculated or — more easily — found in text books on Theoretical Physics (for example, Arfken, 1970 or Morse & Feshbach, 1953). For the case of carbon dioxide diffusion, they are cited in (3.72) and for water vapour diffusion in (3.73). $I_n(x)$ and $K_n(x)$ denote the modified Bessel functions of the first respective second kind of order n according to the conventions of Abramowitz & Stegun, 1972.

The effective conductances are defined as $S_i := D_{CO_2}^{air} \, n_i / \tau_i^2$ and $s_i := D_{H_2O}^{air} \, n_i / \tau_i^2$, resp..

A_i and B_i (resp. a_i and b_i) are arbitrary constants to which definite values will be assigned during the course of the matching procedure.

r	$C^{CO_2}(r)$	$j^{CO_2}(r)$
— r_3		
boundary layer	$A_{bl} + B_{bl} \, \ln\left(\dfrac{r}{R}\right)$	$-S_{bl}\dfrac{B_{bl}}{r}$
— R		
stomatal layer	$A_{st} + B_{st} \, \ln\left(\dfrac{r}{R}\right)$	$-S_{st}\dfrac{B_{st}}{r}$
— r_2		
hypodermal layer	$A_{hy} + B_{hy} \, \ln\left(\dfrac{r}{R}\right)$	$-S_{hy}\dfrac{B_{hy}}{r}$
— r_1		
intracellular air space (outer cortex) — r_c	$A_2 + B_2 \, \ln\left(\dfrac{r}{R}\right) + \dfrac{\chi}{4}r^2$	$-S_{as}\left[\dfrac{B_2}{r} + \dfrac{\chi}{2}r\right]$
	$A_1 \, I_0(kr) + B_1 \, K_0(kr) + \dfrac{\kappa}{k^2}$	$S_{as}\, k\,[-A_1 \, I_1(kr) + B_1 \, K_1(kr)]$
— r_0		

(3.72)

(ii) **Conditions of continuity at inner boundaries.** The solutions cited in (i) should be matched at the (inner) boundaries between the plant's layers such that $C(r)$ and $j(r)$ become continuous functions of r.

The physical basis of the continuity requirement lies in the mobility of the molecules of a gas (or a fluid), which prevents discontinuous concentrations and current densities. Within the various layers, continuity is already guaranteed by the mathematical structure of (3.71). Critical areas, for which continuity has to be explicitly ensured, are the boundaries which separate the layers at $r = R$, r_2, r_1 and r_c[10]. An analogous requirement for the fluxes stems

---

[10] This can be traced to the fact that the differential equation (3.71) is piecewise — one layer, one piece — defined. As pointed out in Section 3.3.4, the effective conductance S changes quite abruptly at the layer boundaries at $r = R$, r_2 and r_1. Additionally, the right hand side of equation (3.71) is discontinuous at $r = r_1$ and $r = r_c$.

r	$C^{\mathrm{H_2O}}(r)$	$j^{\mathrm{H_2O}}(r)$
— r_3 —		
boundary layer	$a_{bl} + b_{bl}\,\ln\left(\dfrac{r}{R}\right)$	$-s_{bl}\dfrac{b_{bl}}{r}$
— R —		
stomatal layer	$a_{st} + b_{st}\,\ln\left(\dfrac{r}{R}\right)$	$-s_{st}\dfrac{b_{st}}{r}$
— r_2 —		
hypodermal layer	$a_{hy} + b_{hy}\,\ln\left(\dfrac{r}{R}\right)$	$-s_{hy}\dfrac{b_{hy}}{r}$
— r_1 —		

$$(3.73)$$

from the fact, that — with the sole exception of the assimilating outer cortex — molecules should nowhere disappear or spontaneously appear. The boundaries between the radial layers are again critical areas (compare Figure 10). The conditions of continuity are explicitly given in equations (3.78) for the case of carbon dioxide and in equations (3.80) for water vapour.

(iii) **Boundary conditions.** The solutions given in (i) and processed in (ii) should be continuously connected to prescribed boundary values for $C(r)$ (and perhaps $j(r)$).

For carbon dioxide diffusion we make the following assumptions:

— The carbon dioxide current shall cease at the inner edge of the photosynthetic active region, that is, $j^{\mathrm{CO_2}}(r)$ should fulfill

$$j^{\mathrm{CO_2}}(r_0) = 0 \qquad (3.74)$$

— We assign the value $C_{atm}^{\mathrm{CO_2}}$ to the carbon dioxide concentration in the free atmosphere outside the boundary layer . The boundary condition at $r = r_3$ reads then

$$C^{\mathrm{CO_2}}(r_3) = C_{atm}^{\mathrm{CO_2}} \qquad (3.75)$$

In the case of water vapour diffusion we assume:

— The inner cortex of rhyniophytic plants is saturated with liquid water, that is supplied by the central vascular bundle and evaporates in the intercellular voids of the outer cortex. The water vapour concentration in the intercellular air space is therefore in equilibrium with the liquid water in the cortex cells. If temperature T and pressure p are given, the water vapour concentration can be calculated from tabulated saturation values $C_{sat}^{\mathrm{H_2O}}$ of water vapour in air above a plane water surface via the Kelvin equation (sometimes called Thomson equation after Lord Kelvins civic name), which considers the pressure drop of water vapour due to capillary effects in the cortex cells (for details see Nobel, 1999, p.

312). With σ denoting the radius of a typical cortex cell, V_l^m the molar volume of water and γ the surface tension in a boundary surface which separates air and liquid water, the boundary condition at $r = r_1$ reads

$$C^{\mathrm{H_2O}}(r_1) = C_{sat}^{\mathrm{H_2O}} \exp\left(\frac{2\, V_l^m\, \gamma}{R_{gas} T\, \sigma} \right) \tag{3.76}$$

— The water vapour concentration $C_{atm}^{\mathrm{H_2O}}$ in the free atmosphere outside the boundary layer may be arbitrarily chosen, according to our assumptions on the prevailing climate, i.e. the boundary condition at $r = r_3$ is

$$C^{\mathrm{H_2O}}(r_3) = C_{atm}^{\mathrm{H_2O}} \tag{3.77}$$

More explicit statements of the boundary conditions can be found in equations (3.79) for the case of carbon dioxide and in equations (3.81) for water vapour.

As part of the matching procedure the hitherto unspecified arbitrary constants A_i, B_i, a_i and b_i are given definite values, because otherwise continuity of $C^{\mathrm{CO_2}}(r)$, $j^{\mathrm{CO_2}}(r)$, $C^{\mathrm{H_2O}}(r)$ and $j^{\mathrm{H_2O}}(r)$ cannot be achieved. In other words, the (total) number of arbitrary constants which are present in the general solutions (3.72) and (3.73) have to be equal to the number of conditions of continuity at $r = R$, r_2, r_1 and r_c, plus the number of boundary conditions given by equations (3.74) to (3.77).

Insertion of the general solutions (3.72) into the continuity and boundary conditions results in the case of carbon dioxide in the following system of ten linear equations for the ten unknowns A_i and B_i:

$$A_{bl} = A_{st}$$
$$A_{st} + B_{st} \ln\left(\frac{r_2}{R}\right) = A_{hy} + B_{hy} \ln\left(\frac{r_2}{R}\right)$$
$$A_{hy} + B_{hy} \ln\left(\frac{r_1}{R}\right) = A_2 + B_2 \ln\left(\frac{r_1}{R}\right) + \frac{\chi}{4}r_1{}^2$$
$$A_2 + B_2 \ln\left(\frac{r_c}{R}\right) + \frac{\chi}{4}r_c{}^2 = A_1 I_0(kr_c) + B_1 K_0(kr_c) + \frac{\kappa}{k^2}$$
$$S_{bl} B_{bl} = S_{st} B_{st}$$
$$S_{st} B_{st} = S_{hy} B_{hy}$$
$$S_{hy} \frac{B_{hy}}{r_1} = S_{as}\left[\frac{B_2}{r_1} + \frac{\chi}{2}r_1\right]$$
$$\frac{B_2}{r_c} + \frac{\chi}{2}r_c = k\left[A_1 I_1(kr_c) - B_1 K_1(kr_c)\right] \tag{3.78}$$

$$0 = k\left[A_1 I_1(kr_0) - B_1 K_1(kr_0)\right]$$
$$C_{atm}^{\mathrm{CO_2}} = A_{bl} + B_{bl} \ln\left(\frac{r_3}{R}\right) \tag{3.79}$$

Equations (3.78) represent the eight conditions of continuity. The two equations (3.79) represent the two boundary conditions.

The system of equations (3.78) and (3.79) can be solved for the A_i and B_i by mathematical standard procedures like matrix inversion. By this step, A_i and B_i become functions of the parameters which describe the anatomy and the photosynthesis apparatus of the plant, and the particulars of the boundary conditions. Note, that quantities like χ, k, and κ or the S_i are just shorthand expressions for complex combinations concerning parameters of anatomy and photosynthesis. Reinsertion of the A_i and B_i back into the solutions (3.72) will almost complete the solution process: C^{CO_2} and j^{CO_2} depend afterwards on anatomical and photosynthetical parameters, the variable r and the parameter r_c which has been defined in (3.69) and (3.70).

What remains to be done (in the case of carbon dioxide diffusion) is to calculate r_c and to explain its significance. Figures 15, 16 and 17 depict typical shapes of the concentration C^{CO_2} in the assimilation layer and a part of the hypodermal layer under qualitatively different conditions.
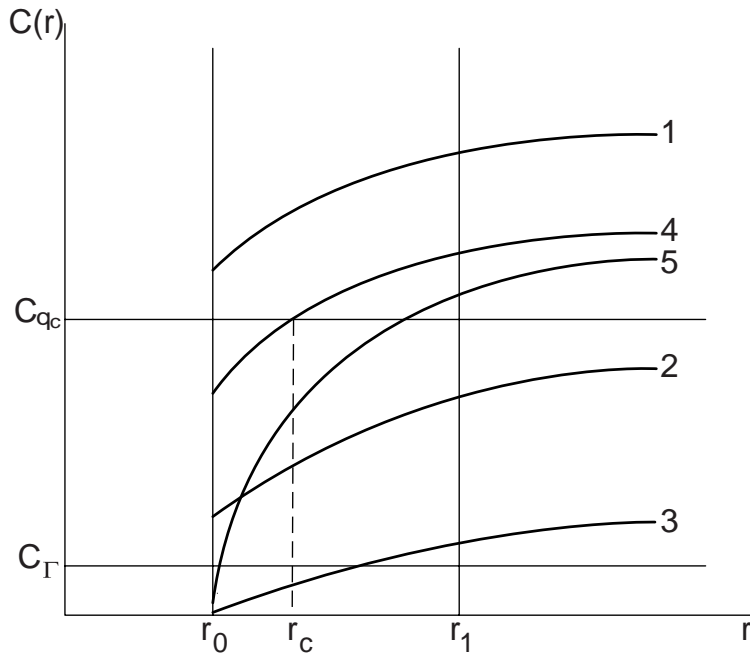
Figure 15: The "standard situations" of assimilation:

— Curve 1: $C^{CO_2} > C_{q_c}$ in the whole assimilation layer, photosynthesis is running everywhere in the saturated mode.

— Curve 2: $C^{CO_2} < C_{q_c}$ in the whole assimilation layer, photosynthesis is running in the linear mode in the whole layer.

— Curve 3: $C^{CO_2} < C_{q_c}$ and $C^{CO_2} < C_{\Gamma_*}$, photosynthesis is running in the linear mode in the whole layer, net *production* of carbon dioxide in the area with $C^{CO_2} < C_{\Gamma_*}$.

— Curve 4: $C^{CO_2} > C_{q_c}$ for $r_c \leq r \leq r_1$, $C^{CO_2} < C_{q_c}$ for $r_0 \leq r \leq r_c$. Photosynthesis is running in saturated mode in the outer zone of the assimilation layer, in the linear mode in the inner sublayer.

— Curve 5: Modification of Curve 4 with net production of carbon dioxide in the area with $C^{CO_2} < C_{\Gamma_*}$.

Figure 15 illustrates several "standard situations" when assimilation runs and the carbon dioxide concentration decreases steadily from its highest value in the atmosphere to the inner border of the assimilation layer at $r = r_0$. Three typical situations (plus two "subsituations") can develop:

— The carbon dioxide concentration is higher than its "threshold-value" C_{q_c} in the whole assimilation layer, i.e. plenty of carbon dioxide is available, photosynthesis runs everywhere in the

saturated mode (Curve 1, Figure 15).

— The carbon dioxide concentration is lower than its "threshold-value" C_{q_c} in the entire assimilation layer, i.e. carbon dioxide is scarce, photosynthesis runs in the linear mode in the whole layer. The less carbon dioxide is available, the less is consumed (Curve 2, Figure 15).

Wherever in the assimilation layer the carbon dioxide concentration drops below the carbon dioxide compensation point C_{Γ_*} net *production* of carbon dioxide takes place (Curve 3, Figure 15).

— The carbon dioxide concentration in the outer zone of the assimilation layer is higher than C_{q_c}, but lower in its inner zone. In this case, net production of carbon dioxide is allowed to take place only in the inner sublayer with $r_0 \leq r \leq r_c$ (r_c denotes the border surface between both sublayers.) (Curve 4, Figure 15).

Similarly as above, the carbon dioxide concentration can drop beyond C_{Γ_*} (Curve 5, Figure 15).
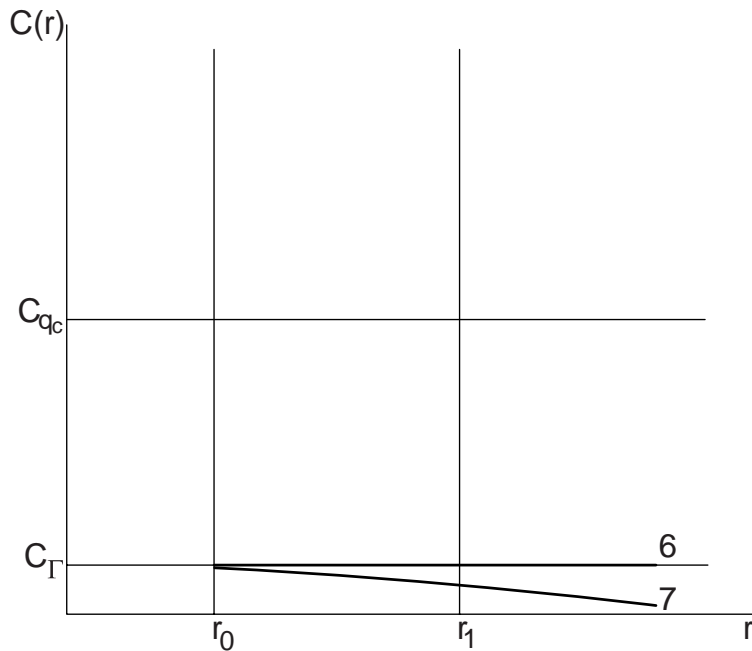
Figure 16: "Non-standard situations" of assimilation:

— Curve 6: $C^{CO_2} = C_{\Gamma_*}$ in the whole plant, carboxylation and oxygenation are performed at identical rates. This situation may develop when the stomata are fully closed.

— Curve 7: $C^{CO_2} < C_{\Gamma_*}$ in the whole plant, C^{CO_2} is produced by photosynthesis (and transported away).

Figure 16 illustrates two "non-standard situations".

— If there is no connection between the free atmosphere and the plant's interior (e.g. when the stomata are fully closed) a situation like the one depicted in Curve 6 of Figure 16 should develop: carboxylation and oxygenation are performed at identical rates, the carbon dioxide concentration attains the constant value C_Γ after some time.

— If the carbon dioxide content of the atmosphere is smaller than C_Γ, we may expect Curve 7 of Figure 16: a continously growing carbon dioxide concentration for decreasing r.
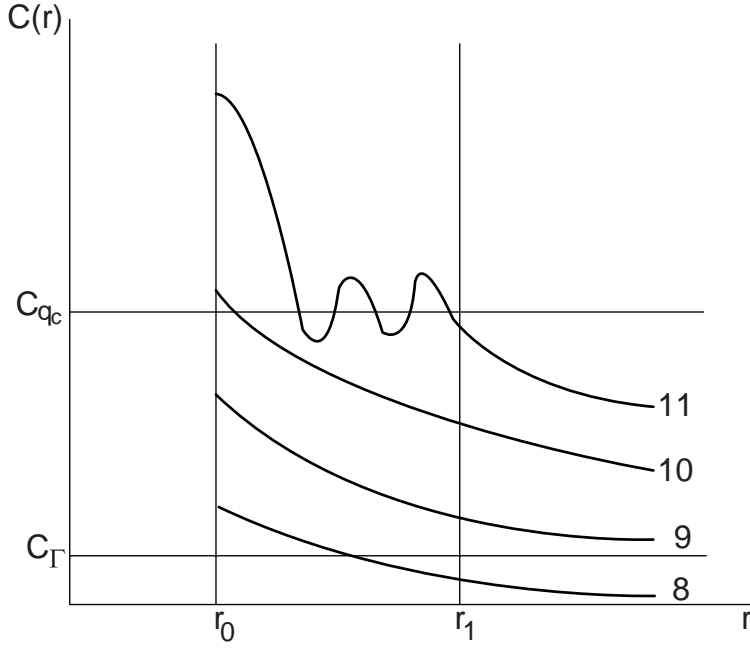
Figure 17: "Hypothetical situations" of assimilation:

— Curve 8: Carbon dioxide is consumed in the interior part of the assimilation layer but produced in the exterior part. This is unrealistic under stationary conditions.

— Curve 9: Carbon dioxide is consumed in the whole assimilation layer, C^{CO_2} increases for decreasing r. This is unrealistic under stationary conditions.

— Curve 10: C^{CO_2} increases for decreasing r. This is unrealistic under stationary conditions.

— Curve 11: Photosynthesis works alternately in saturated and linear modes. This is unrealistic under stationary conditions.

Figure 17, after all, illustrates "hypothetical situations", that should never develop due to physiological reasons — at least not under stationary circumstances.

— Two of them (Curves 8 and 9) are covered by our mathematical model (with $r_c = r_1$).

— However, the situations depicted in Curves 10 and 11 cannot be described within the framework of the model. Curve 10 cannot develop, because the inner zone would work in saturated photosynthesis mode and the outer one in linear mode, whereas the assumption underlying our model is just to the contrary. The situation of Curve 11 would require that the assimilation layer has to split up not only into two — as is assumed in our model — but into six layers, that work alternately in saturated and linear modes[11].

We were forced to postpone the calculation of r_c until now, because the "constants" A_i and B_i became functions of r_c only *after* the application of the conditions of continuity (3.78). Before this step, it makes no sense to apply and solve the equations

$$r_c := \begin{cases} r_0 & \text{if } C^{CO_2}(r = r_0, r_c = r_0) > C_{q_c} \\ r_1 & \text{if } C^{CO_2}(r = r_1, r_c = r_1) < C_{q_c} \\ r_c^* & \text{if } C^{CO_2}(r = r_0, r_c = r_0) < C_{q_c} \text{ and } C^{CO_2}(r = r_1, r_c = r_1) > C_{q_c} \end{cases} \tag{3.69}$$

and

$$C^{CO_2}(r = r_c^*, r_c = r_c^*) = C_{q_c} \tag{3.70}$$

---

[11] If desired, our model can be extended to encompass the situations of Curves 10 and 11.

But meanwhile the functional dependance of A_i and B_i from r_c is known and the calculation of the parameter r_c from (3.69) and (3.70) is possible. Insertion of r_c into $C^{CO_2}(r)$ and $j^{CO_2}(r)$ obtained from (3.72) completes the solution process.

The mathematics of the process of water vapour diffusion is less complex: The six constants a_i and b_i and the expressions for $C^{H_2O}(r)$ and $j^{H_2O}(r)$ are calculated by insertion of the general solutions (3.73) into the continuity and boundary conditions. This leads to a system of six linear equations for the six unknowns a_i and b_i:

$$a_{bl} = a_{st}$$
$$a_{st} + b_{st} \ln\left(\frac{r_2}{R}\right) = a_{hy} + b_{hy} \ln\left(\frac{r_2}{R}\right)$$
$$s_{bl}b_{bl} = s_{st}b_{st}$$
$$s_{st}b_{st} = s_{hy}b_{hy} \tag{3.80}$$

$$C^{H_2O}_{atm} = a_{bl} + b_{bl} \ln\left(\frac{r_3}{R}\right)$$
$$a_{hy} + b_{hy} \ln\left(\frac{r_1}{R}\right) = C^{H_2O}_{sat} \exp\left(\frac{2\,V_l^m\gamma}{R_{gas}T\,\sigma}\right) \tag{3.81}$$

The first and the fourth equation represent the two boundary conditions, the other equations the four conditions of continuity.

The system (3.80) has to be solved for the a_i and b_i which become hereby functions of anatomical parameters of the stomatal and hypodermal layers and of the appropriate boundary conditions. Reinsertion of the a_i and b_i back into the solutions (3.73) will result in the final form of the solutions $C^{H_2O}(r)$ and $j^{H_2O}(r)$.

It should be noted at this point that the use of a computer code, such as MAPLE, is strongly advised for all calculations. Faced with the task of inverting a 10×10-matrix — as presented by equations (3.78) and (3.79) — by traditional pencil-and-paper methods even mathematical hardcore purists resort gratefully to computer codes, which are capable of doing symbolic algebraic manipulations. Even then, the expressions for $C(r)$ and $j(r)$ look frightful and have therefore been shifted to the appendix. It has proven to be economical to transform — whenever possible — arithmetic results obtained with the aid of the computer already *in statu nascendi* into the easier digestable form of a plot.

4. Application of the Model to *Aglaophyton major* and *Rhynia gwynne-vaughanii*

The model as outlined above applies to every axially symmetric plant which qualifies for the approximations stated in Section 3.3. We have to show yet, how the model and data which were obtained from fossilized specimen are connected. The quantities which relate data and model to each other are mainly the effective conductivities for carbon dioxide and water vapour and the radii of the various layers. As the effective conductivities are essentially composed of porosity n and tortuosity τ,

$$\frac{S_i}{D_{\mathrm{CO_2}}} = \frac{s_i}{D_{\mathrm{H_2O}}} = \frac{n_i}{\tau_i{}^2} \tag{4.1}$$

We explain now, how the n_i and the τ_i can be calculated in a general way from measurements carried out with thin sections of fossilized plants. The data are obtained from material which was prepared at the Institute of Geology and Palaeontology of the University of Münster. The methods of preparation will be presented in Section 5. After insertion of data from specimen of *Aglaophyton major* and *Rhynia gwynne-vaughanii* we shall be able to derive actual results.

4.1 Boundary layer

The first barrier encountered by a diffusing molecule is the boundary layer of air which envelopes the plant. If air (or, in general, a fluid) flows around an object, a velocity gradient develops due to the adhesion of the innermost air layer to the object (see, for example, Vogel, 1994). Thickness d_{bl} and kind of the boundary layer (laminar or turbulent) influence its conductance with respect to diffusion. For the present case, we choose the approximation given in Nobel (1999, p. 274) for a cylindrical body of radius R immersed in air with a (free air) wind velocity v:

$$d_{bl} = 5.8 \times 10^{-3}\mathrm{m}\sqrt{\frac{2R}{v}\frac{1}{s}} \tag{4.2}$$

With R as the plants radius we define the outer edge of the boundary layer as

$$r_3 := R + d_{bl} \tag{4.3}$$

As molecules move in air unhindered by any obstacles, porosity and tortuosity take the values

$$n_{bl} = 1 \qquad \text{and} \qquad \tau_{bl} = 1 \tag{4.4} \tag{4.5}$$

leading to

$$\frac{S_{bl}}{D_{\mathrm{CO_2}}} = \frac{s_{bl}}{D_{\mathrm{H_2O}}} = \frac{n_{bl}}{\tau_{bl}{}^2} = 1 \tag{4.6}$$

4.2 Stomatal layer

The effective conductance of the stomatal layer depends on the density of the stomata, their pore size and the diffusivity of the gas. We consider only the case of fully opened stomata, due to two reasons:

(i) stomatal closure requires a corresponding regulation function which is not readily available for Devonian plants, and,

(ii) during the closing process the size of the stomatal pore may drop below a threshold value below which interactions between the diffusing molecules and the cell walls become important. Condition (3.3) is no longer fulfilled and Fick's first law ought to be modified (Jarman, 1974, Leuning, 1983, Reif, 1974).

r_2 denotes the inner edge of the stomatal layer, d_{st} the depth of stomatal pores and thus

$$r_2 := R - d_{st} \qquad (4.7)$$

Fossilized specimen will provide values for the number of stomata per unit surface area, ν_{st}, and for the average area of stomatal pores, a_{st}, of *Aglaophyton major* and *Rhynia gwynne-vaughanii* (see Section 5).

As the pores are shaped like ellipses, numerical values of a_{st} are obtained by measuring the shortest diameter w_{st} and the longest diameter h_{st} of a pore. The pore area is calculated via the equation for the area of an ellipse

$$a_{st} = \frac{\pi}{4} w_{st} h_{st} \qquad (4.8)$$

In order to calculate the porosity we concentrate on a "slice" of length L along the symmetry axis (see Figure). We approximate the stomatal layer between R and r_2 by a thin rectangular plate of thickness d_{st} and side lenghts L and $\pi(R + r_2)$, where the latter is the arithmetic mean between the circumferences of the outer surface (at $r = R$) and the inner surface (at $r = r_2$) of the stomatal layer.

The volume of one stoma is approximately $a_{st}d_{st} = \frac{\pi}{4}w_{st}h_{st}d_{st}$, the number of stomata on the slice of length L is $\nu_{st}L\pi(R + r_2)$, and therefore the pore volume V_p is given by $V_p = \frac{\pi^2}{4}w_{st}h_{st}d_{st}\,\nu_{st}L\pi(R + r_2)$. Because the total volume of the slice is $V = d_{st}L\pi(R + r_2)$ and $n_{st} = V_p/V$ we obtain

$$n_{st} = a_{st}\nu_{st} = \frac{\pi}{4}w_{st}h_{st}\nu_{st} \qquad (4.9)$$

In the case of the stomatal layer, tortuosity results not from obstacles inside the stomata, but from the following effect (see Figure): within the boundary layer, the surfaces of equal concentration of water vapour (or carbon dioxide) are not exactly concentric cylinders (whose centres coincide with

the plant's symmetry axis) but bulge out over the stomata, so that molecules diffusing out of the stomata still experience stomatal conditions although they have already left the stomatal layer in a geometric sense.

Nobel (1999, p. 301, see Figure 18) approximates the "bulge" above a stoma by a little sphere whose centre coincides with the centre of the elliptically shaped cross-section of the stoma and whose radius ρ_{st} is given as half the geometric mean of the longest and shortest diameters w_{st} and h_{st} of the pore,

$$\rho_{st} = \frac{\sqrt{w_{st}h_{st}}}{2} \tag{4.10}$$
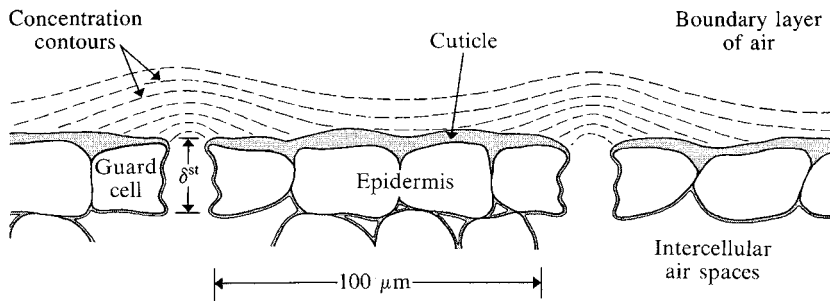
Figure 18: A typical plant epidermis. The broken lines depict the concentration contours of water vapour and carbon dioxide. The quantity δ^{st} in the drawing is the same as the quantity d_{st} in the text.

A molecule diffusing through a stoma will therefore cover an effective path length $l_e = d_{st} + \rho_{st} = d_{st} + \sqrt{w_{st}h_{st}}/2$ under stomatal conditions. With $l = d_{st}$ and $\tau := l_e/l$ we obtain

$$\tau_{st} = \frac{d_{st} + \rho_{st}}{d_{st}} = 1 + \frac{\rho_{st}}{d_{st}} = 1 + \frac{\sqrt{w_{st}h_{st}}}{2\,d_{st}} \tag{4.11}$$

Combining (4.9) and (4.11) we obtain

$$\frac{S_{st}}{D_{CO_2}} = \frac{s_{st}}{D_{H_2O}} = \frac{n_{st}}{\tau_{st}{}^2} = \frac{\pi}{4} \frac{\nu_{st}}{\left(\dfrac{1}{\sqrt{w_{st}h_{st}}} + \dfrac{1}{2d_{st}} \right)^2} \tag{4.12}$$

4.3 Hypodermal channels

When hypodermal channels are present, their contribution to the diffusion conductance has also to be considered. We denote the thickness of the hypodermis by d_{hy} and its lower edge, the boundary to the assimilation layer, by r_1. Thus

$$r_1 := r_2 - d_{hy} = R - (d_{hy} + d_{st}) \tag{4.13}$$

The same ideas as above are used in the derivation of porosity. Hypodermal channels, like stomata, usually show an elliptic cross-sectional shape with a longer axis, h_{hy}, and a shorter axis, w_{hy}. Thus their area is $a_{hy} = (\pi/4)\, h_{hy} w_{hy}$. Because every hypodermal channel is attached to exactly one stoma, the number of hypodermal channels on a slice of length L equals the number of stomata, $\nu_{st} L\pi(R + r_2)$. As the volume of one hypodermal channel is $a_{hy} d_{hy} = \frac{\pi}{4} w_{hy} h_{hy} d_{hy}$ the total pore volume of all channels reads $V_p = \frac{\pi^2}{4} w_{hy} h_{hy} d_{hy}\, \nu_{st} L\pi(R + r_2)$. The total volume of the hypodermal "slice" is $V = d_{hy} L\pi(r_1 + r_2)$, thus

$$n_{hy} = \frac{V_p}{V} = \frac{\pi}{4}\, h_{hy} w_{hy}\, \nu_{st}\, \frac{2R - d_{st}}{2R - (2d_{st} + d_{hy})} \tag{4.14}$$

where we have used (4.7) and (4.13).

Hypodermal channels contain no obstacles for diffusing molecules. Their tortuosity is therefore

$$\tau_{hy} = 1 \tag{4.15}$$

and the effective conductances become

$$\frac{S_{hy}}{D_{CO_2}} = \frac{s_{hy}}{D_{H_2O}} = \frac{n_{hy}}{\tau_{hy}^2} = \frac{\pi}{4}\, h_{hy} w_{hy}\, \nu_{st}\, \frac{2R - d_{st}}{2R - (2d_{st} + d_{hy})} \tag{4.16}$$

4.4 Assimilation layer

The thickness of the assimilation layer is denoted as d_{as} and

$$r_0 := r_1 - d_{as} = R - (d_{as} + d_{hy} + d_{st}) \tag{4.17}$$

represents its inner edge.

The outer cortex consists of cells whose shape is approximately cylindric. As the longitudinal axis of these cells is parallel to the longitudinal axis of the plant, in cross-sectional view, the shape of these cells is similar to circular disks. If we assume, that the cortex cells are either infintely long or that their "end disks" are randomly distributed along the plant axis, rather than lying on common cross-sections, the measurement of the (three-dimensional) porosity reduces two the evaluation of (two-dimensional) cross-sections.

In Section 3.4.2 the specific surface (a_{as}/v_{as}) of a cortex cell was introduced. We denote the length of a cell by L and its radius by σ. The disclike ends are cupped by half spheres with radius σ. The expressions $a_{as} = 2\pi\sigma L + 4\pi\sigma^2$ and $v_{as} = \pi\sigma^2 L + (4/3)\pi\sigma^3$ for the total surface and the volume of the cylinder imply

$$\left(\frac{a_{as}}{v_{as}} \right) = \frac{2\pi\sigma L + 4\pi\sigma^2}{\pi\sigma^2 L + (4/3)\pi\sigma^3} = \frac{2}{\sigma} \times \frac{1 + 2\dfrac{\sigma}{L}}{1 + \dfrac{4}{3}\dfrac{\sigma}{L}} \tag{4.18}$$

For the limit of an infinite long cylindrical cell $(L \to \infty)$ this reduces to

$$\left(\frac{a_{as}}{v_{as}}\right) = \frac{2}{\sigma} \tag{4.19}$$

For the sake of simplicity we will assume further on that this expression is valid.

In order to calculate the tortuosity of the outer cortex, we use a rough approximation: a molecule which diffuses around such a cell has to move along a half circular path with a distance r from the cell centre. The pathlength l_e amounts to $l_e = \pi r$, the direct distance is $l = 2r$, and the following average value results:

$$\tau_{as} = \frac{l_e}{l} = \frac{\pi r}{2r} = \frac{\pi}{2} \approx 1.57 \tag{4.20}$$

Once n_{as} is explicitly known, the effective conductances can be calculated via

$$\frac{S_{as}}{D_{CO_2}} = \frac{s_{as}}{D_{H_2O}} = \frac{n_{as}}{\tau_{as}{}^2} \tag{4.21}$$

Another quantity of interest is the ratio (a_{chl}/a_{as}) of the sum of the surfaces of all chloroplasts a_{chl} within one cortex cell to the surface a_{as} of this cell. It was introduced in (3.54) (Section 3.4.2) in the light of the fact that this ratio can easier be calculated than the individual values a_{chl} and a_{as}. (a_{chl}/a_{as}) is determined by two factors:

(i) Typical chloroplasts tend to look like oblate spheroids, whose shorter axes are about half as long as their two (equally long) longer axes. Inside the cortex cells the chloroplasts seem to be oriented in such a way, that their "equatorial planes" (defined by their longer axes) lie parallel to the surfaces of the cortex cells. Therefore, if we denote the half-length of the longer axes of a cortex cell by R_c, one chloroplast "covers" an area $\pi R_c{}^2$ of the cortex cell's surface area a_{as}. In other words, if the surface of a cortex cell would be entirely packed with chloroplasts, each chloroplast's supply of carbon dioxide would have to diffuse through an area $\pi R_c{}^2$ of the cortex cell's surface, quite irrespective of the chloroplast's surface.

The surface of a chloroplast showing the shape of an oblate spheroid is given by

$$A_\eta = 2\pi R_c{}^2 + \pi R_c{}^2 \frac{\eta^2}{\sqrt{1-\eta^2}} \ln\left(\frac{1+\sqrt{1-\eta^2}}{1-\sqrt{1-\eta^2}}\right) \qquad (0 \le \eta \le 1) \tag{4.22}$$

where R_c is the length of the spheroid's longer and ηR_c the length of its shorter half axis. Therefore the ratio

$$\frac{A_\eta}{\pi R_c{}^2} = 2 + \frac{\eta^2}{\sqrt{1-\eta^2}} \ln\left(\frac{1+\sqrt{1-\eta^2}}{1-\sqrt{1-\eta^2}}\right) \tag{4.23}$$

is one of the two factors, that cause the "area increase" (a_{chl}/a_{as}) experienced by the carbon dioxide diffusion current.

In the degenerate case $\eta = 0$ (the spheroid shrinks to a flat disk of radius R_c) we get $A_0/\pi R_c^2 = 2$ (the factor 2 stems from the fact, that even a degenerate, flat spheroid has *two* sides). $\eta = 1$ (the spheroid becomes a sphere of radius R_c) implies $A_1/\pi R_c^2 = 4$ (as was to be expected). For $\eta = 1/2$ (the spheroid's shorter axis length is $R_c/2$) we arrive at $A_{0.5}/\pi R_c^2 = 2.760$.

Values from the literature for the sizes of chloroplasts differ somewhat: Nultsch, 1996, gives as chloroplast diameter the range 4 μm – 8 μm and as chloroplast depth 2 μm – 3 μm. Moore et. al., 1998, give 5 μm – 10 μm and 3 μm – 4 μm, respectively. Calculating η from the averages over the minima and maxima of these intervals we arrive at $\eta = 3/7 = 0.429$, which implies $A_{0.429}/\pi R_c^2 = 2.606$.

(ii) The second factor contributing to (a_{chl}/a_{as}) is due to the fact that the (inner) surface of a cortex cell is only partially lined with chloroplasts. Following Parkhurst & Mott, 1990, we assume a value of 90 %.

Taking both factors into account the ratio is in the range $1.8 \leq (a_{chl}/a_{as}) \leq 3.6$, where the lower value represents a flat chloroplast and the higher value a sphere-shaped chloroplast. We shall use the value

$$(a_{chl}/a_{as}) = 2.3454 \tag{4.24}$$

as a consequence of the chloroplast sizes just cited from the literature.

5. Plant Material and Methods for Obtaining Relevant Anatomical Data

5.1 General Approach

The data we use have been obtained from ground sections of Rhynie Chert silifications which were prepared at the Institute of Geology and Palaeontology of the University of Münster. They were evaluated partially in Münster and partially in Tübingen.
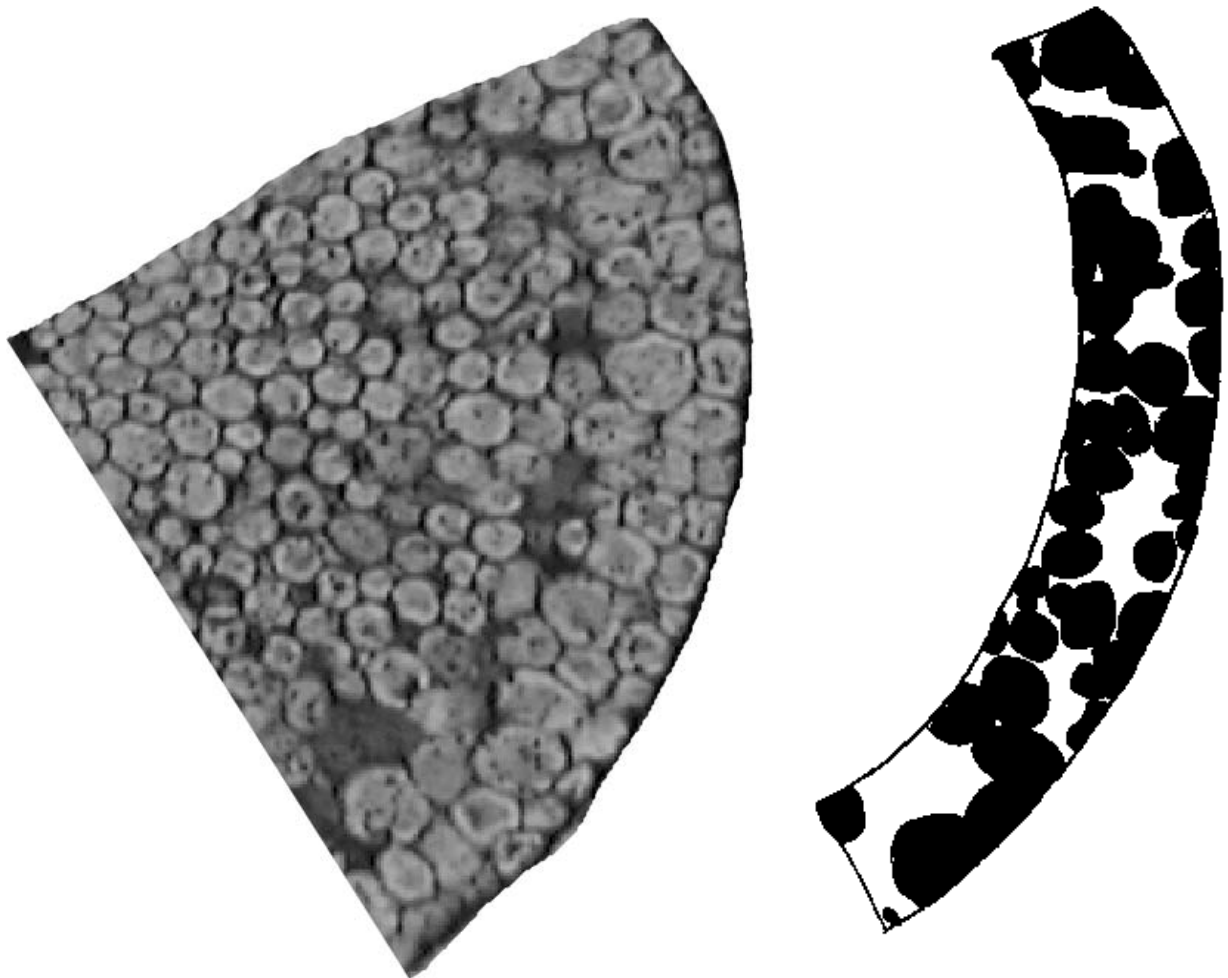
Figures 19 and 20: Left: A sector of a cross-section through *Aglaophyton*. The plane of the cross-section is perpendicular to the symmetry axis of the plant. The dark areas indicate intercellular airspaces, which are most extended in the assimilation layer. The distance from the apex to the circumference of the sector is approximately 1 mm.
Right: The cell/intercellular airspace pattern of the assimilation area of the same photograph. Cortex cells are black, intercellular airspaces are white.

Slices of chert 1 mm to 1.5 mm thick were produced on a diamond saw, glued to biological or geological standard microscope slides with thermoplastic cement (No. 70C Lakeside Brand), and then ground down by using silicon carbide powder. Thermoplastic mounted slices may be removed from the slides by reheating, transferred to a new slide and then turned over, so that both sides of

the slices may be ground down to the plane desired. The ultimate thickness of the slices depends on the nature of the material (50 μm to 100 μm for higher magnifications and several 100 μm for overviews, e.g. of epidermal patterns). They are viewed by transmitted or reflected light without a cover slip, but with a film of oil for all objectives.

Measurements of linear dimensions like the depth of stomatal pores, the length of their long and short axes, and similar quantities for the hypodermal layer were carried out either with an ocular micrometer or from photographs. The thicknesses of the layers were determined from photographs like the one in Figure 9 (in Section 2) or in Figure 19, which allow a clear identification of stomata, hypodermal channels, cells and intercellular airspaces.

Porosities were obtained by copying the cell/intercellular airspace pattern of the assimilation area from photographs as in Figure 19 onto transparent overlays. A typical result is depicted as Figure 20. These overlays were scanned and evaluated with the image processing software OPTIMAS, which determines the total area of the figure and the percentage of its black and white portions. The white areas in Figure 20 represent the intercellular airspaces. Therefore, in the case of Figure 19, the porosity n_{as} is given as the fraction of the white areas of the total area. The justification for this method was outlined in Section 4.4.

5.2 Numerical Values

The numerical values of the parameters which were calculated in a general way in Section 4 are listed in the Tables below. They include

(i) anatomical properties (Table 1),

(ii) environmental parameters (Table 2) and

(iii) biochemical and physiological parameters (Table 3).

The anatomical properties are derived from thin sections of fossilized specimen of *Aglaophyton major* and *Rhynia gwynne-vaughanii* (see Section 5.1).

The environmental parameters represent a Lower Devonian atmosphere as described in the literature (Berner, 1997), an arbitrary chosen atmospheric humidity and wind velocity and a typical value for the irradiance I for moderate latitudes.

In the case of the biochemical and physiological parameters, values from extant C$_3$ plants are applied (data compiled from Harley & Sharkey, 1991, Harley et al., 1992 and Wullschleger, 1993). The value for g_{liq} is from Parkhurst & Mott, 1990. The chosen parameters for V_{max} and J_{max} are at the lower range for modern plants (Wullschleger, 1993). Corresponding values can be found in, for example, fern leaves or conifer needles.

Two remarks concerning the photosynthetic parameters V_{max} and J_{max} and the irradiation I are appropriate:

(i) Values for V_{max} and J_{max} found in the literature cannot be used in our model without precaution, because we do *not* adopt the widespread convention to relate the fluxes V_{max} and

J_{max} to a (in our case particularly) fictitious "leaf area" far away from the chloroplasts, where the carbon dioxide molecules are actually processed. Although it is standard in the field of plant physiology, it is nonetheless a puzzling measure[12]. This is made worse by the fact, that by relating V_{max} and J_{max} to the leaf surface area these biochemical constants become intermingled with the anatomical ratio (A^{mes}/A) of the (total) surface of all mesophyll cells to the (total) leaf area. (In modern leaves, mesophyll cells are the equivalent of the outer cortex cells of rhyniophytic plants.)[13]. Thus, biochemical constants, which should not vary very much among species, get mixed up with the species-specific morphology. In our case this is especially unfortunate, because (i), (A^{mes}/A)-values for extant mesophytic plants, which are the principal source of (modern) data, differ considerably from the (A^{mes}/A)-values of rhyniophytic plants, and, (ii) we use photosynthetic data from extant conifer needles [14].

In order to make values from the literature applicable to rhyniophytic plants we redefine V_{max} and J_{max} according to the following "local" definition: a flux (or a current density) is (i), the number of particles, which cross a small surface element during a small temporal interval, divided by (ii), the area of the surface element they are actually crossing, and divided by (iii), the time interval which actually elapsed during their passage.

Now we connect the usual convention with this "local" definition: Consider a (total) current I_{tot} [mol/s] of molecules streaming into (or out of) the chloroplasts of one leaf under stationary conditions. A^{chl}, A^{mes} and A shall denote the total areas of all chloroplasts, of all mesophyll cells and of the total leaf surface (i.e. area of upper side of leaf plus area of lower side), respectively. If the corresponding fluxes — the symbol j stands for either V_{max} or J_{max} — are defined by

$$j_{chl} := \frac{I_{tot}}{A^{chl}} \qquad j_{mes} := \frac{I_{tot}}{A^{mes}} \qquad j := \frac{I_{tot}}{A} \qquad (5.2)$$

elimination of I_{tot} from (5.2) results in

---

[12] The usual convention is of course convenient for experimentalists performing measurements with plants showing foliage leaves. But from the viewpoint of a theorist, it is absurd. Consider a mid-european cookery-book, which makes extensive use of hen's eggs, but gives the number of hen's eggs used in the recipes not in numbers of hen's eggs but rather as fractions of ostrich eggs or multiples of colibri eggs. Even if the book provides an appendix with conversion tables between typical volumes and typical percentages of white and yellow of the three egg species, it is predictable that many dishes will end up as mathematical and culinary desasters.

[13] Still worse, some authors relate V_{max} and J_{max} to the "projected leaf area", which implies in the case of conifer needles that the specific shape of the needles, the details of the projection procedure and perhaps even contributions from statistics enter the values of V_{max} and J_{max}, too.

[14] In our model, the ratio (A^{mes}/A) is not explicitly used, it is rather hidden in other morphological parameters. If desired, it can be calculated from values in Table 1 via the equation

$$\frac{A^{mes}}{A} = \left(\frac{a_{as}}{v_{as}}\right)(1 - n_{as})\frac{r_1{}^2 - r_0{}^2}{2R} \qquad (5.1)$$

with the results $(A^{mes}/A) = 5.3$ (*Aglaophyton*) and $(A^{mes}/A) = 2.2$ (*Rhynia*).

$$j_{chl} A^{chl} = j_{mes} A^{mes} = jA \tag{5.3}$$

The desired relations between the "locally" defined flux j_{chl} and its "non-local" counterparts j_{mes} and j follow in an obvious way:

$$j_{chl} = j_{mes} \frac{A^{mes}}{A^{chl}} = j_{mes} \frac{A^{mes}}{A} \frac{A}{A^{chl}} = j \frac{A}{A^{chl}} = j \frac{A}{A^{mes}} \frac{A^{mes}}{A^{chl}} \tag{5.4}$$

Because the ratios (A^{chl}/A^{mes}) and (a_{chl}/a_{as}) (defined in Section 3.4.2) amount to the same value, we can write

$$j_{chl} = j \left(\frac{A}{A^{mes}} \right) \left(\frac{a_{as}}{a_{chl}} \right) \tag{5.5}$$

(a_{chl}/a_{as}) was calculated in Section 4.4. In order to obtain values for (A^{mes}/A) we carried out measurement of extant conifer needles. The result was $(A^{mes}/A) = 10$.

Now that the quantities in the parentheses of equation (5.5) are known, the local versions j_{chl} of the quantities V_{max} and J_{max} can be calculated from values in the literature by substituting V_{max} or J_{max} for j on the right hand side of equation (5.5).

(ii) The ultimate energy source for assimilation is provided by the electro-magnetic radiation of the sun. The value of the solar constant $S_\odot$ — the radiation energy per time and area arriving just outside the earth's atmosphere — is

$$S_\odot = 1360 \ \frac{W}{m^2} \tag{5.6}$$

The value of the irradiation I at the assimilation site is quite different from $S_\odot$, due to several reasons:

— According to Larcher, 1994, about 19 % of $S_\odot$ are absorbed in the Stratosphere and the Troposphere (and converted into heat).

— Further 26 % of $S_\odot$ are reflected back into space because radiation is scattered by "air molecules", clouds and mist.

— Thus, 55 % of $S_\odot$ arrive at the surface of the earth. On a global average, 30 % of $S_\odot$ reach the earth unscattered. Contributions to diffuse light are due to Rayleigh scattering by "air molecules" (10 % of $S_\odot$), and to Mie scattering by clouds or mist (15 % of $S_\odot$)[15].

---

[15] Photons travelling through air are scattered chiefly by "air molecules" (Rayleigh scattering) and by bigger objects like water drops in clouds or aerosol (Mie scattering) (see, for example, Roedel, 1994). Rayleigh scattering depends strongly on the wave length λ of the incident light. The light intensity scattered away is proportional to $1/\lambda^4$, which means that even if the sun is at zenit (i.e. noon at the equator) only 76 % of the violet photons ($\lambda = 410$ nm) but 96 % of the red photons ($\lambda = 650$ nm) incident from the sun reach sea level unscattered. At sunrise (or sunset) these percentages shift

It should be noted, that these percentages are valid only on a global scale. Locally, they are apt to wide variations, depending on local weather conditions and air pollution.

— The hitherto given radiation rates encompass the entire electro-magnetic spectrum. Photosynthesis, however, uses only radiation with wavelengths in the range 380 nm $\leq \lambda \leq$ 710 nm. On an average, 45 % – 50 % of the radiation from the sun fall into that range. Here, we use the value 45 %.

— Thus, if the sun is in the zenit (i.e. vertically above a horizontally oriented area on the surface of the earth), the photosynthetically active radiation impinging on this area consists of a term $I_{\oplus}^{direct}$, describing the direct (unscattered) radiation, and of a term $I_{\oplus}^{diffuse}$, describing the diffuse radiation, which has been scattered by air molecules, clouds and mist and was not reflected back into space:

$$I_{\oplus}^{direct} = 0.2454\, S_{\odot} = 334\ \frac{\text{W}}{\text{m}^2} \triangleq 1502\ \frac{\mu\text{mol}}{\text{m}^2\text{s}} \tag{5.7}$$

$$I_{\oplus}^{diffuse} = 0.2045\, S_{\odot} = 278\ \frac{\text{W}}{\text{m}^2} \triangleq 1251\ \frac{\mu\text{mol}}{\text{m}^2\text{s}} \tag{5.8}$$

where we have used the relation 1 W/m$^2 \triangleq 4.5\ \mu$mol/m^{2}s to convert radiation energy to number of photons[16].

— Due to their axially symmetric shape rhyniophytic plants can exploit radiation coming from the sun only partially. The plant tissue of an upright standing telome of radius R and length (i.e. height) L absorbs all photons which impinge on the rectangle resulting from projecting the telome onto a plane situated perpendicular to the direction of the incoming light rays. If the sun is elevated above the horizon by an angle Θ, the area of this rectangle is given by $2R \times L \times \cos\Theta$. Therefore, the number of unscattered photons which are absorbed per unit time by the whole telome is $2R\, L \cos\Theta \times I_{\oplus}^{direct}$.

The rate of photons which were originally (i.e. outside the atmosphere) directed onto the telome but became scattered away from their straight path while traversing the atmosphere

---

to 0.0065 % (violet photons) and 21 % (red photons). Reflecting upon these ratios for a moment, it should become clear, that the blueness of the sky, the redness of the sunset, the waneness of the winter sun, and the ease of sunburning at midday in summer are all consequences of the $1/\lambda^4$ dependance of Rayleigh scattering in the atmosphere (Jackson, 1975).

Mie scattering is proportional only to $1/\lambda$. Nonetheless, in clear weather, it extracts about the same percentage of blue photons from incident light as Rayleigh scattering, but high humidity or clouds increase the amount of diffuse light considerably.

[16] This conversion is necessarily an approximate one, since it depends on the energy distribution among the photons, which form the radiation. For photons of a fixed wavelength (i.e. fixed energy) the following relations hold:

1 mol photons $\triangleq 1.8 \times 10^5$ J (for red photons, $\lambda = 650$ nm)

1 mol photons $\triangleq 2.7 \times 10^5$ J (for violet photons, $\lambda = 450$ nm)

The value 1 W/m$^2 \triangleq 4.5\ \mu$mol/m^{2}s is obtained by taking the (unweighted) average over red and violet photons.

is given by $2R\,L\cos\Theta \times I_{\oplus}^{diffuse}$. Since they represent, by assumption, diffuse light, we have to distribute them uniformly onto the entire telome surface area $2\pi R\,L$. The result is

$$I_{\Theta}^{diffuse} := \frac{2R\,L\cos\Theta}{2\pi R\,L}\,I_{\oplus}^{diffuse} = \frac{\cos\Theta}{\pi}\,I_{\oplus}^{diffuse} = \cos\Theta \times 398\,\frac{\mu\mathrm{mol}}{\mathrm{m^2s}} \qquad (5.9)$$

Note, that at noon local time the angle Θ is connected with the geographic latitude B of a location via $\Theta = 90^{\circ} - B$.

— A correct desription of the situation ought to take into account that the irradiance is constant (and equal to $I_{\Theta}^{diffuse}$) on the shadow side of a telome, but varies on the sunny side of the telome according to $I_{\Theta}^{diffuse} + I_{\oplus}^{direct}\sin\varphi$. ($\varphi$ denotes the angle between (i) the plane spanned by the telome axis and the straight line connecting the sun and any point on the telome axis, and (ii) the plane spanned by the telome axis and one of the terminators on the telome surface. The terminators lie at $\varphi = 0^{\circ}$ and $\varphi = 180^{\circ}$, the brightest (vertical) line on the telome surface lies at $\varphi = 90^{\circ}$.) Driving accuracy that far would complicate computations considerably, since it would be tempting to include also effects such as the movement of chloroplasts in response to varying levels and wavelenghts of the incident light. (Chloroplasts seem to distribute themselves uniformly across the (inner) surface of a mesophyll cell, if the incident light is not too intensive. In intense light, however, they lump together at the bright end of the mesophyll cells. See Augustynowicz & Gabrys̀, 1999.)

Therefore, and because the cited ratio between direct and diffuse irradiation is valid only on a global scale (global in a spatial and temporal sense), we ignore these effects and proceed with the averaging process one step further. That is, we distribute also the unscattered component $I_{\oplus}^{direct}$ of the impinging light evenly onto the telome surface. The result is similar to the one derived for the diffuse light

$$I_{\Theta}^{direct} := \frac{2R\,L\cos\Theta}{2\pi R\,L}\,I_{\oplus}^{direct} = \frac{\cos\Theta}{\pi}\,I_{\oplus}^{direct} = \cos\Theta \times 478\,\frac{\mu\mathrm{mol}}{\mathrm{m^2s}} \qquad (5.10)$$

It should be noted, that the averaging procedure for $I_{\oplus}^{direct}$ leads to erraneous results even without the effect of chloroplast movement, because assimilation depends either not at all (if limited by Rubisco activity, equation (3.34)) or in a non-linear manner (if limited by electron transport, equations (3.35) and (3.36)) on the irradiance. Consider a situation in which the chloroplasts on the sunny side of the telome act in saturated photosynthesis mode, while their counterparts on the shadow side are idle. The combined assimilation rate of all chloroplasts in this situation will, in general, be different from the total assimilation rate of all chloroplasts of the whole telome, if they act under an averaged irradiance and are photosynthesizing in linear mode.

— Combining equations (5.9) and (5.10) we arrive at

$$I_\Theta := I_\Theta^{direct} + I_\Theta^{diffuse} = \frac{\cos\Theta}{\pi}\,(I_\oplus^{direct} + I_\oplus^{diffuse}) = \cos\Theta \times 877 \,\frac{\mu\text{mol}}{\text{m}^2\text{s}} \qquad (5.11)$$

for the total (and averaged) amount of photosynthetically active radiation incident on the surface of a telome. For a location at a geographic latitude $B = 45°$ values for $I_\Theta(\Theta)$ vary between sunrise and noon from $I_\Theta(\Theta = 0°) = 877\ \mu\text{mol/m}^2\text{s}$ to $I_\Theta(\Theta = 45°) = 620\ \mu\text{mol/m}^2\text{s}$.

Our ultimate goal is to obtain an expression for the irradiance I at the assimilating site. The calculation of this quantity follows the same reasoning which led to (5.5). The substitutions

$$j_{chl} \leftrightarrow I \qquad \text{and} \qquad j \leftrightarrow I_\Theta \qquad (5.12)$$

equation (5.1) and equation (5.11) lead to

$$I = \left(\frac{a_{as}}{a_{chl}}\right)\left(\frac{v_{as}}{a_{as}}\right)\frac{1}{1 - n_{as}}\frac{2\,R}{r_1{}^2 - r_0{}^2}\,I_\Theta$$

$$= \left(\frac{a_{as}}{a_{chl}}\right)\left(\frac{v_{as}}{a_{as}}\right)\frac{1}{1 - n_{as}}\frac{2\,R}{r_1{}^2 - r_0{}^2}\frac{\cos\Theta}{\pi}\,(I_\oplus^{direct} + I_\oplus^{diffuse}) \qquad (5.13)$$

On substitution of the values from Tables 1, 2 and 3 we obtain from equation (5.13) for the irradiance I at the assimilating site

$$I_{Aglaophyton} = 49.82\,\frac{\mu\text{mol}}{\text{m}^2\text{s}} \qquad (5.14)$$

and

$$I_{Rhynia} = 122.47\,\frac{\mu\text{mol}}{\text{m}^2\text{s}} \qquad (5.15)$$

The difference in the numerical values stems from the factor $2\,R/(r_1{}^2 - r_0{}^2)$.

Table 1 — Anatomical Properties :

Boundary layer:

Parameter	Aglaophyton	Rhynia	Units	Description
r_3	2.685×10^{-3}	1.29×10^{-3}	m	Outer edge of boundary layer
d_{bl}	0.435×10^{-3}	0.29×10^{-3}	m	Thickness of boundary layer
n_{bl}	1	1	–	Porosity of boundary layer
τ_{bl}	1	1	–	Tortuosity of boundary layer
$n_{bl}/\tau_{bl}{}^2$	1	1	–	Effective Conductance of boundary layer

Stomatal layer:

Parameter	Aglaophyton	Rhynia	Units	Description
R	2.25×10^{-3}	1.0×10^{-3}	m	Radius of plant
d_{st}	0.03×10^{-3}	0.015×10^{-3}	m	Depth of stomatal pore
h_{st}	0.039×10^{-3}	0.029×10^{-3}	m	Long axis of cross section of stoma
w_{st}	0.0105×10^{-3}	0.010×10^{-3}	m	Short axis of cross section of stoma
a_{st}	3.216×10^{-10}	2.277×10^{-10}	m^2	Surface area of stomatal pore
ν_{st}	1.0×10^6	1.75×10^6	m^{-2}	Number density of stomata
n_{st}	0.32×10^{-3}	0.399×10^{-3}	–	Porosity of stomatal layer
τ_{st}	1.34	1.57	–	Tortuosity of stomatal layer
$n_{st}/\tau_{st}{}^2$	0.18×10^{-3}	0.16×10^{-3}	–	Effective conductance of stomatal layer

Hypodermal layer:

Parameter	Aglaophyton	Rhynia	Units	Description
r_2	2.22×10^{-3}	0.985×10^{-3}	m	Outer edge of hypodermal layer
d_{hy}	0.075×10^{-3}	0.105×10^{-3}	m	Thickness of hypodermal layer
h_{hy}	0.04×10^{-3}	0.03×10^{-3}	m	Long axis of cross section of hypodermal channel
w_{hy}	0.03×10^{-3}	0.02×10^{-3}	m	Short axis of cross section of hypodermal channel
a_{hy}	9.42×10^{-10}	4.71×10^{-10}	m^2	Area of cross section of hypodermal channel
n_{hy}	0.96×10^{-3}	0.87×10^{-3}	–	Porosity of hypodermal layer
τ_{hy}	1	1	–	Tortuosity of hypodermal layer
$n_{hy}/\tau_{hy}{}^2$	0.96×10^{-3}	0.87×10^{-3}	–	Effective conductance of hypodermal layer

Assimilation layer:

Parameter	Aglaophyton	Rhynia	Units	Description
r_1	2.145×10^{-3}	0.88×10^{-3}	m	Outer edge of assimilation layer
d_{as}	0.25×10^{-3}	0.10×10^{-3}	m	Thickness of assimilation layer
r_0	1.895×10^{-3}	0.78×10^{-3}	m	Inner edge of assimilation layer
σ	55×10^{-6}	50×10^{-6}	m	Radius of a cortex cell

(a_{as}/v_{as})	36364	40000	m^{-1}	Specific surface of a cortex cell
(a_{chl}/a_{as})	2.345	2.345	–	Sum of surfaces of all chloroplasts within a cortex cell over surface of one cortex cell
g_{liq}	0.5×10^{-3}	0.5×10^{-3}	mmol m^{-2} s^{-1}Pa^{-1}	Liquid phase conductance for carbon dioxide in water from cell wall to chloroplast
n_{as}	0.35	0.35	–	Porosity of assimilation layer
τ_{as}	1.571	1.571	–	Tortuosity of assimilation layer
$n_{as}/\tau_{as}{}^2$	0.142	0.142	–	Effective conductance of assimilation layer

Table 2 — Environmental Parameters :

Parameter	Value	Units	Description
$C_{atm}^{CO_2}$	168	mmol m^{-3}	Atmospheric carbon dioxide concentration during Lower Devonian
$C_{atm}^{CO_2}$	14	mmol m^{-3}	Atmospheric carbon dioxide concentration of today
$C_{atm}^{H_2O}$	480	mmol m^{-3}	Atmospheric water vapour concentration (equivalent to a relative humidity of 50 %)
$C_{sat}^{H_2O}$	960.3	mmol m^{-3}	Saturation value of water vapour at 20° C and 1 atm
T	20	°C	Temperature
R_{gas}	8.3143×10^{-3}	m^3 Pa mmol^{-1} (°K)$^{-1}$	Gas constant
V_l^m	1.805×10^{-8}	m^3 mmol^{-1}	Molar volume of water at 20° C
γ	0.0728	Pa m	Surface tension of water at 20° C
v_{atm}	0.8	m s^{-1}	Atmospheric wind velocity
D_{CO_2}	1.51×10^{-5}	m^2 s^{-1}	Diffusion constant of carbon dioxide in air at 20° C
D_{H_2O}	2.42×10^{-5}	m^2 s^{-1}	Diffusion constant of water vapour in air at 20° C
$I_{Aglaophyton}$	49.82×10^{-3}	mmol m^{-2} s^{-1}	Irradiance at assimilation site
I_{Rhynia}	122.47×10^{-3}	mmol m^{-2} s^{-1}	Irradiance at assimilation site
Θ	45°	–	Angular elevation of sun above horizon

Table 3 — Biochemical and Physiological Parameters :

Parameter	Value	Units	Description
p_o	20260	Pa	Partial pressure of oxygen at chloroplasts
τ	2822	–	Specificity factor for Rubisco
V_{max}	0.512×10^{-3}	mmol m^{-2} s^{-1}	Local maximum carboxylation rate
K_c	63.6	Pa	Michaelis-Menten constant for carboxylation
K_o	34825	Pa	Michaelis-Menten constant for oxygenation
J	——	mmol m^{-2} s^{-1}	Potential rate of electron transport
J_{max}	1.364×10^{-3}	mmol m^{-2} s^{-1}	Light-saturated rate of electron transport
α	0.2	–	Efficiency of light conversion

6. Results

The most direct results of our calculations are the solutions (3.72) and (3.73) of the differential equation (3.71) and of Fick's first law (3.1) — the local concentrations of carbon dioxide and of water vapour, and the corresponding fluxes.

Most interesting for application in fields as plant physiology, ecophysiology or climatology are the assimilation rate $j^{CO_2}(R)$ and the transpiration rate $j^{H_2O}(R)$, and especially the dependance of these rates from the variables, which "define" the plant and its environment. These can be grouped into three categories:

(i) Five variables defining the environmental conditions, i.e. the atmospheric carbon dioxide and water vapour concentrations $C_{atm}^{CO_2}$ and $C_{atm}^{H_2O}$, the atmospheric wind velocity v_{atm}, the irradiance I of photosynthetic active electromagnetic radiation and the temperature T[17].

(ii) Twenty variables defining the plant anatomy, i.e. the axis radius R, the thicknesses d_{st}, d_{hy} and d_{as} of the various layers[18], the porosities d_{bl}, d_{st}, d_{hy} and d_{as} and the tortuosities n_{bl}, n_{st}, n_{hy} and n_{as}, the number density of stomata ν_{st}, the long and short axes of the cross sections of the stomata and the hypodermal channels h_{st}, h_{hy}, w_{st} and w_{hy}, respectively, the radius of a cortex cell σ, the sum of surfaces of all chloroplasts within a cortex cell over the surface of one cortex cell (a_{chl}/a_{as}) and the liquid phase conductance for carbon dioxide in water from cell wall to chloroplast g_{liq}.

(iii) Eight variables describing the physiological and biochemical behaviour, i.e. the partial pressure of oxygen at chloroplasts p_o, the specificity factor for Rubisco τ, the local maximum carboxylation rate V_{max}, the light-saturated rate of electron transport J_{max}, the Michaelis-Menten constants for carboxylation K_c and for oxygenation K_o, the potential rate of electron transport J and the efficiency of light conversion α.

The most straightforward (and most reliable) approach to investigate the behaviour of the assimilation and transpiration rates under variation of the 33 variables[19] cited in (i), (ii) and (iii), would be to write down $j^{CO_2}(R)$ and $j^{H_2O}(R)$ as functions of these variables and to determine their extrema,

---

[17] Although the temperature T emerges in various formulas, in its present state, our model does *not* simulate a true temperature dependance, because

— "constants" like the diffusion constants, the Michaelis-Menten constants or the molar volume of water are in reality — but not in the framework of our model — functions of T. They are, at least as fitted curves, available from the literature,

— a worthwhile extension of the model should incorporate the temperature not only as an "external parameter", but as a "dynamic variable". This is a necessary prerequisite for a realistic description of thermodynamic feedback effects like transpiration. (Transpiration rate is a function of plant temperature, plant temperature is influenced by the amount of heat needed for transpiration, etc..)

[18] Note that d_{bl} is not an independent parameter, it is rather a function of the atmospheric wind velocity v_{atm}.

[19] To be more precise, the assimilation rate depends only on 32 variables (not on $C_{atm}^{H_2O}$), the transpiration rate merely on 17 of the 33 variables mentioned, chiefly because it is not involved in photosynthesis.

their singularities and their asymptotic behaviour. This is in principle possible, but fails in practice due to the sheer length of the expressions.

The second best route to results would consist in displaying the 33 independent variables plus the dependant variable (i.e. the assimilation rate or the transpiration rate) in a 34-dimensional space by assigning one coordinate axis to each variable. Thus, the functional dependance of the dependant variable would be illustrated as a (hyper-)surface in that space. Note, that this approach would encompass not only *Aglaophyton* and *Rhynia* and their environment in a single picture. It would even comprise *every* combination of plant and environment, which can be "defined" by the admissable ranges of the numerical values of the 33 variables[20].

Unfortunately, human visual perception is restricted to three dimensions. Therefore, we resort to displaying the assimilation and transpiration rates as functions of only one or two independent variables, while assigning the remaining variables the numerical values appropriate for *Aglaophyton* or *Rhynia*. This means, that we explore the 33-dimensional neighbourhood of *Aglaophyton* and *Rhynia* in digestable two- or three-dimensional bites. This proceeding, however, has a drawback: Varying only one or two variables while fixing all others, is like exploring the sea from a small island, with the restriction that one may move only either along the meridian or along the parallel of the latitude on which the island is located. Choosing, for instance, the island of Madeira as a basis for such an exploration, the continent of Europe would go undetected. Of course it is possible, to refine the "exploration mesh" by defining hypothetical islands (or plants) and to explore their neighbourhood as well. But the basic problem remains, to condense the wealth of information provided by our model into a conceivable form without unwittingly throwing away the most interesting messages.

Because the principal goal of this thesis is the construction of the model presented, we restrict the presentation of results to some examples, which illustrate its possibilities, rather than giving the rhyniophytic plants a systematic and full 34-dimensional treatment. Reluctantly obeying some regulations on the form of the thesis which are beyond scientific comprehension, we give first a somewhat bare skeleton of results. The discussion of the results is postponed to the next section.

---

[20] For a similar approach to treating the shells of gastropods, coiled cephalopods, bivalves and brachiopods on a common footing, see the section on Theoretical Morphology in Raup & Stanley, 1978.

6.1 Local Fluxes and Local Concentrations of Carbon Dioxide and Water Vapour

By using the values given in Tables 1, 2 and 3 the following results shown in the Figures 21, 22, 23 and 24 concerning the local concentrations and fluxes of water vapour and carbon dioxide are obtained.
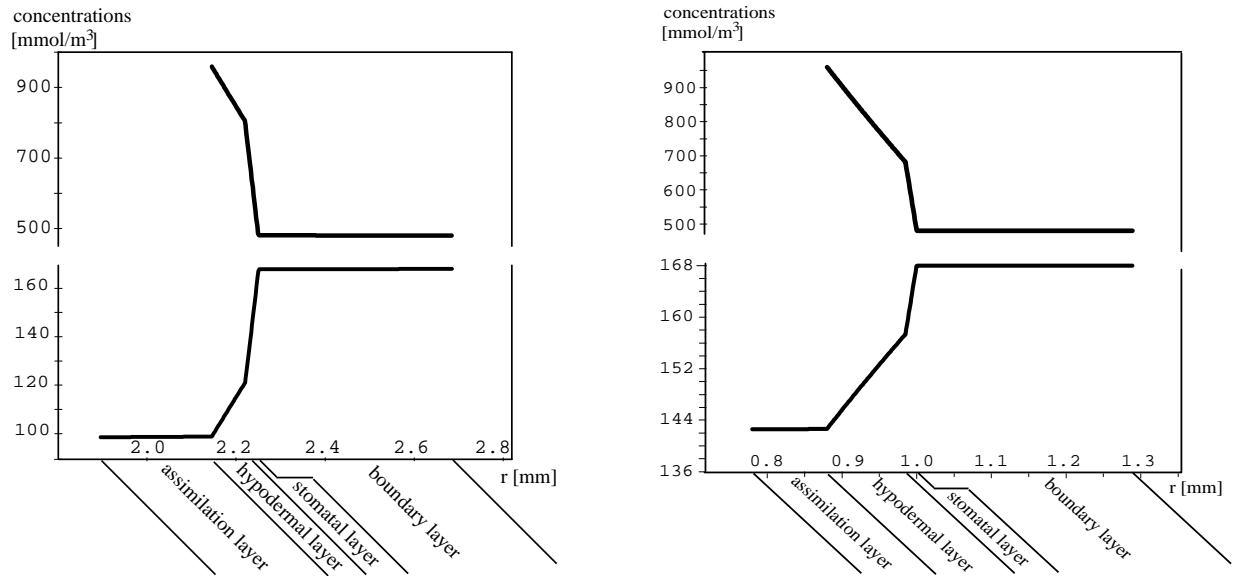
Figures 21 and 22: Water vapour and carbon dioxide concentrations of *Aglaophyton* (left) and *Rhynia* (right) as a function of *r*. Water vapour concentrations (upper curves) and carbon dioxide concentrations (lower curves) are not to the same scale.
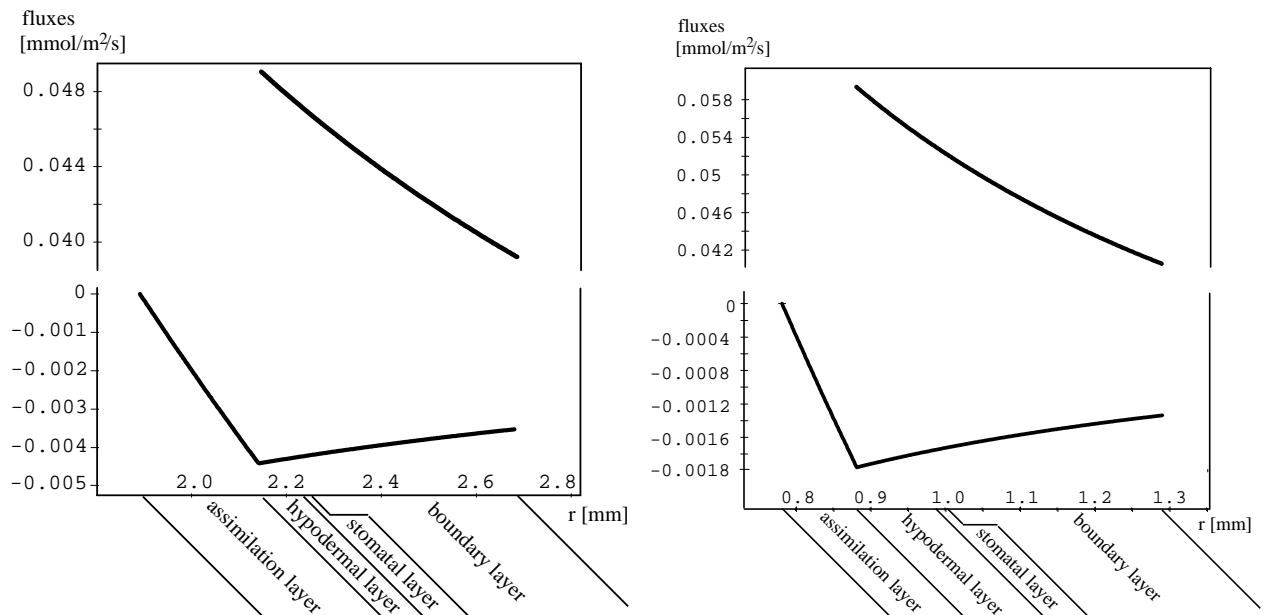
Figures 23 and 24: Water vapour and carbon dioxide fluxes inside *Aglaophyton* (left) and *Rhynia* (right) as a function of *r*. Water vapour fluxes (upper curves) and carbon dioxide fluxes (lower curves) are not at the same scale. Carbon dioxide fluxes have a negative sign, as carbon dioxide flows *into* the plant.

6.2 Transpiration and Assimilation Rates and their Dependance on Environmental Conditions
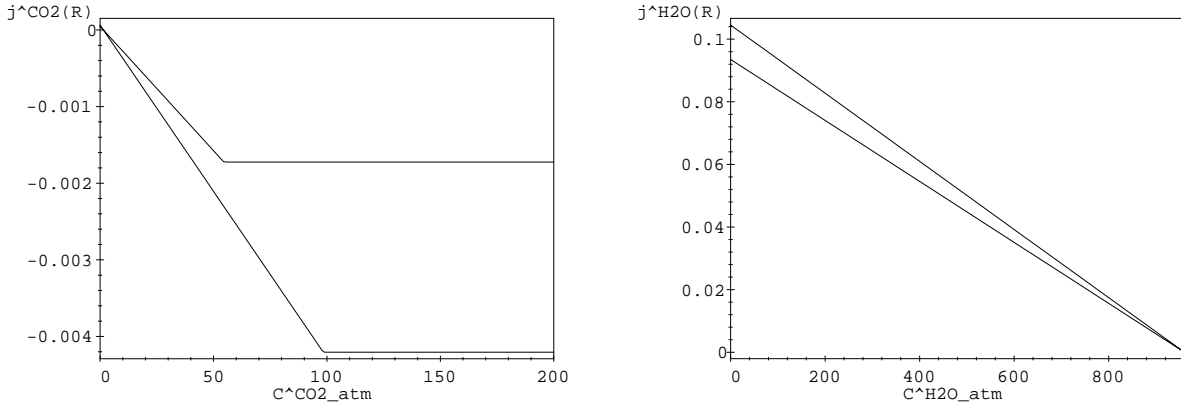
Figures 25 and 26: Left: Carbon dioxide fluxes at the surface of *Aglaophyton* (lower curve) and of *Rhynia* (upper curve) as a function of the atmospheric carbon dioxide concentration $C_{atm}^{CO_2}$. Note that the Lower Devonian value $C_{atm}^{CO_2} = 168$ mmol/m^3 lies in the "saturated" regions of both curves, whereas the value of today, $C_{atm}^{CO_2} = 14$ mmol/m^3, is to be found in their "linear" regions. Carbon dioxide fluxes have a negative sign, as carbon dioxide flows *into* the plant.
Right: Water vapour fluxes at the surface of *Aglaophyton* (lower curve) and of *Rhynia* (upper curve) as a function of the atmospheric water vapour concentration $C_{atm}^{H_2O}$. $C_{atm}^{H_2O} = 960$ mmol/m^3 corresponds to a relative humidity of 100 % at a temperature of 20 °C.
Concentrations are given in units of mmol/m^3, fluxes in mmol/m^2/s.
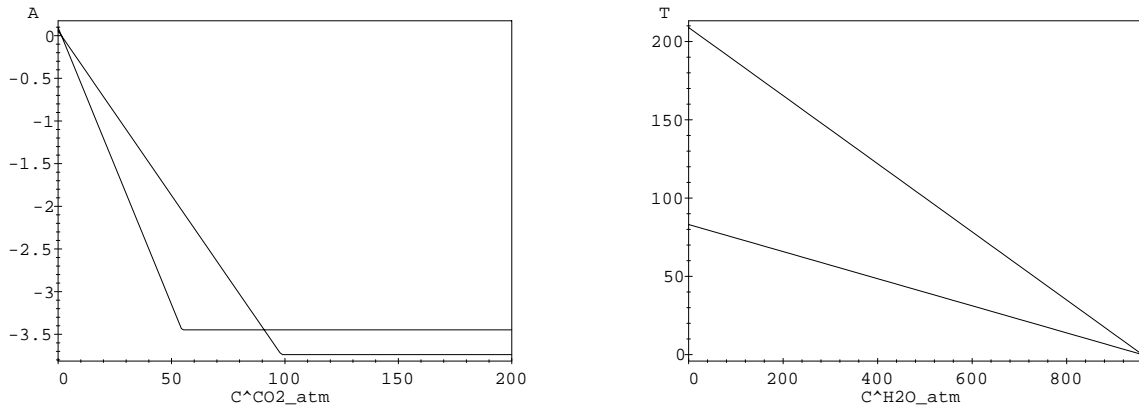
Figures 27 and 28: Left: Assimilation rate per plant volume of *Aglaophyton* (lower curve) and of *Rhynia* (upper curve) as a function of the atmospheric carbon dioxide concentration $C_{atm}^{CO_2}$.
The Lower Devonian value $C_{atm}^{CO_2} = 168$ mmol/m^3 lies in the "saturated" regions of both curves, today's value $C_{atm}^{CO_2} = 14$ mmol/m^3 in their "linear" regions. Assimilation rates have a negative sign, as carbon dioxide flows *into* the plant.
Right: Transpiration rate per plant volume of *Aglaophyton* (lower curve) and of *Rhynia* (upper curve) as a function of the atmospheric water vapour concentration $C_{atm}^{H_2O}$. $C_{atm}^{H_2O} = 960$ mmol/m^3 corresponds to a relative humidity of 100 % at a temperature of 20 °C.
Concentrations are given in units of mmol/m^3, assimilation and transpiration rates per plant volume in mmol/m^2/s.

Figure 29 shows the dependance of the assimilation rate $j^{CO_2}(R)$ on the irradiance I for *Aglaophyton* and *Rhynia*, respectively.
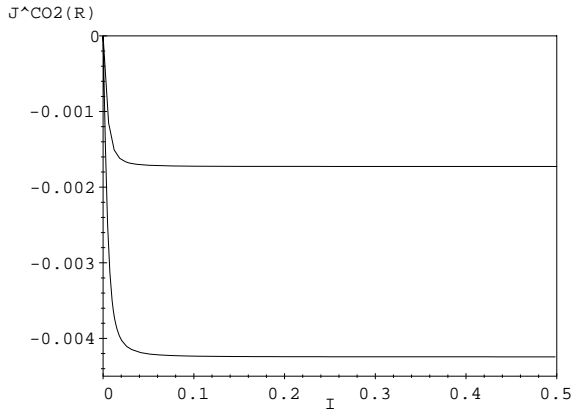
J^CO2(R)

Figure 29: Assimilation rates $j^{CO_2}(R)$ of *Aglaophyton* (lower curve) and *Rhynia* (upper curve) as a function of the irradiance I. The values of I used in the model are $I = 0.050$ mmol/m^2/s (*Aglaophyton*) and $I = 0.122$ mmol/m^2/s (*Rhynia*). $j^{CO_2}(R)$ and I are in units of mmol/m^2/s. (mmol CO_2-molecules in the former and mmol photons in the latter case.) Assimilation rates have a negative sign, as carbon dioxide flows *into* the plant.

6.3 The Water Use Efficiency and its Dependance on Atmospheric Conditions

The water use efficiency (WUE) is defined by

$$\text{WUE} := \frac{\text{number of CO}_2 \text{ molecules fixed per time}}{\text{number of H}_2\text{O molecules transpired per time}} = \frac{|\mathcal{A}|}{\mathcal{T}} = \frac{|j^{\text{CO}_2}(R)|}{j^{\text{H}_2\text{O}}(R)} \qquad (6.1)$$

With the numerical values of Tables 1, 2 and 3 we obtain

$$\text{WUE}_{Aglaophyton} = 0.0899 \approx 45 \times \text{WUE}_{\text{extant}} \qquad (6.2)$$

$$\text{WUE}_{Rhynia} = 0.0329 \approx 16 \times \text{WUE}_{\text{extant}} \qquad (6.3)$$

where $\text{WUE}_{\text{extant}} = 0.0020$ is a typical average value for extant C_3 plants (see, for example, Kramer, 1983).
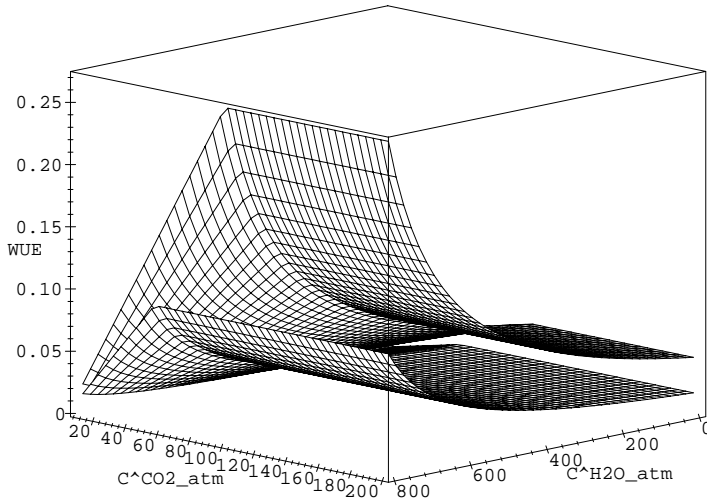
Figure 30: Water use efficiency WUE of *Aglaophyton* (upper surface) and *Rhynia* (lower surface) as a function of the atmospheric carbon dioxide $C_{atm}^{\text{CO}_2}$ and water vapour $C_{atm}^{\text{H}_2\text{O}}$ concentrations. Concentrations are given in units of mmol/m^3. In the scale of the figure, the plane $\text{WUE}_{\text{extant}} = 0.0020$ is identical to the bottom of the cube.
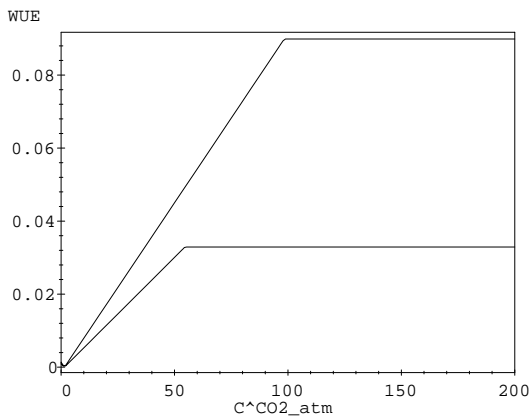
Figure 31: Water use efficiency WUE of *Aglaophyton* (upper curve) and *Rhynia* (lower curve) as a function of the atmospheric carbon dioxide concentration $C_{atm}^{\text{CO}_2}$ at a water vapour concentration of $C_{atm}^{\text{H}_2\text{O}} = 480$ mmol/m^3 (equivalent to a relative humidity of 50 %). Concentrations are given in units of mmol/m^3. During the Lower Devonian, the atmospheric carbon dioxide concentration amounted to about 168 mmol/m^3, nowadays it has the value 14 mmol/m^3.

Figure 30 displays the water use efficiency as a function of the atmospheric carbon dioxide and of the water vapour concentrations. Figure 31 is a (vertical) section through Figure 30 at a water vapour concentration $C_{atm}^{\text{H}_2\text{O}} = 480$ mmol/m^3 (equivalent to a relative humidity of 50 %).

6.4 Dependance of Water Use Efficiency, Transpiration and Assimilation Rates on Plant Anatomy

Figure 32 displays the water use efficiency of *Aglaophyton* (upper surface) and *Rhynia* (lower surface) as a function of the stomatal density ν_{st} and the thickness d_{hy} of the hypodermal layer.

Figures 33 and 34 show carbon dioxide fluxes $j^{CO_2}(R)$ and the water vapour fluxes $j^{H_2O}(R)$ at the surface of *Aglaophyton* (lower surface) and of *Rhynia* (upper surface), respectively, as a function of the stomatal density ν_{st} and the thickness d_{hy} of the hypodermal layer.

Figure 35 is the counterpart of Figure 33 for the recent atmospheric carbon dioxide content.
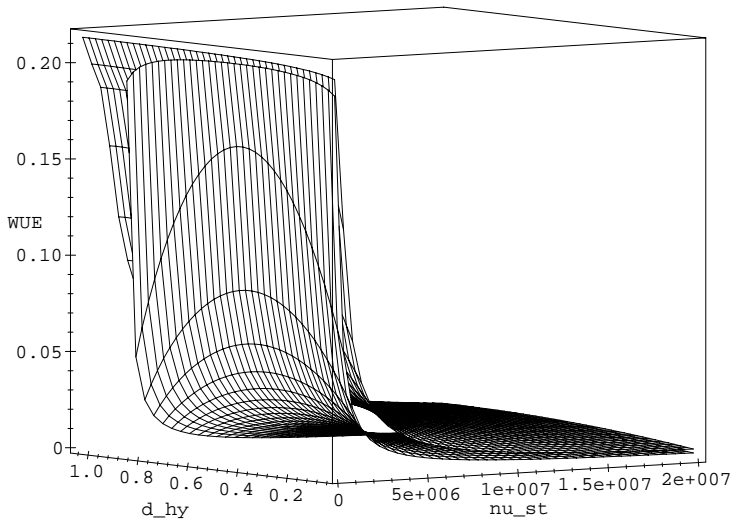
Figure 32: Water use efficiency (WUE) of *Aglaophyton* (upper surface) and *Rhynia* (lower surface) as a function of the stomatal density ν_{st} and the thickness d_{hy} of the hypodermal layer. The stomatal density is given in $1/m^2$, the thickness of the hypodermal layer in mm. *Aglaophyton*'s actual position in the (ν_{st}, d_{hy})-plane is at $(\nu_{st}, d_{hy}) = (10^6/m^2, 0.075\,mm)$ *Rhynia*'s position is at $(\nu_{st}, d_{hy}) = (1.75 \times 10^6/m^2, 0.105\,mm)$
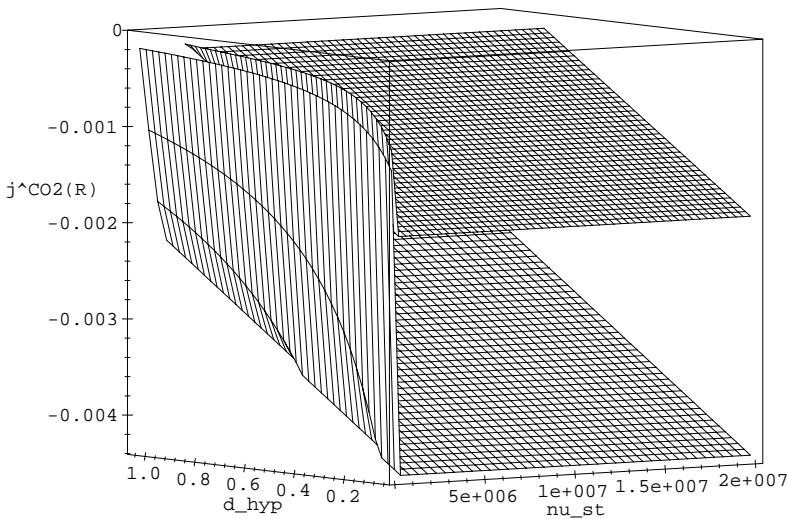
Figure 33: Carbon dioxide fluxes $j^{CO_2}(R)$ at the surface of *Aglaophyton* (lower surface) and of *Rhynia* (upper surface) as a function of the stomatal density ν_{st} and the thickness d_{hy} of the hypodermal layer. The stomatal density is given in $1/m^2$, the thickness of the hypodermal layer in mm. $j^{CO_2}(R)$ has units mmol/m^3. *Aglaophyton*'s actual position in the (ν_{st}, d_{hy})-plane is at $(\nu_{st}, d_{hy}) = (10^6/m^2, 0.075\,mm)$ *Rhynia*'s position is at $(\nu_{st}, d_{hy}) = (1.75 \times 10^6/m^2, 0.105\,mm)$ Note, that carbon dioxide fluxes have a negative sign.
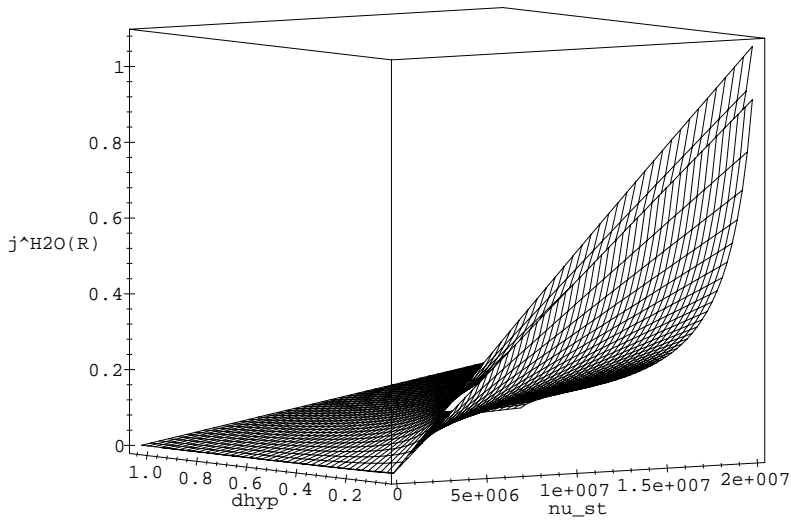
Figure 34: Water vapour fluxes $j^{\mathrm{H_2O}}(R)$ at the surface of *Aglaophyton* (lower surface) and of *Rhynia* (upper surface) as a function of the stomatal density ν_{st} and the thickness d_{hy} of the hypodermal layer. The stomatal density is given in $1/\mathrm{m}^2$, the thickness of the hypodermal layer in mm. $j^{\mathrm{H_2O}}(R)$ has units $\mathrm{mmol/m}^3$. *Aglaophyton*'s actual position in the (ν_{st}, d_{hy})-plane is at $(\nu_{st}, d_{hy}) = (10^6/\mathrm{m}^2, 0.075\,\mathrm{mm})$ *Rhynia*'s position is at $(\nu_{st}, d_{hy}) = (1.75 \times 10^6/\mathrm{m}^2, 0.105\,\mathrm{mm})$
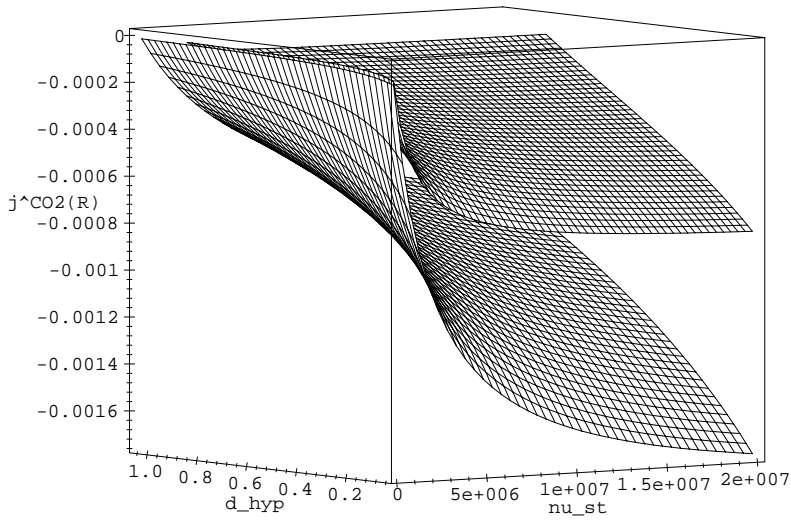
Figure 35: Carbon dioxide fluxes $j^{\mathrm{CO_2}}(R)$ at the surface of *Aglaophyton* (lower surface) and of *Rhynia* (upper surface) in today's atmosphere with $C_{atm}^{\mathrm{CO_2}} = 14$ $\mathrm{mmol/m}^3$. $j^{\mathrm{CO_2}}(R)$ is — as in Figure 33 — a function of the stomatal density ν_{st} and the thickness d_{hy} of the hypodermal layer. Values of all other parameters are as in Figure 33.

Figures 36 and 37 display the assimilation rate $j^{CO_2}(R)$ and the relative carbon dioxide concentration $C^{CO_2}(r_0)/C^{CO_2}_{atm}$ at the inner edge of the assimilation layer, respectively, as functions of the ratio (a_{chl}/a_{as}). (a_{chl}/a_{as}) denotes the sum of the surfaces of all chloroplasts within a cortex cell divided by the surface of one cortex cell.
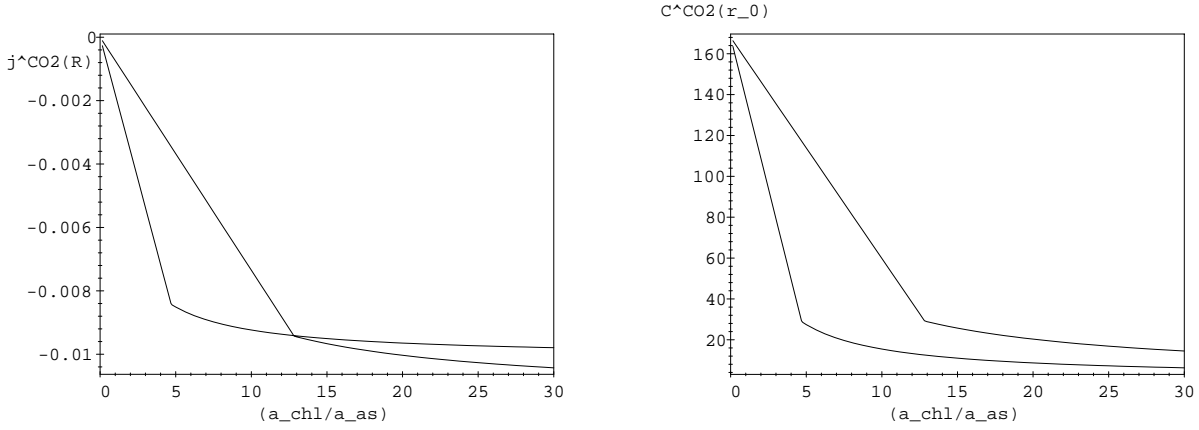
Figures 36 and 37: Left: Assimilation rates $j^{CO_2}(R)$ as functions of (a_{chl}/a_{as}) for *Aglaophyton* (lower curve) and *Rhynia* (upper curve). Assimilation rates have a negative sign, as carbon dioxide flows *into* the plant.

Right: Carbon dioxide concentrations $C^{CO_2}(r_0)$ at the inner edge of the assimilation layer as functions of (a_{chl}/a_{as}) for *Aglaophyton* (lower curve) and *Rhynia* (upper curve).

(a_{chl}/a_{as}) denotes the sum of the surfaces of all chloroplasts within a cortex cell divided by the surface of one cortex cell.

$j^{CO_2}(R)$ is in units of mmol/m²/s, $C^{CO_2}(r_0)$ is in units of mmol/m³/s and (a_{chl}/a_{as}) is a dimensionless quantity.

6.5 Dependance of the Assimilation Rate on the Liquid Phase Conductance of Carbon Dioxide

Figure 38 displays the assimilation rate $j^{CO_2}(R)$ as a function of the liquid phase conductance g_{liq} of carbon dioxide in liquid water from cortex cell wall to the chloroplasts for *Aglaophyton* and *Rhynia*, respectively.
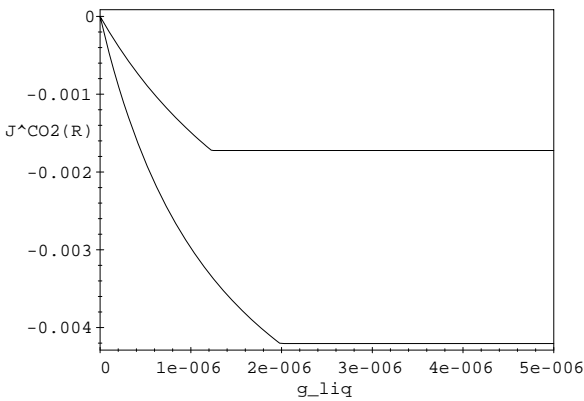
Figure 38: Assimilation rates $j^{CO_2}(R)$ of *Aglaophyton* (lower curve) and *Rhynia* (upper curve) as a function of the liquid phase conductance g_{liq} of carbon dioxide in liquid water from cortex cell wall to the chloroplasts. The value $g_{liq} = 0.5 \times 10^{-3}$ mmol/m²/s/Pa used in the model lies far beyond the right end of the graph. $j^{CO_2}(R)$ is in units of mmol/m²/s, g_{liq} in units of mmol/m²/s/Pa. Assimilation rates have a negative sign, as carbon dioxide flows *into* the plant.

6.6 Dependance of the Assimilation Rate on the Specificity Factor for Rubisco

Figures 39 and 40 display the assimilation rate $j^{CO_2}(R)$ and the carbon dioxide concentration $C^{CO_2}(r_0)$ at the inner edge of the assimilation layer, respectively, as functions of the specificity factor τ for Rubisco for *Aglaophyton* and *Rhynia*, respectively. For the definition of τ recall equation (3.38), Section 3.4.1.
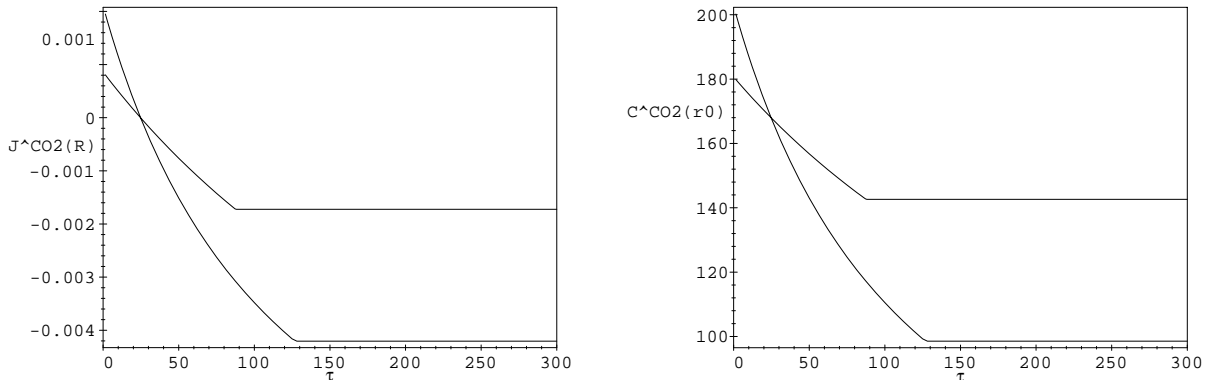
Figures 39 and 40: Left: Assimilation rates $j^{CO_2}(R)$ of *Aglaophyton* (lower curve) and *Rhynia* (upper curve) as a function of the specificity factor τ for Rubisco. $j^{CO_2}(R)$ is in units of mmol/m^2/s, τ is without dimension. Assimilation rates have a negative sign, as carbon dioxide flows *into* the plant.
Right: Carbon dioxide concentration $C^{CO_2}(r_0)$ at the inner edge of the assimilation layer as function of the specificity factor τ for Rubisco for *Aglaophyton* (lower curve) and *Rhynia* (upper curve). $C^{CO_2}(r_0)$ is in units of mmol/m^3, τ is without dimension.
The value $\tau = 2822$ used in the model lies far beyond the right end of both graphs.

6.7 Dependance of the Assimilation Rate on the Efficiency of Light Conversion

Figure 41 displays the assimilation rate $j^{CO_2}(R)$ as a function of the efficiency of light conversion α for *Aglaophyton* and *Rhynia*, respectively.
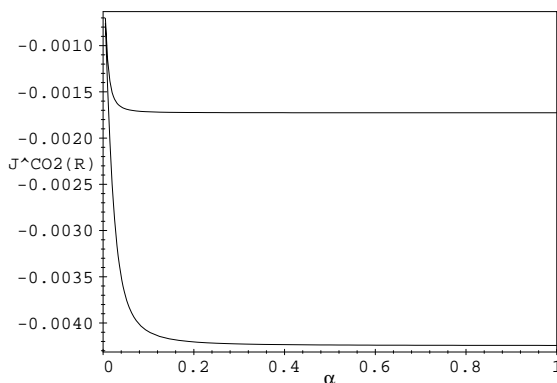
Figure 41: Assimilation rates $j^{CO_2}(R)$ of *Aglaophyton* (lower curve) and *Rhynia* (upper curve) as a function of the efficiency of light conversion α. $j^{CO_2}(R)$ is in units of mmol/m^2/s, α is without dimension. The model employs the value $\alpha = 0.2$. Assimilation rates have a negative sign, as carbon dioxide flows *into* the plant.

6.8 Dependance of the Assimilation Rate on V_{max} and J_{max}

Figures 42 to 45 display the the assimilation rate $j^{CO_2}(R)$ as a function of the local maximum carboxylation rate V_{max} and the light-saturated rate of electron transport J_{max} for *Aglaophyton* and *Rhynia*, respectively.
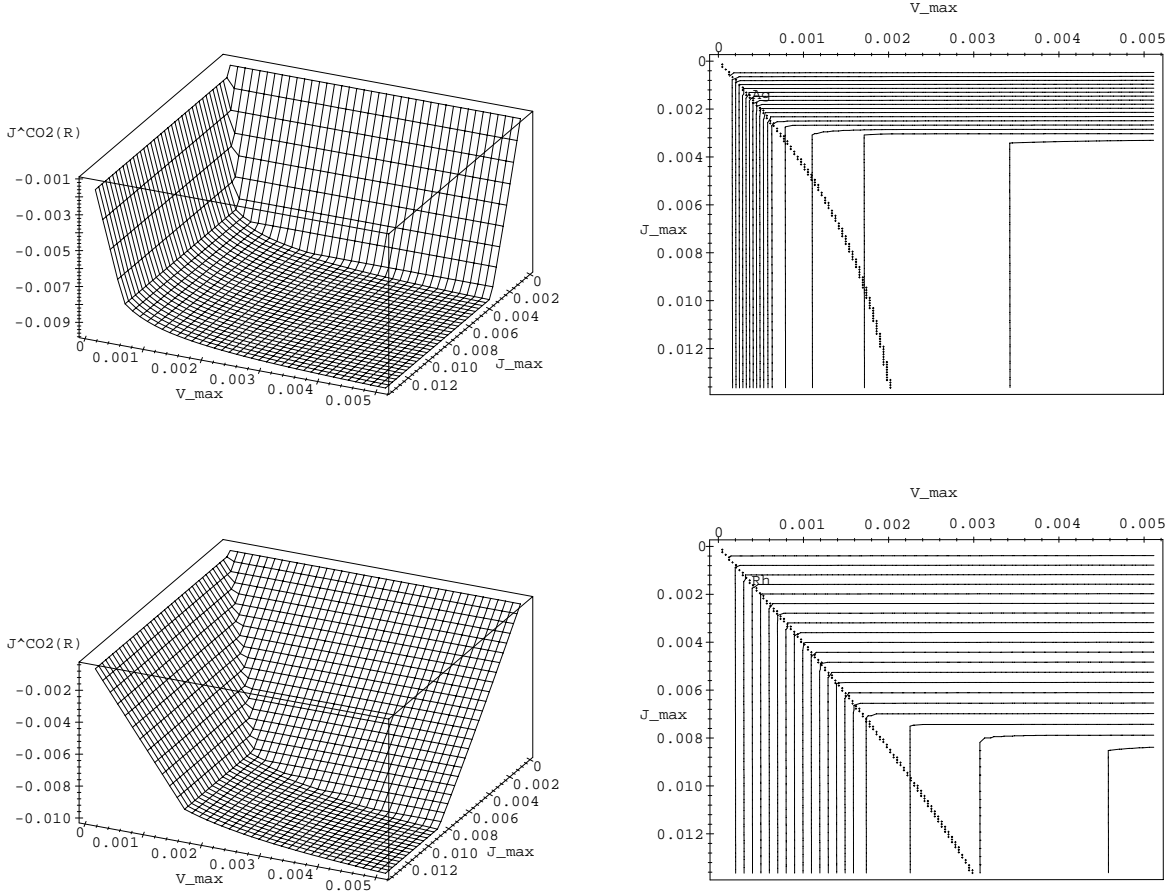
Figures 42, 43, 44 and 45: Assimilation rates $j^{CO_2}(R)$ of *Aglaophyton* (upper pictures) and *Rhynia* (lower pictures) as functions of the local maximum carboxylation rate V_{max} and the light-saturated rate of electron transport J_{max}. All quantities are in units of mmol/m^2/s. Assimilation rates have a negative sign, as carbon dioxide flows *into* the plant.

Left: Three-dimensional views.

Right: The same pictures displayed as contour plots. The positions of *Aglaophyton* and *Rhynia* on the (V_{max}, J_{max})-plane are marked by 'Ag' and 'Rh', respectively.

Points lying "northeast" of the crossed line fulfill the condition $V_{max} < J/4$, that is, photosynthesis is limited by the maximum rate of carboxylation. On the other hand, for points "southwest" of the crossed line the condition $V_{max} > J/4$ is valid, that is, photosynthesis is limited by the light-saturated rate of electron transport.

Intervals between adjacent contour lines amount to $\triangle j^{CO_2}(R) = 0.0005$ mmol/m^2/s.

Upper, right picture: The contour line close to 'Ag' corresponds to $j^{CO_2}(R) = -0.00425$ mmol/m^2/s, the one at the top to $j^{CO_2}(R) = -0.0015$ mmol/m^2/s, and the one encircling the "south-east"-corner to $j^{CO_2}(R) = -0.0095$ mmol/m^2/s.

Lower, right picture: The contour line close to 'Rh' corresponds to $j^{CO_2}(R) = -0.00175$ mmol/m^2/s, the one at the top to $j^{CO_2}(R) = -0.0005$ mmol/m^2/s, and the one encircling the "south-east"-corner to $j^{CO_2}(R) = -0.01$ mmol/m^2/s.

7. Discussion

7.1 Local Fluxes and Local Concentrations of Carbon Dioxide and Water Vapour

By using the values given in Tables 1, 2 and 3 the results shown in Figures 23 and 24 concerning the local fluxes of water vapour and carbon dioxide are obtained.

It is apparent that the fluxes are quite smooth functions of r outside the assimilation layer. This is to be expected from the plants' axial symmetry and from the principle of mass conservation, which forces the fluxes to vary inversely proportional to r wherever sources or sinks are absent. Formally this result can be derived from the principle of mass conservation (equation (3.4)): In the absence of sources (i.e. $Q = 0$) and under stationary conditions (i.e. $\partial C/\partial t = 0$), axial and translatorial symmetry with respect to the z-axis imply

$$0 = \operatorname{div} \vec{j} + Q - \frac{\partial C}{\partial t} = \frac{1}{r} \frac{\partial (r\, j_r)}{\partial r} \tag{7.1}$$

where the definition of the divergence, equation (9.6), has been used, too. The last equation is equivalent to

$$r\, j_r = \text{const.} \tag{7.2}$$

from which follows

$$j_r = \frac{\text{const.}}{r} \tag{7.3}$$

The local concentrations of water vapour and carbon dioxide plotted in Figures 21 and 22 against r behave less smoothly than the fluxes, because their gradients $dC(r)/dr = -(1/S)\, j(r)$ (see equation (3.5)) are dominated by the factor $1/S$ which leaps considerably from layer to layer, exhibiting the following ratios, which are valid both for carbon dioxide and water vapour diffusion:

$$1/S_{bl} : 1/S_{st} : 1/S_{hy} : 1/S_{as} \approx 1 : 5560 : 1036 : 7 \qquad (Aglaophyton) \tag{7.4}$$

$$1/S_{bl} : 1/S_{st} : 1/S_{hy} : 1/S_{as} \approx 1 : 6166 : 1144 : 7 \qquad (Rhynia) \tag{7.5}$$

This causes steep gradients of both carbon dioxide and water vapour in the stomatal and hypodermal layers, whereas in the boundary layer and — in the case of carbon dioxide — in the assimilation layer, the concentrations of both gases remain almost constant.

In a Lower Devonian atmosphere with $C_{atm}^{CO_2} = 168$ mmol/m^3 and $C_{atm}^{H_2O} = 480$ mmol/m^3, the intercellular carbon dioxide concentrations inside the assimilating tissue amount to about 99 mmol/m^3 (Aglaophyton) and 143 mmol/m^3 (Rhynia), which are roughly 59 % and 85 % of the external values.

Extant plants show intercellular carbon dioxide concentrations of about 70 % of the atmospheric concentration (von Caemmerer & Evans, 1991).

7.2 Transpiration and Assimilation Rates and their Dependance on Environmental Conditions

The local fluxes of carbon dioxide and water vapour at the plant surface give the assimilation rate and the transpiration rate per plant surface area[21]. In a Lower Devonian atmosphere the values of the assimilation rates and the transpiration rates (from equations (3.72) and (3.73)) amount to about

$$|j^{\text{CO}_2}(R)| = 4.20 \ \frac{\mu\text{mol}}{\text{m}^2 \ \text{s}} \qquad j^{\text{H}_2\text{O}}(R) = 47 \ \frac{\mu\text{mol}}{\text{m}^2 \ \text{s}} \qquad (\textit{Aglaophyton}) \qquad (7.6)$$

$$|j^{\text{CO}_2}(R)| = 1.72 \ \frac{\mu\text{mol}}{\text{m}^2 \ \text{s}} \qquad j^{\text{H}_2\text{O}}(R) = 52 \ \frac{\text{mmol}}{\text{m}^3 \ \text{s}} \qquad (\textit{Rhynia}) \qquad (7.7)$$

The assimilation rates are in the range of the results of Raven, 1993 and Beerling & Woodward, 1997. Compared to extant plants all values are low. Today's ferns, shade leaves of angiosperms, or conifer needles assimilate with a rate of about 6 μmol/m^2/s (Larcher, 1997). The transpiration rates of *Aglaophyton* and *Rhynia* are extremely low, as leaves of, for example, extant herbaceous plants may reach transpiration rates of more than 5000 μmol/m^2/s (Larcher, 1997). The tiny xylem strands of rhyniophytic plants thus appear to be sufficient for the obviously low water demand of the plant axes.

The dependance of the transpiration and assimilation rates from the atmospheric water vapour and carbon dioxide contents is illustrated in Figures 25 and 26. The transpiration rates depend in an approximately linear way from the atmospheric water vapour concentration, with high transpiration rates corresponding to low atmospheric water vapour concentrations and *vice versa*, as is to be expected. The assimilation rates, however, show saturation behaviour: if the atmospheric carbon dioxide concentrations are smaller than $C_{atm}^{\text{CO}_2} = 80$ mmol/m^3 (*Aglaophyton*) and $C_{atm}^{\text{CO}_2} = 46$ mmol/m^3 (*Rhynia*) they are approximately linear functions of $C_{atm}^{\text{CO}_2}$, for higher values of $C_{atm}^{\text{CO}_2}$ they remain almost constant. This reflects the saturation behaviour of the model of photosynthesis which we introduced in Section 3.4.3 (see equation (3.63) and Figure 14): The carbon dioxide flux into the plant is driven by the difference between the carbon dioxide concentrations of the atmosphere and the intercellular airspaces (see the discussion of Fick's law in Section 3.1). The lower carbon dioxide concentration inside the plant is caused by photosynthesis, whose output depends on the carbon dioxide concentration close to the chloroplasts (see equation (3.63) and Figure 14). If the atmospheric carbon dioxide concentration increases, starting from a *low* level,

---

[21] We remind the reader of the discussion of the porous medium approximation in Section 3.3.1: The rates given are *not* those which one would actually measure in or close to a stoma, they are rather average values, identical to the sum of all molecules diffusing (at the same moment) through all stomata divided by the plant's surface area.

photosynthesis performs in the "linear mode" of Figure 14 and is thus able to appreciate the increasing carbon dioxide concentration by assimilating greater quantities of carbon dioxide, which in turn increases the carbon dioxide influx from outside the plant. If, however, the atmospheric carbon dioxide concentration increases from an initially *high* level, photosynthesis works already in the "saturated mode", so that the carbon dioxide influx into the chloroplasts is independent from the carbon dioxide concentration around the chloroplasts. As there are no other carbon dioxide sinks in the plant, the overall carbon dioxide influx remains constant. This explanantion is confirmed by calculating the carbon dioxide concentrations C_{q_c} (equation (3.64)) for *Aglaophyton* and *Rhynia*. C_{q_c} divides the carbon dioxide consumption per time and chloroplast area $A_{lin}^{chl}(C)$ (equation (3.63)) into a linear and a saturated branch. The values of C_{q_c} coincide — as is to be expected — with the carbon dioxide concentrations, at which the assimilation rates in Figures 25 and 27 switch between their linear and saturation modes.

As far as ecophysiologic performance is concerned, it is desirable for a plant to live under conditions which enable high assimilation rates, because this is the prerequisite for a sufficient production of structural material and energy. A second criterion for a successful existence consists in the requirement to transpire as little water vapour as possible. A superficial examination of Figures 25 and 26 seems to suggest that *Aglaophyton* is better than *Rhynia* with respect to both conditions. But this conclusion should be inferred with caution, because the crucial quantities are not the fluxes per plant surface area and time. Far more important are the fluxes per plant volume and time, because the assimilational demands of a plant are not proportional to its surface, but rather to the amount of living tissue, which is — at least in the case of plants which do not produce wood — approximately proportional to the volume of the plant.

We therefore define the quantity $\mathcal{A}$, the assimilation rate per plant volume, by

$$\mathcal{A} := \frac{j^{\mathrm{CO_2}}(R) \times 2\pi R\,L}{\pi R^2\,L} = \frac{2}{R}\,j^{\mathrm{CO_2}}(R) \tag{7.8}$$

where L is the length and R the radius of a cylindrical telome. The telomes (outer) surface is $2\pi R\,L$, its volume $\pi R^2\,L$. For the Lower Devonian atmosphere with $C_{atm}^{\mathrm{CO_2}} = 168$ mmol/m^3 this leads to

$$\mathcal{A}_{Aglaophyton} = 3.74\ \frac{\mathrm{mmol}}{\mathrm{m^3\ s}} \qquad \text{and} \qquad \mathcal{A}_{Rhynia} = 3.45\ \frac{\mathrm{mmol}}{\mathrm{m^3\ s}} \tag{7.9}$$

With respect to water loss we define the transpiration rate per plant volume, $\mathcal{T}$, in analogy to $\mathcal{A}$

$$\mathcal{T} := \frac{j^{\mathrm{H_2O}}(R) \times 2\pi R\,L}{\pi R^2\,L} = \frac{2}{R}\,j^{\mathrm{H_2O}}(R) \tag{7.10}$$

but with a different argument: $\mathcal{T}$ becomes important, if the plant loses more water by transpiration than its roots (or rhizoids) can supply. If we assume somewhat crudely, that on an average all cells are equally threatened from drying up, a plant with a low $\mathcal{T}$-value will be better off during

a temporary drought than a plant with a high $\mathcal{T}$-value. For a relative humidity of 50 % (i,e. $C_{atm}^{\mathrm{H_2O}} = 480$ mmol/m^3 at a temperature of $20\,^\circ$C) we get

$$\mathcal{T}_{Aglaophyton} = 41.6\,\frac{\mathrm{mmol}}{\mathrm{m^3\ s}} \qquad \text{and} \qquad \mathcal{T}_{Rhynia} = 104.8\,\frac{\mathrm{mmol}}{\mathrm{m^3\ s}} \tag{7.11}$$

Equations (7.9) and (7.11) imply $\mathcal{A}_{Aglaophyton}\,/\mathcal{A}_{Rhynia} = 1.08$ and $\mathcal{T}_{Rhynia}\,/\mathcal{T}_{Aglaophyton} = 2.52$. Thus we may conclude, that *Aglaophyton* assimilated (in the sense of assimilation rate per plant volume, as defined in equation (7.8)) only slightly better but lost much less water by transpiration than *Rhynia*. Figures 27 and 28 display $\mathcal{A}$ and $\mathcal{T}$ for wider ranges of $C_{atm}^{\mathrm{CO_2}}$ and $C_{atm}^{\mathrm{H_2O}}$.

As a high atmospheric carbon dioxide content probably represents a prerequisite for the evolution of early terrestrial plants such as *Aglaophyton* or *Rhynia*, Figure 27 gives a partial answer to the question, to which limit of the atmospheric carbon dioxide concentration rhyniophytic plants were able to exist. As mentioned before, the graph shows that the assimilation rate is roughly constant and fully saturated over a wide range of atmospheric carbon dioxide concentrations above $C_{atm}^{\mathrm{CO_2}} = 99$ mmol/m^3 (*Aglaophyton*) and $C_{atm}^{\mathrm{CO_2}} = 55$ mmol/m^3 (*Rhynia*). Thus we can conclude that lower values than the 168 mmol/m^3, which are commonly accepted as the Lower Devonian atmospheric carbon dioxide concentration, are sufficient for a saturation of the assimilation process. Therefore, *Aglaophyton* and *Rhynia* may well have been able to exist under a wide range of atmospheric carbon dioxide concentrations.

The irradiance I is another environmental variable which influences the assimilation rate[22]. Figure 29 shows the dependance of the assimilation rate $j^{\mathrm{CO_2}}(R)$ on I. Obviously, for $I \gtrsim 0.04$ mmol/m^2/s (*Aglaophyton*) and $I \gtrsim 0.02$ mmol/m^2/s (*Rhynia*) the assimilation rate is saturated with respect to I. This corresponds to the saturation behaviour of the rate of carboxylation if limited by electron transport, $W_j(q, I)$ (see equations (3.35) and (3.36)).

The irradiance value for *Aglaophyton*, $I_{Aglaophyton} = 0.05$ mmol/m^2/s, which we have chosen for the calculations in our model lies just inside the saturated range, the value for *Rhynia*, $I_{Rhynia} = 0.122$ mmol/m^2/s, however, lies well inside the saturated range.

7.3 The Water Use Efficiency and its Dependance on Atmospheric Conditions

All land plants face a common problem: Whenever they open their stomata to allow the carbon dioxide molecules to diffuse from the outside to the internal assimilating tissue, they simultaneously lose water by transpiration. As it is obviously favourable for a plant to conserve water vapour, different plant groups developed different strategies in order to achieve this. A quantitative measure for the efficiency of such strategies is provided by the water use efficiency (WUE). It is defined by

---

[22] In principle, the transpiration rate depends on I, too. In the framework of our model, however, we ignore the heat transfer between plant and environment caused by electro-magnetic radiation.

$$\text{WUE} := \frac{\text{number of CO}_2 \text{ molecules fixed per time}}{\text{number of H}_2\text{O molecules transpired per time}} = \frac{|\mathcal{A}|}{\mathcal{T}} = \frac{|j^{\text{CO}_2}(R)|}{j^{\text{H}_2\text{O}}(R)} \qquad (7.12)$$

Taking the water use efficiency as the sole measure for the performance of a plant can be misleading due to several reasons:

(i) If the transpiration rate $\mathcal{T}$ in the denominator of (7.11) becomes close to zero, the fraction WUE will attain *very* high values, even if the plants assimilation rate $\mathcal{A}$ becomes so small, that it cannot sustain the plant's energetic requirements.

(ii) In a real plant, the value of the water use efficiency varies strongly due to temporal stomatal closure or variations in environmental conditions.

In order to avoid these drawbacks, other long-term parameters — such as the amount of water used per vegetational period divided by the dry matter produced during that time — are often used.

With the numerical values of Tables 1, 2 and 3 we obtain

$$\text{WUE}_{Aglaophyton} = 0.0899 \approx 45 \times \text{WUE}_{\text{extant}} \qquad (7.13)$$

$$\text{WUE}_{Rhynia} = 0.0329 \approx 16 \times \text{WUE}_{\text{extant}} \qquad (7.14)$$

where $\text{WUE}_{\text{extant}} = 0.0020$ is a typical average value for extant C_3 plants (see, for example, Kramer, 1983). The question arises, whether these relatively high values are due to environmental conditions — during the Lower Devonian the atmospheric carbon dioxide concentration was twelve times as high as it is today —, or if the high water use efficiencies calculated in equations (7.13) and (7.14) are based on the morphological design of rhyniophytic plant axes. A partial answer can be obtained by consulting Figures 30 and 31. Figure 30 displays the water use efficiency as a function of the atmospheric carbon dioxide and of the water vapour concentrations. Figure 31 is a (vertical) section through Figure 30 at a water vapour concentration $C_{atm}^{\text{H}_2\text{O}} = 480$ mmol/m^3 (equivalent to a relative humidity of 50 %). The figures show, that for a given water vapour concentration the water use efficiency is almost constant for a wide range of carbon dioxide concentrations around the Lower Devonian value of $C_{atm}^{\text{CO}_2} = 168$ mmol/m^3. It approaches zero more or less linearly, if the carbon dioxide concentration drops below the values $C_{atm}^{\text{CO}_2} = 99$ mmol/m^3 (*Aglaophyton*) and $C_{atm}^{\text{CO}_2} = 55$ mmol/m^3 (*Rhynia*). Under recent atmospheric conditions, *Aglaophyton*'s and *Rhynia*'s water use efficiencies would be

$$\text{WUE}_{Aglaophyton, \text{ today}} = 0.0116 \approx 5.8 \times \text{WUE}_{\text{extant}} \qquad (7.15)$$

$$\text{WUE}_{Rhynia, \text{ today}} = 0.0078 \approx 3.9 \times \text{WUE}_{\text{extant}} \qquad (7.16)$$

This means that under present day conditions both plants would perform below their respective optima of water use efficiency, but still more efficient than extant plants. However, we should not

ignore the possibility that although the fraction WUE attains high values, the plants assimilation rate $\mathcal{A}$ becomes so small under present day conditions, that it cannot sustain the plant's energetic requirements.

Nonetheless, we may conclude from Figure 30 that the water use efficiencies are not independent from the atmospheric carbon dioxide and water vapour content, because in this case the surfaces in Figure 30 would be planes with WUE=$const.$.

7.4 Dependance of Water Use Efficiency, Transpiration and Assimilation Rates on Plant Anatomy

There remains the question, to what extent the morphology of rhyniophytic plants is responsible for their high water use efficiency. Their low water losses perhaps matched the probably low water absorbing capacity of these plants, which is suggested by the absence of true roots in rhyniophytic plants. Although mycorrhizal fungi were present in rhyniophytic plants, it is assumed that the plants' water consumption was supplied by the plants' own underground rhizoids. Edwards et al., 1998 suggested that rhyniophytic plants achieved low water losses by a low stomatal density and the presence of a hypodermal layer in the plant axes. Figure 32 displays the water use efficiency of *Aglaophyton* (upper surface) and *Rhynia* (lower surface) as a function of the stomatal density ν_{st} and the thickness d_{hy} of the hypodermal layer.

It is apparent from Figure 32, that the water use efficiencies show "threshold behaviour" with respect to the variable ν_{st}: if ν_{st} is varied below a value of $\nu_{st} \approx 0.8 \times 10^7$, the water use efficiencies change drastically, whereas for greater values of ν_{st} the water use efficiencies vary only slowly. The d_{hy}-dependance of the water use efficiencies is not very distinct in comparison with the effect which is exerted by ν_{st}.

Both *Aglaophyton* and *Rhynia* occupy positions on the lower flanks of the strongly varying sectors of the WUE-surfaces above the (ν_{st}, d_{hy})-planes. Figures 33 and 34 show, that the plants have good reason to do so: From Figure 33 it is apparent that the best positions for good assimilation performance are to be found on a strip of the (ν_{st}, d_{hy})-plane with small d_{hy}-values above the carbon dioxide ν_{st}-thresholds, the latter being at about $\nu_{st} \approx 0.5 \times 10^6$ (*Aglaophyton*) and $\nu_{st} \approx 1.5 \times 10^6$ (*Rhynia*). Why the positions of *Aglaophyton* and *Rhynia* are located close to (but above) the carbon dioxide ν_{st}-thresholds becomes obvious from Figure 34: The transpiration rates are smooth functions and show the behaviour one would intuitively expect: They are small for small values of ν_{st} and high values of d_{hy}, they increase for increasing ν_{st}- and decreasing d_{hy}-values and they have their maxima where ν_{st} and d_{hy} attain their respective maxima and minima. Therefore, the actual ν_{st} and d_{hy} values of *Aglaophyton* and *Rhynia* represent good compromise solutions.

We may pursue this line of reasoning still further: Figure 35 is the counterpart of Figure 33 for the recent atmospheric carbon dioxide content: the surfaces in Figure 35 are much smoother than the ones in Figure 33, the carbon dioxide ν_{st}-threshold is much less conspicuous. Thus it is obvious that *Aglaophyton* and *Rhynia* were best adapted to the Lower Devonian atmosphere, or, as was

stated by Edwards, 1998, "it could be argued that high carbon dioxide concentration 'permitted' the minimizing of numbers of stomata (...)".

Figures 36 and 37 depict the assimilation rate $j^{CO_2}(R)$ and the carbon dioxide concentration $C^{CO_2}(r_0)$ at the inner edge of the assimilation layer, respectively, as functions of the ratio (a_{chl}/a_{as}). (a_{chl}/a_{as}) denotes the sum of the surfaces of all chloroplasts within a cortex cell divided by the surface of one cortex cell. The shape of both curves is no surprise:

— $(a_{chl}/a_{as}) \to 0$ means that all chloroplasts disappear, with the consequence that assimilation ceases, which implies a uniform carbon dioxide level equal to $C^{CO_2}_{atm}$ throughout the plant.

— $(a_{chl}/a_{as}) \to \infty$ stands for a growing assimilation capacity which exceeds beyond a certain (a_{chl}/a_{as})-ratio the carbon dioxide supply, the latter being limited by the effective conductances $S_i = D\,n_i/\tau^2$ (see Section 3.3.1) within the plants various layers. This implies saturation behaviour for both curves.

In Section 4.4. we used geometric arguments to confine the ratio (a_{chl}/a_{as}) to the interval $1.8 \leq (a_{chl}/a_{as}) \leq 3.6$. The values 1.8 and 3.6 correspond to completely flat and to sphere-shaped chloroplasts, respectively. A depth/diameter ratio of $\eta = 3/7$ (the value of modern chloroplasts) implies $(a_{chl}/a_{as}) = 2.345$, which is near the midpoint of that interval. In view of the fact that assimilation rate and carbon dioxide concentration show their highest variation within the interval $1.8 \leq (a_{chl}/a_{as}) \leq 3.6$ (the assimilation rates of both *Aglaophyton* and *Rhynia* vary by a factor of two between the endpoints of the interval), it is quite unfortunate that (a_{chl}/a_{as}) cannot be measured from fossilized material.

7.5 Dependance of the Assimilation Rate on the Liquid Phase Conductance of Carbon Dioxide

Figure 38 displays the assimilation rate $j^{CO_2}(R)$ as a function of g_{liq} for *Aglaophyton* and *Rhynia*, respectively. g_{liq} denotes the liquid phase conductance of carbon dioxide in liquid water from the cortex cell wall to the chloroplasts. The message of the picture is an agreeable one, since for

$$g_{liq} \gtrsim 1.4 \times 10^{-6} \ \frac{\text{mmol}}{\text{m}^2 \text{ s Pa}} \tag{7.17}$$

the assimilation rate is nearly constant and the value $g_{liq} = 0.5 \times 10^{-3}$ mmol/m²/s/Pa used in the model lies far beyond this threshold. In other words, we need not bother about an accurate value for g_{liq} as long as we can be sure that the inequality (7.17) holds.

7.6 Dependance of the Assimilation Rate on the Specificity Factor for Rubisco

Figure 39 displays the assimilation rates $j^{CO_2}(R)$ of *Aglaophyton* and *Rhynia* as functions of the specificity factor τ for Rubisco. Figure 40 displays the carbon dioxide concentrations $C^{CO_2}(r_0)$ at

the inner edge of the assimilation layer as functions of τ, again for *Aglaophyton* and *Rhynia*. For the definition of τ recall equation (3.38), Section 3.4.1.

The abscissae of both pictures end at $\tau = 300$, since both function pairs attain for $\tau \gtrsim 130$ constant values, which remain constant even beyond the value $\tau = 2822$ used in the model. That is, for $\tau \gtrsim 130$ (*Aglaophyton*) and $\tau \gtrsim 90$ (*Rhynia*) the assimilation rates and the carbon dioxide levels inside the respective plants are effectively independent of τ.

On the other hand, decreasing values of τ make the concentration

$$C_{\Gamma_*} = \frac{1}{R_{gas}T} \times \frac{p_o}{2\,\tau} \tag{7.18}$$

which is equivalent to the carbon dioxide compensation point

$$\Gamma_* = \frac{p_o}{2\,\tau} \tag{7.19}$$

increase. Eventually, for $\tau \lesssim 28$, C_{Γ_*} increases even beyond $C_{atm}^{\mathrm{CO_2}}$. Then carbon dioxide is produced and the carbon dioxide flux is directed outwards.

7.7 Dependance of the Assimilation Rate on the Efficiency of Light Conversion

Figure 41 shows that for $\alpha \gtrsim 0.16$ the assimilation rates of both *Aglaophyton* and *Rhynia* are more or less saturated. For $0 \leq \alpha \lesssim 0.16$, however, they respond very strongly to a variation of α. The value $\alpha = 0.2$ we chose for our model lies thus just outside this "critical" area.

7.8 Dependance of the Assimilation Rate on V_{max} and J_{max}

Figures 42 and 43 display the assimilation rate of *Aglaophyton* as functions of the local maximum carboxylation rate V_{max} and the light-saturated rate of electron transport J_{max}. The left picture displays a three-dimensional view of the situation, the right one displays it as a contour plot. Figures 44 and 45 are the equivalent pictures in the case of *Rhynia*. Points lying "northeast" of the crossed lines in the contour plots fulfill the condition

$$V_{max} < J/4 \tag{7.20}$$

that is, photosynthesis is limited by the maximum rate of carboxylation. On the other hand, for points "southwest" of the crossed line the condition

$$V_{max} > J/4 \tag{7.21}$$

is valid, and photosynthesis is limited by the light-saturated rate of electron transport. Note, that the ordinates in Figures 43 and 45 display not J but J_{max} which is connected to J (see Section 3.4.1) via the definition

$$J := \frac{\alpha I}{\sqrt{1 + \left(\frac{\alpha I}{J_{max}} \right)^2}} \qquad (7.22)$$

Assimilation rates which obey the equation $V_{max} = J/4$ (i.e. they lie on the crossed lines in Figures 43 and 45) show a peculiar behaviour: if we want to change the assimilation rate connected with any of these points, we must change V_{max} and J_{max} simultaneously. Variation of only one of the two variables does not change the assimilation rate, the new (V_{max}, J_{max})-pair lies on the same isohypse as the old one. Note that the (V_{max}, J_{max})-pairs we have chosen for *Aglaophyton* and *Rhynia* are very close to the crossed lines.

The positions of both *Aglaophyton* and *Rhynia* correspond to comparatively low values of the assimilation rate. As the values of V_{max} and J_{max} bear no influence on the water vapour fluxes, both plants would be better off with higher values of V_{max} and J_{max} — at least with respect to water use efficiency and to their general assimilation ability. This would place them closer to the bottom of the "assimilation plane" and to higher assimilation rates. As the fossil record tells us nothing about the Lower Devonian values of the biochemical parameters of photosynthesis, the outcome of our calculation might be interpreted as a clue that higher values of V_{max} and J_{max} should be chosen.

The high intercellular carbon dioxide concentration of *Rhynia* — in Section 7.1 the value 85 % was calculated — is perhaps a hint into the same direction: Beerling & Woodward, 1997, concluded from stable carbon isotope measurements (δ^{13}C) of fossilized plant material that the intercellular carbon dioxide concentration amounted to about 70 % of the external value in all phanerozoic land plants. Recalculation of *Rhynia* shows, that this value is produced by our model, if we double the values of V_{max} and J_{max} given in Table 3 and leave all other parameters as before. (The doubling of V_{max} and J_{max} leads, by the way, to a doubling of both *Rhynia*'s assimilation rate and of its water use efficiency.)

On may wonder, whether this line of thought is really convincing, as it obviously applies only for *Rhynia* and not for *Aglaophyton*. But, first, it cannot be excluded, that the biochemical parameters V_{max} and J_{max} were different for the different rhyniophytic species *Aglaophyton* and *Rhynia*. A second argument in favour of this interpretation will be given in the next section.

7.9 Concluding Remarks on Physiological and Biochemical Parameters

As we have emphasized before, some uncertainties exist for our approach. This concerns mainly the biochemical parameters of photosynthesis. Since it is obviously impossible to conduct physiological measurements on fossil plants, many quantities must be estimated, or taken from results obtained with extant plants. However, the uncertainties in the biochemical parameters do not all have the same quality, as can be seen from the way, in which they influence the assimilation rate: Increasing or decreasing of input values may or may not have an effect on the simulation results, depending

on the parameters. The validity of the results must then be checked by using additional criteria. To see this more clearly, we shortly reexamine a few results calculated above.

— The specificity factor for Rubisco, τ, was found to exert influence on the assimilation rate only for small values very far away from its modern value. These values are so small, that there exists only a remote possibility that they had ever any influence at all.

— The dependance of the assimilation rate on the efficiency of light conversion, α, allows statements, which could be characterized as being "confident towards one side" of the α-interval: if α is shifted to higher values than $\alpha = 0.16$ (which is not much below the value $\alpha = 0.2$ we chose for the model) the assimilation rate remains unchanged, but for values below $\alpha = 0.16$ the assimilation rate changes drastically. That is, if during the Lower Devonian, by some reason we do not know (or cannot imagine), more than 16 % of the irradiating photons escaped absorption on their way from the plant surfaces to the assimilating sites, our results do not change. But if the absorbing tissue of the Lower Devonian rhyniophytes was slightly more opaque than we assume it to have been, the predictions of our model are misleading.

— Now to the question, which values should be used for V_{max} and J_{max}. If we insist on the (V_{max}, J_{max})-pairs we have chosen, the accompanying assimilation rate is in a "critical" range, in the sense that simultaneous variation of both variables produces massive changes of the assimilation rate, even if the variations in V_{max} and J_{max} are only small.

On the other hand, the situation could be still more critical: As we pointed out in Section 7.8, the (V_{max}, J_{max})-values we have chosen for *Aglaophyton* and *Rhynia* are very close to the crossed lines in Figures 43 and 45 (representing the equality $V_{max} = J/4$), with the consequence that in order to change the assimilation rate, V_{max} and J_{max} must be changed simultaneously. Perhaps this behaviour can be understood as a selection criterion on the (V_{max}, J_{max})-pairs in terms of stability: Fluctuations around (V_{max}, J_{max})-pairs lying *on* the crossed lines, and concerning only one of the two variables, do not change the assimilation rate, whereas fluctuations around (V_{max}, J_{max})-pairs lying *off* the crossed lines do affect the assimilation rate irrespective of the fact, whether only one or both variables fluctuate. Note, however, that the (V_{max}, J_{max})-pairs producing the most "stable" assimilation rates lie on the "bottom planes" of Figures 42 and 44, which correspond to saturation states of the assimilation, as can be seen from pictures (not included here) spanning still larger (V_{max}, J_{max})-intervals.

— The dependance of the assimilation rate on the ratio (a_{chl}/a_{as}) illustrates a situation in which model-immanent criteria lead nowhere: The fact that the curves in Figures 36 and 37 show saturation behaviour for $(a_{chl}/a_{as}) \gtrsim 13$ certainly represents a model-immanent criterion, but this knowledge is of little value, because it is quite improbable that the ratio (a_{chl}/a_{as}) (the sum of the surfaces of all chloroplasts within a cortex cell divided by the surface of one cortex cell) ever reached such high values.

We may draw the following conclusions from these examples:

(i) The internal mathematical machinery of the model indicates quite clearly whether a biochem-

ical or physiological parameter must be known with high accuracy, or whether its exact knowledge is less crucial, if the model is supposed to produce reliable results. (a_{chl}/a_{as}) falls into the first, τ and α fall into the second of these categories, and V_{max} and J_{max} are somewhere in between.

(ii) It is necessary to supplement the information obtainable from criteria inherent to the model with arguments and/or data from "outside" the model.

Apart from these considerations, our results demonstrate that the design of rhyniophytic plants is well-adapted to Lower Devonian conditions. Taking into account the probably poor water absorption capability of rhyniophytic plants, the high values of their water use efficiency were on the one hand absolutely necessary in order to avoid water stress. On the other hand, the high carbon dioxide concentration of the Lower Devonian atmosphere guaranteed sufficient carbon dioxide influx.

The results furthermore appear to confirm a suggestion of Kerp and Hass (personal communication) that *Aglaophyton* and *Rhynia* occupied different ecological niches in the sense that *Aglaophyton* represented a longer-lived species than *Rhynia*. It seems plausible that a fast-growing species with a short individual life-span like *Rhynia* showed higher assimilation rates (and accordingly higher values of the biochemical parameters V_{max} and J_{max}, as discussed at the end of Section 7.8) than a slower-growing species like *Aglaophyton*.

More research is required, however, in order to confirm specific suggestions like these, and to yield more detailed information about ecophysiological ranges of the rhyniophytic plant group in general.

8. References

Abramowitz, M. Stegun, I. (1972) *Handbook of Mathematical Functions*, New York: Dover Publications.

Arfken, G. (1970) *Mathematical Methods for Physicists*, New York: Academic Press.

Aris, R. (1975) *The mathematical theory of diffusion and reaction in permeable catalysts. The theory of the steady state.*, London: Oxford University Press.

Augustinowicz, J. & Gabryś, H. (1999) Chloroplast movements in fern leaves: correlation of movement dynamics and environmental flexibility of the species. *Plant, Cell and Environment* **22**, 1239-1248.

Bateman, R.M., Crane, P.R., DiMichele, W.A., Kenrick, P.R., Rowe, N.P., Speck, T. & Stein, W. (1998) Early evolution of land plants: phylogeny, physiology, and ecology of the primary terrestrial radiation. *Annual Review of Ecology and Systematics* **29**, 263-292.

Beerling, D.J. & Woodward, F.L.S. (1997) Changes in land plant function over the Phanerozoic: reconstructions based on the fossil record. *Botanical Journal of the Linnean Society* **124**, 137-153.

Berner, R.A. (1997) The rise of plants and their effect on weathering and atmospheric CO_2. *Science* **276**, 544–545.

von Caemmerer, S. & Evans, J.R. (1991) Determination of the average partial pressure of CO_2 in chloroplasts from leaves of several C_3 plants. *Australian Journal of Plant Physiology* **18**, 287-306.

Edwards, D. (1986) *Aglaophyton major*, a non-vascular land plant from the Devonian Rhynie Chert. *Bot. J. Linn. Soc.* **93**, 173–204.

Edwards, D. (1998) Climate signals in Paleozoic land plants. *Philosophical Transactions of the Royal Society of London, Series* **B 353**, 141–157.

Edwards, D., Kerp, H. & Hass, H. (1998) Stomata in early land plants: an anatomical and eco-physiological approach. *Journal of Experimental Botany* **49**, 255–278.

Farquhar, G.D., von Caemmerer, S. & Berry, J.A. (1980) A Biochemical Model of Photosynthetic CO_2 Assimilation in Leaves of C_3 Species. *Planta* **149**, 78–90.

Farquhar, G.D., Ehleringer, J.R. & Hubick, K.T. (1989) Carbon isotope discrimination and photosynthesis. *Annual Review of Plant Physiology and Plant Molecular Biology* **40**, 503–537.

Grathwohl, P. (1998) *Diffusion in natural media: Contaminant Transport, Sorption/Desorption and Dissolution Kinetics*, Boston: Kluwer Academic Publishers.

Harley, J.L & Smith, S.S. (1983) *Mycorrhizal symbiosis*, New York: Academic Press.

Harley, P.C. & Sharkey, T.D. (1991) An improved model of C_3 photosynthesis at high CO_2: Reversed O_2 sensitivity explained the lack of glycerate re-entry into the chloroplast. *Photosynthesis Research* **27**, 169-178.

Harley, P.C., Thomas, R.B., Reynolds, J.F. & Strain, B.R. (1992) Modelling the photosynthesis of cotton grown in elevated CO_2. *Plant, Cell and Environment* **15**, 271-282.

Jackson, J.D. (1975) *Classical Electrodynamics*, New York: John Wiley & Sons.

Jarman, P.D. (1974) The diffusion of carbon dioxide and water vapour through stomata. *J. Exp. Bot.* **25**, 927–936.

Kenrick, P. & Crane, P.R. (1997) The origin and early evolution of plants on land. *Nature* **389**, 33-39.

Kirschbaum, M.U.F. & Farquhar, G.D. (1984) Temperature dependance of whole leaf photosynthesis in *Eucalyptus pauciflora* Sieb. ex Spreng.. *Aust. J. Plant Physiol.* **11**, 519–538.

Konrad, W., Roth-Nebelsick, A., Kerp, H., Hass, H. (2000) Transpiration and Assimilation of Early Devonian Land Plants with Axially Symmetric Telomes — Simulations on the Tissue Level. *Journal of Theoretical Biology* (in the press)

Kramer, P.J. (1983) *Water relations of plants*, New York: Academic Press.

Larcher, W. (1997) *Physiological Plant Ecology, 3rd ed.*, New York: Springer-Verlag.

Leuning, R. (1983) Transport of gases into leaves. *Plant, Cell and Environment* **6**, 181–194.

Li Tai-Bo (1962) *Gedichte*, Stuttgart: Philipp Reclam Jun..

Longstreth, D.J., Hartsock & T.L., Nobel, P.S. (1980) Mesophyll cell properties for some C_3 and C_4 species with high photosynthetic rates. *Physiol. Plant.* **48**, 494–498.

Moore, R., Clark, W.D. & Vodopich, D.S. (1998) *Botany*, Boston: McGraw-Hill Book Company.

Morse, P.M., Feshbach, H. (1953) *Methods of Theoretical Physics*, New York: McGraw-Hill Book Company.

Nobel, P.S. (1999) *Physicochemical and Environmental Plant Physiology*, San Diego, Academic Press .

Nultsch, W. (1996) *Allgemeine Botanik*, Stuttgart: Georg Thieme Verlag .

Parkhurst, D.F. (1994) Diffusion of CO_2 and other gases inside leaves. *Phytol.* **126**, 449–479.

Parkhurst, D.F. & Mott, K.A. (1990) Intercellular Diffusion Limits to CO_2 Uptake in Leaves. *Plant Physiol.* **94**, 1024–1032.

Raup, D.M. & Stanley, S.M. (1978) *Principals of Paleontology*, New York: W. H. Freeman and Company.

Raven, J.A. (1977) The evolution of vascular land plants in relation to supracellular transport processes. *Advances in Botanical Research* **5**, 153-219.

Raven, J.A. (1993) The evolution of vascular plants in relation to quantitative functioning of dead water-conducting cells and stomata. *Biological Review* **68**, 337-363.

Raven, J.A. (1994) The significance of the distance from photosynthesizing cells to vascular tissue in extant and early vascular plants. *Botanical Journal of Scotland* **47**, 65-81.

Reif, F. (1974) *Fundamentals of statistical and thermal physics*, Boston: McGraw-Hill.

Remy, W. & Hass, H. (1996) New information on gametophytes and sporophytes of *Aglaophyton major* and inferences about possible environmental adaptations. *Review of Palaeobotany and Palynology* **90**, 175-193.

Robinson, J.M. (1994) Speculations on carbon dioxide starvation, Late Tertiary evolution of stomatal regulation and floristic modernization. *Plant, Cell and Environment* **17**, 345-354.

Roedel, W. (1994) *Physik unserer Umwelt: Die Atmosphäre*, Berlin, Heidelberg, New York: Springer.

Stanley, M.S. (1989) *Earth and Life through Time*, New York: W. H. Freeman and Company.

Taylor, T.N. & Taylor, E.L. (1997) The distribution and interactions of some Paleozoic fungi. *Review of Palaeobotany and Palynology* **95**, 83-94.

Vogel, S. (1994) *Life in Moving Fluids*, Princeton: Princeton University Press.

Waechter, F.K. (1981) *Es lebe die Freihei*, Zürich: Diogenes-Verlag.

Wullschleger, S.D. (1993) Biochemical Limitations to Carbon Assimilation in C_3 Plants — A Retrospective Analysis of the A/C_i Curves from 109 Species. *J. Exp. Bot.* **14**, 907–920.

Zimmermann, W. (1959) *Die Phylogenie der Pflanzen*, Stuttgart: Fischer

9. Appendix I: Some Mathematical Definitions

In cartesian coordinates x, y and z the differential operators gradient grad, divergence div and the Laplace-operator Δ are defined by

$$\text{grad}\, f(x, y, z) := \frac{\partial f}{\partial x}\, \vec{e_x} + \frac{\partial f}{\partial y}\, \vec{e_y} + \frac{\partial f}{\partial z}\, \vec{e_z} \tag{9.1}$$

$$\text{div}\, \vec{F}(x, y, z) := \frac{\partial F_x}{\partial x} + \frac{\partial F_y}{\partial y} + \frac{\partial F_z}{\partial z} \tag{9.2}$$

$$\Delta f(x, y, z) := \frac{\partial^2 f}{\partial x^2} + \frac{\partial^2 f}{\partial y^2} + \frac{\partial^2 f}{\partial z^2} \tag{9.3}$$

$f(x, y, z)$ denotes a (scalar) function, $\vec{F}(x, y, z) = F_x(x, y, z)\vec{e_x} + F_y(x, y, z)\vec{e_y} + F_z(x, y, z)\vec{e_z}$ a vector field, and $\vec{e_x}$, $\vec{e_y}$ and $\vec{e_z}$ is the system of orthonormal unit vectors related to the cartesian coordinates x, y and z.

In polar coordinates (r, φ, z), defined by

$$
\begin{aligned}
x &= r \cos \varphi \\
y &= r \sin \varphi \\
z &= z
\end{aligned}
\tag{9.4}
$$

$$0 \leq r < \infty \qquad 0 \leq \varphi < 2\pi \qquad -\infty < z < \infty$$

and with $\vec{e_r}$, $\vec{e_\varphi}$ and $\vec{e_z}$ the system of orthonormal unit vectors in the directions r, φ and z, respectively, the expressions (9.1) through (9.3) become

$$\text{grad}\, f(r, \varphi, z) = \frac{\partial f}{\partial r}\, \vec{e_r} + \frac{1}{r}\frac{\partial f}{\partial \varphi}\, \vec{e_\varphi} + \frac{\partial f}{\partial z}\, \vec{e_z} \tag{9.5}$$

$$\text{div}\, \vec{F}(r, \varphi, z) = \frac{1}{r}\frac{\partial (r\, F_r)}{\partial r} + \frac{1}{r}\frac{\partial F_\varphi}{\partial \varphi} + \frac{\partial F_z}{\partial z} \tag{9.6}$$

and

$$\Delta f(x, y, z) = \frac{1}{r}\frac{\partial}{\partial r}\left(r\frac{\partial f}{\partial r}\right) + \frac{1}{r^2}\frac{\partial^2 f}{\partial \varphi^2} + \frac{\partial^2 f}{\partial z^2} \tag{9.7}$$

10. Appendix II: MAPLE Code

10.1 Solutions of the Basic Equations

The code in the file `diffgl` corresponds to the content of Section 3. The continuity and boundary conditions from Section 3.5 are applied on the general solutions of the differential equation given in Section 3.5 and solved for the integration constants A_i, B_i, a_i and b_i, as described in Section 3.5. They are stored in the files `diffsol` and `diffsol.m`[23] [24].

File `diffgl`:
```
#
alias(sim=simplify,ev=evalf);
#
# *********************************************************************
# berechnung der CO2-konzentration, des CO2-flusses, der
# wasserdampf-konzentration und des wasserdampf-flusses fuer eine
# axialsymmetrische pflanze aus der stationaeren
# diffusionsgleichung
#
# die CO2-konzentration ausserhalb der pflanze und der CO2-verbrauch
# durch die photosynthese sind vorgegeben  (neumannsche randbedingungen)
#
# die wasserdampf-konzentration ausserhalb der pflanze und die
# wasserdampf-konzentration im mesophyll sind vorgegeben
# (dirichletsche randbedingungen)
# *********************************************************************
# zu berechnende groessen:
#
# C(r)         CO2-konzentration als funktion von r (mol/m^3)
# J(r)         CO2-stromdichte als funktion von r (mol/m^2/s)
#
# c(r)         wasserdampf-konzentration als funktion von r (mol/m^3)
# j(r)         wasserdampf-stromdichte als funktion von r (mol/m^2/s)
#
# *********************************************************************
# sonstige groessen:
#
# Ai,Bi,ai,bi        integrationskonstanten
# BesselI(n,k*r)     modifizierte Besselfunktion der ersten art der ordnung n
# BesselK(n,k*r)     modifizierte Besselfunktion der zweiten art der ordnung n
#
# *********************************************************************
# die loesungen der diffusionsgleichung in den radialen abschnitten:
# !!! wasserdampf !!!
#
#     | c_r3
#     |--------------------------------------------------| r=r3
#     | boundary layer                                   |
#     |                                                  |
cbl:=r -> abl+bbl*ln(r/R);
jbl:=unapply(-sbl*D(cbl)(r),r);
#     |                                                  |
#     |--------------------------------------------------| r=R
#     | stomata                                          |
```

---

[23] The content of `diffsol` and `diffsol.m` is identical, the latter one is written in internal MAPLE format.

[24] The "commentary symbol" in MAPLE is `#`. MAPLE ignores anything in a line after an `#`.

```
#     |                                               |
cst:=r -> ast+bst*ln(r/R);
jst:=unapply(-sst*D(cst)(r),r);
#     |                                               |
#     |---------------------------                    | r=r2
#     | hypodermis                                    |
#     |                                               |
chyp:=r -> ahyp+bhyp*ln(r/R);
jhyp:=unapply(-shyp*D(chyp)(r),r);
#     |                                               |
#     |-----------------------------------------------| r=r1
#     | mesophyll                                     |
#     | c_r1                                          |
#     |                                               |
#     |-----------------------------------------------| r=r0
#     |                                               |
#     |                                               |
#     |---------- symmetrieachse ---------------------| r=0
#
#
#
# die loesungen der diffusionsgleichung in den radialen abschnitten:
# !!! kohlendioxid !!!
#
#     | C_r3
#     |-----------------------------------------------| r=r3
#     | boundary layer                                |
#     |                                               |
Cbl:=r -> Abl+Bbl*ln(r/R);
Jbl:=unapply(-Sbl*D(Cbl)(r),r);
#     |                                               |
#     |-----------------------------------------------| r=R
#     | stomata                                       |
#     |                                               |
Cst:=r -> Ast+Bst*ln(r/R);
Jst:=unapply(-Sst*D(Cst)(r),r);
#     |                                               |
#     |-------------------------                      | r=r2
#     | hypodermis                                    |
#     |                                               |
Chyp:=r -> Ahyp+Bhyp*ln(r/R);
Jhyp:=unapply(-Shyp*D(Chyp)(r),r);
#     |                                               |
#     |-----------------------------------------------| r=r1
#     | mesophyll                                     |
#     |                                               |
C2:=r -> A2+B2*ln(r/R)+chi/4*r^2;
J2:=unapply(-Sias*D(C2)(r),r);
#     |                                               |
#     |                                               |
C1:=r -> A1*BesselI(0,k*r)+B1*BesselK(0,k*r)+kappa/k^2;
J1:=unapply(-Sias*D(C1)(r),r);
#     |                                               |
#     |-----------------------------------------------| r=r0
#     |                                               |
#     |                                               |
#     |---------- symmetrieachse ---------------------| r=0
#
#
# die oben aufgefuehrten physikalischen, morphologischen und
# pflanzenphysiologischen parameter stecken alle in den "effektiven
# leitfaehigkeiten" Si und si sowie in den konstanten k,
# kappa und chi drinnen
```

```
#
# die nun folgenden rand- und stetigkeitsbedingungen dienen dazu, die
# integrationskonstanten Ai,ai,bi und Bi durch Si, si, k, kappa, chi und r0,
# rc, r1, r2, R und r3 auszudruecken
# *********************************************************************
# randbedingungen:
#
# die konzentrationen an der aussenkante des boundary layers (bei r=r3)
# sind vorgegeben:
#
# wasserdampf:
#
e1:=cbl(r3)=c_r3;
#
# ebenso an der aussenkante des mesophylls (bei r=r1)
#
e2:=chyp(r1)=c_r1;
#
# kohlendioxid:
#
e3:=Cbl(r3)=C_r3;
#
# an der innenkante des mesophylls (bei r=r0) soll der (radial zur
# symmetrieachse hin gerichtete) CO2-strom gegen null gehen:
#
e4:=J1(r0)=0;
#
# *********************************************************************
# stetigkeitsbedingungen an den inneren grenzflaechen:
#
# wasserdampf-konzentrationen:
#
# grenze hypodermis/stomata (bei r=r2):
e5:=chyp(r2)=cst(r2);
#
# grenze stomata/boundary layer (bei r=R):
e6:=cst(R)=cbl(R);
#
# CO2-konzentrationen:
#
# grenze mesophyll 1 / mesophyll 2 (bei r=rc):
e7:=C1(rc)=C2(rc);
#
# grenze mesophyll 2 / hypodermis (bei r=r1):
e9:=C2(r1)=Chyp(r1);
#
# grenze hypodermis/epidermis (bei r=r2):
e10:=Chyp(r2)=Cst(r2);
#
# grenze epidermis/boundary layer (bei r=R):
e11:=Cst(R)=Cbl(R);
#
# ----------------------------------------------------------------
# stetigkeitsbedingungen fuer die stromdichten an den inneren grenzflaechen:
#
# wasserdampf:
#
# grenze hypodermis/stomata (bei r=r2):
e12:=jhyp(r2)=jst(r2);
#
# grenze stomata/boundary layer (bei r=R):
e13:=jst(R)=jbl(R);
#
```

```
# CO2:
#
# grenze mesophyll 1 / mesophyll 2 (bei r=rc):
e14:=J1(rc)=J2(rc);
#
# grenze mesophyll 2 / hypodermis-cuticula (bei r=r1):
e16:=J2(r1)=Jhyp(r1);
#
# grenze hypodermis/stomata (bei r=r2):
e17:=Jhyp(r2)=Jst(r2);
#
# grenze stomata/boundary layer (bei r=R):
e18:=Jst(R)=Jbl(R);
#
# ***********************************************************************
# das sind 16 gleichungen:
eq:={e1,e2,e3,e4,e5,e6,e7,e9,e10,e11,e12,e13,e14,e16,e17,e18};
#
# fuer 16 unbekannte groessen:
leq:={ahyp,ast,abl,bhyp,bst,bbl,A1,A2,Ahyp,Ast,Abl,B1,B2,Bhyp,Bst,Bbl};
#
# maple bekommt den befehl, das gleichungssystem eq nach leq aufzuloesen:
sol:=solve(eq,leq);
#
assign(sol); # programmiertechnischer befehl
#
# -------------------------------------------------------------------
# jetzt muss maple die loesungen der einzelnen radialen abschnitte
# zu einer gesamtloesung fuer die konzentrationen durch die pflanze
# hindurch zusammensetzen.
#
# wasserdampf:
#
cr1:=r -> c_r1;
cr3:=r -> c_r3;
#
c:=r -> piecewise(r>r3,undefined,r>R,cbl(r),r>r2,cst(r),\
r>r1,chyp(r),r=r1,cr1(r));
#
cn:=r -> evalf(simplify(c(r)));
#
# CO2:
#
Cr0:=r -> evalf(C1(r0));
Cr3:=r -> C_r3;
#
#C:=r -> C1(r0)*Hl(r,r0)+C1(r)*H(r,r0,rc)+C2(r)*H(r,rc,r1)\
#+Chyp(r)*H(r,r1,r2)+Cst(r)*H(r,r2,R)+Cbl(r)*H(r,R,r3)+C_r3*Hr(r,r3);
#
C:=r -> piecewise(r>r3,undefined,r>R,Cbl(r),r>r2,Cst(r),\
r>r1,Chyp(r),r>rc,C2(r),r>r0,C1(r),r=r0,Cr0(r));
#
Cn:=r -> evalf(simplify(C(r)));
#
# -------------------------------------------------------------------
# sowie die stroeme durch boundary layer, stomata, hypodermis und mesophyll:
#
# wasserdampf:
#
j:=r -> piecewise(r>r3,undefined,r>R,jbl(r),r>r2,jst(r),r>r1,jhyp(r));
#
jn:=r -> evalf(simplify(j(r)));
#
```

```
# CO2:
#
Jr0:=r -> evalf(J1(r0));
#
J:=r -> piecewise(r>r3,undefined,r>R,Jbl(r),r>r2,Jst(r),r>r1,Jhyp(r),\
r>rc,J2(r),r>r0,J1(r),r=r0,Jr0(r));
#
Jn:=r -> evalf(simplify(J(r)));
#
# ----------------------------------------------------------------
save c,cn,cr1,cr3,chyp,cst,cbl,j,jn,jhyp,jst,jbl,C,Cn,Cr0,Cr3,\
C1,C2,Chyp,Cst,Cbl,J,Jn,Jr0,J1,J2,Jhyp,Jst,Jbl,ahyp,ast,abl,bhyp,bst,bbl,\
A1,A2,Ahyp,Ast,Abl,B1,B2,Bhyp,Bst,Bbl,diffsol;
#
save c,cn,cr1,cr3,chyp,cst,cbl,j,jn,jhyp,jst,jbl,C,Cn,Cr0,Cr3,\
C1,C2,Chyp,Cst,Cbl,J,Jn,Jr0,J1,J2,Jhyp,Jst,Jbl,ahyp,ast,abl,bhyp,bst,bbl,\
A1,A2,Ahyp,Ast,Abl,B1,B2,Bhyp,Bst,Bbl,'diffsol.m';
#
# *********************************************************************
#
```

File diffsol:

```
c := proc (r) options operator, arrow; piecewise(r3 < r,undefined,R < r,cbl(
r),r2 < r,cst(r),r1 < r,chyp(r),r = r1,cr1(r)) end;
cn := proc (r) options operator, arrow; evalf(simplify(c(r))) end;
cr1 := proc (r) options operator, arrow; c_r1 end;
cr3 := proc (r) options operator, arrow; c_r3 end;
chyp := proc (r) options operator, arrow; ahyp+bhyp*ln(r/R) end;
cst := proc (r) options operator, arrow; ast+bst*ln(r/R) end;
cbl := proc (r) options operator, arrow; abl+bbl*ln(r/R) end;
j := proc (r) options operator, arrow; piecewise(r3 < r,undefined,R < r,jbl(
r),r2 < r,jst(r),r1 < r,jhyp(r)) end;
jn := proc (r) options operator, arrow; evalf(simplify(j(r))) end;
jhyp := proc (r) options operator, arrow; -shyp*bhyp/r end;
jst := proc (r) options operator, arrow; -sst*bst/r end;
jbl := proc (r) options operator, arrow; -sbl*bbl/r end;
H := proc (x, a, b) options operator, arrow; Heaviside((x-a)/R)-Heaviside((x
-b)/R) end;
Hl := proc (x, a) options operator, arrow; 1-Heaviside((x-a)/R) end;
Hr := proc (x, b) options operator, arrow; Heaviside((x-b)/R) end;
C := proc (r) options operator, arrow; piecewise(r3 < r,undefined,R < r,Cbl(
r),r2 < r,Cst(r),r1 < r,Chyp(r),rc < r,C2(r),r0 < r,C1(r),r = r0,Cr0(r)) end
;
Cn := proc (r) options operator, arrow; evalf(simplify(C(r))) end;
Cr0 := proc (r) options operator, arrow; evalf(C1(r0)) end;
Cr3 := proc (r) options operator, arrow; C_r3 end;
C1 := proc (r) options operator, arrow; A1*BesselI(0,k*r)+B1*BesselK(0,k*r)+
kappa/k^2 end;
C2 := proc (r) options operator, arrow; A2+B2*ln(r/R)+1/4*chi*r^2 end;
Chyp := proc (r) options operator, arrow; Ahyp+Bhyp*ln(r/R) end;
Cst := proc (r) options operator, arrow; Ast+Bst*ln(r/R) end;
Cbl := proc (r) options operator, arrow; Abl+Bbl*ln(r/R) end;
J := proc (r) options operator, arrow; piecewise(r3 < r,undefined,R < r,Jbl(
r),r2 < r,Jst(r),r1 < r,Jhyp(r),rc < r,J2(r),r0 < r,J1(r),r = r0,Jr0(r)) end
;
Jn := proc (r) options operator, arrow; evalf(simplify(J(r))) end;
Jr0 := proc (r) options operator, arrow; evalf(J1(r0)) end;
J1 := proc (r) options operator, arrow; -Sias*(A1*BesselI(1,k*r)*k-B1*
BesselK(1,k*r)*k) end;
J2 := proc (r) options operator, arrow; -Sias*(B2/r+1/2*chi*r) end;
Jhyp := proc (r) options operator, arrow; -Shyp*Bhyp/r end;
```

```
Jst := proc (r) options operator, arrow; -Sst*Bst/r end;
Jbl := proc (r) options operator, arrow; -Sbl*Bbl/r end;
ahyp := (c_r3*sbl*ln(r1/R)*sst-shyp*ln(r3/R)*sst*c_r1-c_r1*sbl*ln(r2/R)*sst+
c_r1*sbl*shyp*ln(r2/R))/(-shyp*ln(r3/R)*sst+sbl*ln(r1/R)*sst-sbl*ln(r2/R)*
sst+sbl*shyp*ln(r2/R));
ast := (-shyp*ln(r3/R)*sst*c_r1+c_r3*sbl*ln(r1/R)*sst-c_r3*sbl*ln(r2/R)*sst+
c_r3*sbl*shyp*ln(r2/R))/(-shyp*ln(r3/R)*sst+sbl*ln(r1/R)*sst-sbl*ln(r2/R)*
sst+sbl*shyp*ln(r2/R));
abl := (-shyp*ln(r3/R)*sst*c_r1+c_r3*sbl*ln(r1/R)*sst-c_r3*sbl*ln(r2/R)*sst+
c_r3*sbl*shyp*ln(r2/R))/(-shyp*ln(r3/R)*sst+sbl*ln(r1/R)*sst-sbl*ln(r2/R)*
sst+sbl*shyp*ln(r2/R));
bhyp := -sbl*sst*(c_r3-c_r1)/(-shyp*ln(r3/R)*sst+sbl*ln(r1/R)*sst-sbl*ln(r2/
R)*sst+sbl*shyp*ln(r2/R));
bst := -shyp*sbl*(c_r3-c_r1)/(-shyp*ln(r3/R)*sst+sbl*ln(r1/R)*sst-sbl*ln(r2/
R)*sst+sbl*shyp*ln(r2/R));
bbl := -sst*shyp*(c_r3-c_r1)/(-shyp*ln(r3/R)*sst+sbl*ln(r1/R)*sst-sbl*ln(r2/
R)*sst+sbl*shyp*ln(r2/R));
A1 := -1/4/(-Sst*Sbl*k*rc*ln(rc/R)*Shyp*BesselK(1,k*rc)*BesselI(1,k*r0)+Sst*
Sbl*k*rc*ln(rc/R)*Shyp*BesselK(1,k*r0)*BesselI(1,k*rc)-Sst*Sbl*k*rc*Sias*ln(
r1/R)*BesselK(1,k*rc)*BesselI(1,k*r0)+Sst*Sbl*k*rc*Sias*ln(r1/R)*BesselK(1,k
*r0)*BesselI(1,k*rc)+Sst*Sbl*k*rc*ln(r1/R)*Shyp*BesselK(1,k*rc)*BesselI(1,k*
r0)-Sst*Sbl*k*rc*ln(r1/R)*Shyp*BesselK(1,k*r0)*BesselI(1,k*rc)-Sst*Sbl*Shyp*
BesselK(0,k*rc)*BesselI(1,k*r0)-Sst*Sbl*Shyp*BesselK(1,k*r0)*BesselI(0,k*rc)
+Sias*rc*k*ln(r2/R)*Sbl*Sst*BesselK(1,k*rc)*BesselI(1,k*r0)-Sias*rc*k*ln(r2/
R)*Sbl*Sst*BesselK(1,k*r0)*BesselI(1,k*rc)-Sias*rc*k*ln(r2/R)*Sbl*Shyp*
BesselK(1,k*rc)*BesselI(1,k*r0)+Sias*rc*k*ln(r2/R)*Sbl*Shyp*BesselK(1,k*r0)*
BesselI(1,k*rc)+Sias*rc*k*Shyp*ln(r3/R)*Sst*BesselK(1,k*rc)*BesselI(1,k*r0)-
Sias*rc*k*Shyp*ln(r3/R)*Sst*BesselK(1,k*r0)*BesselI(1,k*rc))*(2*k^2*Sias*chi
*rc^2*ln(r2/R)*Sbl*Sst-2*k^2*Sias*chi*rc^2*ln(r2/R)*Sbl*Shyp+2*k^2*Sias*chi*
rc^2*Shyp*ln(r3/R)*Sst-2*k^2*r1^2*Sias*chi*ln(r2/R)*Sbl*Sst+2*k^2*r1^2*Sias*
chi*ln(r2/R)*Sbl*Shyp-2*k^2*r1^2*Sias*chi*Shyp*ln(r3/R)*Sst+4*k^2*C_r3*Sst*
Sbl*Shyp-2*Sst*Sbl*chi*rc^2*k^2*ln(rc/R)*Shyp-2*Sst*Sbl*chi*rc^2*k^2*Sias*ln
(r1/R)+2*Sst*Sbl*chi*rc^2*k^2*ln(r1/R)*Shyp+2*Sst*Sbl*chi*r1^2*k^2*Sias*ln(
r1/R)-Sst*Sbl*chi*r1^2*k^2*Shyp+Sst*Sbl*Shyp*chi*rc^2*k^2-4*Sst*Sbl*Shyp*
kappa)/k^2*BesselK(1,k*r0);
A2 := 1/4*(-4*C_r3*Sst*Sbl*Shyp*k^2*rc*ln(rc/R)*BesselK(1,k*rc)*BesselI(1,k*
r0)+2*k*r1^2*Sias*chi*ln(r2/R)*Sbl*Sst*BesselK(0,k*rc)*BesselI(1,k*r0)+2*k*
r1^2*Sias*chi*ln(r2/R)*Sbl*Sst*BesselK(1,k*rc)*BesselI(0,k*r0)-2*k*r1^2*Sias
*chi*ln(r2/R)*Sbl*Shyp*BesselK(0,k*rc)*BesselI(1,k*r0)-2*k*Sias*chi*rc^2*
Shyp*ln(r3/R)*Sst*BesselK(0,k*rc)*BesselI(1,k*r0)-2*k*Sias*chi*rc^2*Shyp*ln(
r3/R)*Sst*BesselK(1,k*r0)*BesselI(0,k*rc)+2*k*Sias*chi*rc^2*ln(r2/R)*Sbl*
Shyp*BesselK(0,k*rc)*BesselI(1,k*r0)+2*k*Sias*chi*rc^2*ln(r2/R)*Sbl*Shyp*
BesselK(1,k*r0)*BesselI(0,k*rc)-2*k*Sias*chi*rc^2*ln(r2/R)*Sbl*Sst*BesselK(0
,k*rc)*BesselI(1,k*r0)-2*k*Sias*chi*rc^2*ln(r2/R)*Sbl*Sst*BesselK(1,k*r0)*
BesselI(0,k*rc)-2*r1^2*Sias*chi*ln(r2/R)*Sbl*Shyp*k^2*rc*ln(rc/R)*BesselK(1,
k*rc)*BesselI(1,k*r0)-4*Sias*rc*Shyp*ln(r3/R)*Sst*BesselK(1,k*r0)*BesselI(1,
k*rc)*kappa+2*r1^2*Sias*chi*ln(r2/R)*Sbl*Sst*k^2*rc*ln(rc/R)*BesselK(1,k*rc)
*BesselI(1,k*r0)-2*r1^2*Sias*chi*ln(r2/R)*Sbl*Sst*k^2*rc*ln(rc/R)*BesselK(1,
k*r0)*BesselI(1,k*rc)-4*k*C_r3*Sst*Sbl*Shyp*BesselK(1,k*r0)*BesselI(0,k*rc)+
2*r1^2*Sias*chi*Shyp*ln(r3/R)*Sst*k^2*rc*ln(rc/R)*BesselK(1,k*rc)*BesselI(1,
k*r0)-2*r1^2*Sias*chi*Shyp*ln(r3/R)*Sst*k^2*rc*ln(rc/R)*BesselK(1,k*r0)*
BesselI(1,k*rc)-4*k*C_r3*Sst*Sbl*Shyp*BesselK(0,k*rc)*BesselI(1,k*r0)-Sias*
rc^3*ln(r2/R)*Sbl*Shyp*BesselK(1,k*r0)*BesselI(1,k*rc)*chi*k^2+2*k*r1^2*Sias
*chi*Shyp*ln(r3/R)*Sst*BesselK(1,k*r0)*BesselI(0,k*rc)-2*k*r1^2*Sias*chi*ln(
r2/R)*Sbl*Shyp*BesselK(1,k*r0)*BesselI(0,k*rc)+Sias*rc^3*ln(r2/R)*Sbl*Shyp*
BesselK(1,k*rc)*BesselI(1,k*r0)*chi*k^2-Sias*rc^3*ln(r2/R)*Sbl*Sst*BesselK(1
,k*rc)*BesselI(1,k*r0)*chi*k^2+4*Sias*rc*ln(r2/R)*Sbl*Sst*BesselK(1,k*rc)*
BesselI(1,k*r0)*kappa+4*Sias*rc*ln(r2/R)*Sbl*Shyp*BesselK(1,k*r0)*BesselI(1,
k*rc)*kappa+Sias*rc^3*ln(r2/R)*Sbl*Sst*BesselK(1,k*r0)*BesselI(1,k*rc)*chi*k
^2-4*Sias*rc*ln(r2/R)*Sbl*Sst*BesselK(1,k*r0)*BesselI(1,k*rc)*kappa-4*Sias*
rc*ln(r2/R)*Sbl*Shyp*BesselK(1,k*rc)*BesselI(1,k*r0)*kappa+2*k*r1^2*Sias*chi
*Shyp*ln(r3/R)*Sst*BesselK(0,k*rc)*BesselI(1,k*r0)+2*r1^2*Sias*chi*ln(r2/R)*
Sbl*Shyp*k^2*rc*ln(rc/R)*BesselK(1,k*r0)*BesselI(1,k*rc)+4*C_r3*Sst*Sbl*Shyp
```

```
*k^2*rc*ln(rc/R)*BesselK(1,k*r0)*BesselI(1,k*rc)-Sias*rc^3*Shyp*ln(r3/R)*Sst
*BesselK(1,k*rc)*BesselI(1,k*r0)*chi*k^2+4*Sias*rc*Shyp*ln(r3/R)*Sst*BesselK
(1,k*rc)*BesselI(1,k*r0)*kappa+Sias*rc^3*Shyp*ln(r3/R)*Sst*BesselK(1,k*r0)*
BesselI(1,k*rc)*chi*k^2-ln(r1/R)*rc^3*BesselK(1,k*rc)*BesselI(1,k*r0)*Sst*
Sbl*Shyp*chi*k^2+4*ln(r1/R)*rc*BesselK(1,k*rc)*BesselI(1,k*r0)*Sst*Sbl*Shyp*
kappa+ln(r1/R)*rc^3*BesselK(1,k*r0)*BesselI(1,k*rc)*Sst*Sbl*Shyp*chi*k^2-4*
ln(r1/R)*rc*BesselK(1,k*r0)*BesselI(1,k*rc)*Sst*Sbl*Shyp*kappa-2*ln(r1/R)*rc
^2*chi*k*Sst*Sbl*Shyp*BesselK(0,k*rc)*BesselI(1,k*r0)-2*ln(r1/R)*rc^2*chi*k*
Sst*Sbl*Shyp*BesselK(1,k*r0)*BesselI(0,k*rc)+ln(r1/R)*rc^3*Sias*BesselK(1,k*
rc)*BesselI(1,k*r0)*Sst*Sbl*chi*k^2-4*ln(r1/R)*rc*Sias*BesselK(1,k*rc)*
BesselI(1,k*r0)*Sst*Sbl*kappa-ln(r1/R)*rc^3*Sias*BesselK(1,k*r0)*BesselI(1,k
*rc)*Sst*Sbl*chi*k^2+4*ln(r1/R)*rc*Sias*BesselK(1,k*r0)*BesselI(1,k*rc)*Sst*
Sbl*kappa+2*ln(r1/R)*rc^2*Sias*chi*k*Sst*Sbl*BesselK(0,k*rc)*BesselI(1,k*r0)
+2*ln(r1/R)*rc^2*Sias*chi*k*Sst*Sbl*BesselK(1,k*rc)*BesselI(0,k*rc)-2*chi*r1
^2*k^2*Sias*ln(r1/R)*Sst*Sbl*rc*ln(rc/R)*BesselK(1,k*rc)*BesselI(1,k*r0)+2*
chi*r1^2*k^2*Sias*ln(r1/R)*Sst*Sbl*rc*ln(rc/R)*BesselK(1,k*r0)*BesselI(1,k*
rc)-2*chi*r1^2*k*Sias*ln(r1/R)*Sst*Sbl*BesselK(0,k*rc)*BesselI(1,k*r0)-2*chi
*r1^2*k*Sias*ln(r1/R)*Sst*Sbl*BesselK(1,k*r0)*BesselI(0,k*rc)+chi*r1^2*k^2*
Sst*Sbl*rc*ln(rc/R)*Shyp*BesselK(1,k*rc)*BesselI(1,k*r0)-chi*r1^2*k^2*Sst*
Sbl*rc*ln(rc/R)*Shyp*BesselK(1,k*r0)*BesselI(1,k*rc)+chi*r1^2*k*Sst*Sbl*Shyp
*BesselK(0,k*rc)*BesselI(1,k*r0)+chi*r1^2*k*Sst*Sbl*Shyp*BesselK(1,k*r0)*
BesselI(0,k*rc))/k/(-Sst*Sbl*k*rc*ln(rc/R)*Shyp*BesselK(1,k*rc)*BesselI(1,k*
r0)+Sst*Sbl*k*rc*ln(rc/R)*Shyp*BesselK(1,k*r0)*BesselI(1,k*rc)-Sst*Sbl*k*rc*
Sias*ln(r1/R)*BesselK(1,k*rc)*BesselI(1,k*r0)+Sst*Sbl*k*rc*Sias*ln(r1/R)*
BesselK(1,k*r0)*BesselI(1,k*rc)+Sst*Sbl*k*rc*ln(r1/R)*Shyp*BesselK(1,k*rc)*
BesselI(1,k*r0)-Sst*Sbl*k*rc*ln(r1/R)*Shyp*BesselK(1,k*r0)*BesselI(1,k*rc)-
Sst*Sbl*Shyp*BesselK(0,k*rc)*BesselI(1,k*r0)-Sst*Sbl*Shyp*BesselK(1,k*r0)*
BesselI(0,k*rc)+Sias*rc*k*ln(r2/R)*Sbl*Sst*BesselK(1,k*rc)*BesselI(1,k*r0)-
Sias*rc*k*ln(r2/R)*Sbl*Sst*BesselK(1,k*r0)*BesselI(1,k*rc)-Sias*rc*k*ln(r2/R
)*Sbl*Shyp*BesselK(1,k*rc)*BesselI(1,k*r0)+Sias*rc*k*ln(r2/R)*Sbl*Shyp*
BesselK(1,k*r0)*BesselI(1,k*rc)+Sias*rc*k*Shyp*ln(r3/R)*Sst*BesselK(1,k*rc)*
BesselI(1,k*r0)-Sias*rc*k*Shyp*ln(r3/R)*Sst*BesselK(1,k*r0)*BesselI(1,k*rc))
;
Ahyp := 1/4*(-4*C_r3*Sst*Sbl*Shyp*k^2*rc*ln(rc/R)*BesselK(1,k*rc)*BesselI(1,
k*r0)+2*k*r1^2*Sias*chi*ln(r2/R)*Sbl*Sst*BesselK(0,k*rc)*BesselI(1,k*r0)+2*k
*r1^2*Sias*chi*ln(r2/R)*Sbl*Sst*BesselK(1,k*r0)*BesselI(0,k*rc)-2*k*r1^2*
Sias*chi*ln(r2/R)*Sbl*Shyp*BesselK(0,k*rc)*BesselI(1,k*r0)-2*k*Sias*chi*rc^2
*Shyp*ln(r3/R)*Sst*BesselK(0,k*rc)*BesselI(1,k*r0)-2*k*Sias*chi*rc^2*Shyp*ln
(r3/R)*Sst*BesselK(1,k*r0)*BesselI(0,k*rc)+2*k*Sias*chi*rc^2*ln(r2/R)*Sbl*
Shyp*BesselK(0,k*rc)*BesselI(1,k*r0)+2*k*Sias*chi*rc^2*ln(r2/R)*Sbl*Shyp*
BesselK(1,k*r0)*BesselI(0,k*rc)-2*k*Sias*chi*rc^2*ln(r2/R)*Sbl*Sst*BesselK(0
,k*rc)*BesselI(1,k*r0)-2*k*Sias*chi*rc^2*ln(r2/R)*Sbl*Sst*BesselK(1,k*r0)*
BesselI(0,k*rc)-2*r1^2*Sias*chi*ln(r2/R)*Sbl*Shyp*k^2*rc*ln(rc/R)*BesselK(1,
k*rc)*BesselI(1,k*r0)-4*Sias*rc*Shyp*ln(r3/R)*Sst*BesselK(1,k*r0)*BesselI(1,
k*rc)*kappa+2*r1^2*Sias*chi*ln(r2/R)*Sbl*Sst*k^2*rc*ln(rc/R)*BesselK(1,k*rc)
*BesselI(1,k*r0)-2*r1^2*Sias*chi*ln(r2/R)*Sbl*Sst*k^2*rc*ln(rc/R)*BesselK(1,
k*r0)*BesselI(1,k*rc)-4*k*C_r3*Sst*Sbl*Shyp*BesselK(1,k*r0)*BesselI(0,k*rc)+
2*r1^2*Sias*chi*ln(r2/R)*Sbl*Shyp*k^2*rc*ln(r1/R)*BesselK(1,k*rc)*BesselI(1,
k*r0)-2*r1^2*Sias*chi*ln(r2/R)*Sbl*Shyp*k^2*rc*ln(r1/R)*BesselK(1,k*r0)*
BesselI(1,k*rc)+2*r1^2*Sias*chi*Shyp*ln(r3/R)*Sst*k^2*rc*ln(rc/R)*BesselK(1,
k*rc)*BesselI(1,k*r0)-2*r1^2*Sias*chi*Shyp*ln(r3/R)*Sst*k^2*rc*ln(rc/R)*
BesselK(1,k*r0)*BesselI(1,k*rc)-2*r1^2*Sias*chi*ln(r2/R)*Sbl*Sst*k^2*rc*ln(
r1/R)*BesselK(1,k*rc)*BesselI(1,k*r0)+2*r1^2*Sias*chi*ln(r2/R)*Sbl*Sst*k^2*
rc*ln(r1/R)*BesselK(1,k*r0)*BesselI(1,k*rc)-2*r1^2*Sias*chi*Shyp*ln(r3/R)*
Sst*k^2*rc*ln(r1/R)*BesselK(1,k*rc)*BesselI(1,k*r0)-4*k*C_r3*Sst*Sbl*Shyp*
BesselK(0,k*rc)*BesselI(1,k*r0)-Sias*rc^3*ln(r2/R)*Sbl*Shyp*BesselK(1,k*r0)*
BesselI(1,k*rc)*chi*k^2+2*k*r1^2*Sias*chi*Shyp*ln(r3/R)*Sst*BesselK(1,k*r0)*
BesselI(0,k*rc)-2*k*r1^2*Sias*chi*ln(r2/R)*Sbl*Shyp*BesselK(1,k*r0)*BesselI(
0,k*rc)-4*C_r3*Sst*Sbl*k^2*rc*Sias*ln(r1/R)*BesselK(1,k*rc)*BesselI(1,k*r0)+
4*C_r3*Sst*Sbl*k^2*rc*Sias*ln(r1/R)*BesselK(1,k*r0)*BesselI(1,k*rc)+4*C_r3*
Sst*Sbl*Shyp*k^2*rc*ln(r1/R)*BesselK(1,k*rc)*BesselI(1,k*r0)-4*C_r3*Sst*Sbl*
Shyp*k^2*rc*ln(r1/R)*BesselK(1,k*r0)*BesselI(1,k*rc)-Sias*rc*ln(r2/R)*Sbl*
Shyp*BesselK(1,k*rc)*BesselI(1,k*r0)*chi*r1^2*k^2+Sias*rc^3*ln(r2/R)*Sbl*
```

```
Shyp*BesselK(1,k*rc)*BesselI(1,k*r0)*chi*k^2+Sias*rc*ln(r2/R)*Sbl*Sst*
BesselK(1,k*rc)*BesselI(1,k*r0)*chi*r1^2*k^2-Sias*rc^3*ln(r2/R)*Sbl*Sst*
BesselK(1,k*rc)*BesselI(1,k*r0)*chi*k^2+4*Sias*rc*ln(r2/R)*Sbl*Sst*BesselK(1
,k*rc)*BesselI(1,k*r0)*kappa+4*Sias*rc*ln(r2/R)*Sbl*Shyp*BesselK(1,k*r0)*
BesselI(1,k*rc)*kappa-Sias*rc*ln(r2/R)*Sbl*Sst*BesselK(1,k*r0)*BesselI(1,k*
rc)*chi*r1^2*k^2+Sias*rc^3*ln(r2/R)*Sbl*Sst*BesselK(1,k*r0)*BesselI(1,k*rc)*
chi*k^2-4*Sias*rc*ln(r2/R)*Sbl*Sst*BesselK(1,k*r0)*BesselI(1,k*rc)*kappa-4*
Sias*rc*ln(r2/R)*Sbl*Shyp*BesselK(1,k*rc)*BesselI(1,k*r0)*kappa+Sias*rc*ln(
r2/R)*Sbl*Shyp*BesselK(1,k*r0)*BesselI(1,k*rc)*chi*r1^2*k^2+Sias*rc*Shyp*ln(
r3/R)*Sst*BesselK(1,k*rc)*BesselI(1,k*r0)*chi*r1^2*k^2-Sias*rc*Shyp*ln(r3/R)
*Sst*BesselK(1,k*r0)*BesselI(1,k*rc)*chi*r1^2*k^2+2*k*r1^2*Sias*chi*Shyp*ln(
r3/R)*Sst*BesselK(0,k*rc)*BesselI(1,k*r0)+2*r1^2*Sias*chi*ln(r2/R)*Sbl*Shyp*
k^2*rc*ln(rc/R)*BesselK(1,k*r0)*BesselI(1,k*rc)+4*C_r3*Sst*Sbl*Shyp*k^2*rc*
ln(rc/R)*BesselK(1,k*r0)*BesselI(1,k*rc)-Sias*rc^3*Shyp*ln(r3/R)*Sst*BesselK
(1,k*rc)*BesselI(1,k*r0)*chi*k^2+4*Sias*rc*Shyp*ln(r3/R)*Sst*BesselK(1,k*rc)
*BesselI(1,k*r0)*kappa+Sias*rc^3*Shyp*ln(r3/R)*Sst*BesselK(1,k*r0)*BesselI(1
,k*rc)*chi*k^2+2*r1^2*Sias*chi*Shyp*ln(r3/R)*Sst*k^2*rc*ln(r1/R)*BesselK(1,k
*r0)*BesselI(1,k*rc))/k/(-Sst*Sbl*k*rc*ln(rc/R)*Shyp*BesselK(1,k*rc)*BesselI
(1,k*r0)+Sst*Sbl*k*rc*ln(rc/R)*Shyp*BesselK(1,k*r0)*BesselI(1,k*rc)-Sst*Sbl*
k*rc*Sias*ln(r1/R)*BesselK(1,k*rc)*BesselI(1,k*r0)+Sst*Sbl*k*rc*Sias*ln(r1/R
)*BesselK(1,k*r0)*BesselI(1,k*rc)+Sst*Sbl*k*rc*ln(r1/R)*Shyp*BesselK(1,k*rc)
*BesselI(1,k*r0)-Sst*Sbl*k*rc*ln(r1/R)*Shyp*BesselK(1,k*r0)*BesselI(1,k*rc)-
Sst*Sbl*Shyp*BesselK(0,k*rc)*BesselI(1,k*r0)-Sst*Sbl*Shyp*BesselK(1,k*r0)*
BesselI(0,k*rc)+Sias*rc*k*ln(r2/R)*Sbl*Sst*BesselK(1,k*rc)*BesselI(1,k*r0)-
Sias*rc*k*ln(r2/R)*Sbl*Sst*BesselK(1,k*r0)*BesselI(1,k*rc)-Sias*rc*k*ln(r2/R
)*Sbl*Shyp*BesselK(1,k*rc)*BesselI(1,k*r0)+Sias*rc*k*ln(r2/R)*Sbl*Shyp*
BesselK(1,k*r0)*BesselI(1,k*rc)+Sias*rc*k*Shyp*ln(r3/R)*Sst*BesselK(1,k*rc)*
BesselI(1,k*r0)-Sias*rc*k*Shyp*ln(r3/R)*Sst*BesselK(1,k*r0)*BesselI(1,k*rc))
;
Ast := 1/4*(4*C_r3*k^2*Sias*rc*ln(r2/R)*Sbl*Sst*BesselK(1,k*rc)*BesselI(1,k*
r0)-4*C_r3*k^2*Sias*rc*ln(r2/R)*Sbl*Shyp*BesselK(1,k*rc)*BesselI(1,k*r0)+4*
C_r3*k^2*Sias*rc*ln(r2/R)*Sbl*Shyp*BesselK(1,k*r0)*BesselI(1,k*rc)-4*C_r3*k^
2*Sias*rc*ln(r2/R)*Sbl*Sst*BesselK(1,k*r0)*BesselI(1,k*rc)-4*C_r3*Sst*Sbl*
Shyp*k^2*rc*ln(rc/R)*BesselK(1,k*rc)*BesselI(1,k*r0)-2*k*Sias*chi*rc^2*Shyp*
ln(r3/R)*Sst*BesselK(0,k*rc)*BesselI(1,k*r0)-2*k*Sias*chi*rc^2*Shyp*ln(r3/R)
*Sst*BesselK(1,k*r0)*BesselI(0,k*rc)-4*Sias*rc*Shyp*ln(r3/R)*Sst*BesselK(1,k
*r0)*BesselI(1,k*rc)*kappa-4*k*C_r3*Sst*Sbl*Shyp*BesselK(1,k*r0)*BesselI(0,k
*rc)+2*r1^2*Sias*chi*Shyp*ln(r3/R)*Sst*k^2*rc*ln(rc/R)*BesselK(1,k*rc)*
BesselI(1,k*r0)-2*r1^2*Sias*chi*Shyp*ln(r3/R)*Sst*k^2*rc*ln(rc/R)*BesselK(1,
k*r0)*BesselI(1,k*rc)-2*r1^2*Sias*chi*Shyp*ln(r3/R)*Sst*k^2*rc*ln(r1/R)*
BesselK(1,k*rc)*BesselI(1,k*r0)-4*k*C_r3*Sst*Sbl*Shyp*BesselK(0,k*rc)*
BesselI(1,k*r0)+2*k*r1^2*Sias*chi*Shyp*ln(r3/R)*Sst*BesselK(1,k*r0)*BesselI(
0,k*rc)-4*C_r3*Sst*Sbl*k^2*rc*Sias*ln(r1/R)*BesselK(1,k*rc)*BesselI(1,k*r0)+
4*C_r3*Sst*Sbl*k^2*rc*Sias*ln(r1/R)*BesselK(1,k*r0)*BesselI(1,k*rc)+4*C_r3*
Sst*Sbl*Shyp*k^2*rc*ln(r1/R)*BesselK(1,k*rc)*BesselI(1,k*r0)-4*C_r3*Sst*Sbl*
Shyp*k^2*rc*ln(r1/R)*BesselK(1,k*r0)*BesselI(1,k*rc)+Sias*rc*Shyp*ln(r3/R)*
Sst*BesselK(1,k*rc)*BesselI(1,k*r0)*chi*r1^2*k^2-Sias*rc*Shyp*ln(r3/R)*Sst*
BesselK(1,k*r0)*BesselI(1,k*rc)*chi*r1^2*k^2+2*k*r1^2*Sias*chi*Shyp*ln(r3/R)
*Sst*BesselK(0,k*rc)*BesselI(1,k*r0)+4*C_r3*Sst*Sbl*Shyp*k^2*rc*ln(rc/R)*
BesselK(1,k*r0)*BesselI(1,k*rc)-Sias*rc^3*Shyp*ln(r3/R)*Sst*BesselK(1,k*rc)*
BesselI(1,k*r0)*chi*k^2+4*Sias*rc*Shyp*ln(r3/R)*Sst*BesselK(1,k*rc)*BesselI(
1,k*r0)*kappa+Sias*rc^3*Shyp*ln(r3/R)*Sst*BesselK(1,k*r0)*BesselI(1,k*rc)*
chi*k^2+2*r1^2*Sias*chi*Shyp*ln(r3/R)*Sst*k^2*rc*ln(r1/R)*BesselK(1,k*r0)*
BesselI(1,k*rc))/k/(-Sst*Sbl*k*rc*ln(rc/R)*Shyp*BesselK(1,k*rc)*BesselI(1,k*
r0)+Sst*Sbl*k*rc*ln(rc/R)*Shyp*BesselK(1,k*r0)*BesselI(1,k*rc)-Sst*Sbl*k*rc*
Sias*ln(r1/R)*BesselK(1,k*rc)*BesselI(1,k*r0)+Sst*Sbl*k*rc*Sias*ln(r1/R)*
BesselK(1,k*r0)*BesselI(1,k*rc)+Sst*Sbl*k*rc*ln(r1/R)*Shyp*BesselK(1,k*rc)*
BesselI(1,k*r0)-Sst*Sbl*k*rc*ln(r1/R)*Shyp*BesselK(1,k*r0)*BesselI(1,k*rc)-
Sst*Sbl*Shyp*BesselK(0,k*rc)*BesselI(1,k*r0)-Sst*Sbl*Shyp*BesselK(1,k*r0)*
BesselI(0,k*rc)+Sias*rc*k*ln(r2/R)*Sbl*Sst*BesselK(1,k*rc)*BesselI(1,k*r0)-
Sias*rc*k*ln(r2/R)*Sbl*Sst*BesselK(1,k*r0)*BesselI(1,k*rc)-Sias*rc*k*ln(r2/R
)*Sbl*Shyp*BesselK(1,k*rc)*BesselI(1,k*r0)+Sias*rc*k*ln(r2/R)*Sbl*Shyp*
BesselK(1,k*r0)*BesselI(1,k*rc)+Sias*rc*k*Shyp*ln(r3/R)*Sst*BesselK(1,k*rc)*
```

```
BesselI(1,k*r0)-Sias*rc*k*Shyp*ln(r3/R)*Sst*BesselK(1,k*r0)*BesselI(1,k*rc))
;
Abl := 1/4*(4*C_r3*k^2*Sias*rc*ln(r2/R)*Sbl*Sst*BesselK(1,k*rc)*BesselI(1,k*
r0)-4*C_r3*k^2*Sias*rc*ln(r2/R)*Sbl*Shyp*BesselK(1,k*rc)*BesselI(1,k*r0)+4*
C_r3*k^2*Sias*rc*ln(r2/R)*Sbl*Shyp*BesselK(1,k*r0)*BesselI(1,k*rc)-4*C_r3*k^
2*Sias*rc*ln(r2/R)*Sbl*Sst*BesselK(1,k*r0)*BesselI(1,k*rc)-4*C_r3*Sst*Sbl*
Shyp*k^2*rc*ln(rc/R)*BesselK(1,k*rc)*BesselI(1,k*r0)-2*k*Sias*chi*rc^2*Shyp*
ln(r3/R)*Sst*BesselK(0,k*rc)*BesselI(1,k*r0)-2*k*Sias*chi*rc^2*Shyp*ln(r3/R)
*Sst*BesselK(1,k*r0)*BesselI(0,k*rc)-4*Sias*rc*Shyp*ln(r3/R)*Sst*BesselK(1,k
*r0)*BesselI(1,k*rc)*kappa-4*k*C_r3*Sst*Sbl*Shyp*BesselK(1,k*r0)*BesselI(0,k
*rc)+2*r1^2*Sias*chi*Shyp*ln(r3/R)*Sst*k^2*rc*ln(rc/R)*BesselK(1,k*rc)*
BesselI(1,k*r0)-2*r1^2*Sias*chi*Shyp*ln(r3/R)*Sst*k^2*rc*ln(rc/R)*BesselK(1,
k*r0)*BesselI(1,k*rc)-2*r1^2*Sias*chi*Shyp*ln(r3/R)*Sst*k^2*rc*ln(r1/R)*
BesselK(1,k*rc)*BesselI(1,k*r0)-4*k*C_r3*Sst*Sbl*Shyp*BesselK(0,k*rc)*
BesselI(1,k*r0)+2*k*r1^2*Sias*chi*Shyp*ln(r3/R)*Sst*BesselK(1,k*r0)*BesselI(
0,k*rc)-4*C_r3*Sst*Sbl*k^2*rc*Sias*ln(r1/R)*BesselK(1,k*rc)*BesselI(1,k*r0)+
4*C_r3*Sst*Sbl*k^2*rc*Sias*ln(r1/R)*BesselK(1,k*r0)*BesselI(1,k*rc)+4*C_r3*
Sst*Sbl*Shyp*k^2*rc*ln(r1/R)*BesselK(1,k*rc)*BesselI(1,k*r0)-4*C_r3*Sst*Sbl*
Shyp*k^2*rc*ln(r1/R)*BesselK(1,k*r0)*BesselI(1,k*rc)+Sias*rc*Shyp*ln(r3/R)*
Sst*BesselK(1,k*rc)*BesselI(1,k*r0)*chi*r1^2*k^2-Sias*rc*Shyp*ln(r3/R)*Sst*
BesselK(1,k*r0)*BesselI(1,k*rc)*chi*r1^2*k^2+2*k*r1^2*Sias*chi*Shyp*ln(r3/R)
*Sst*BesselK(0,k*rc)*BesselI(1,k*r0)+4*C_r3*Sst*Sbl*Shyp*k^2*rc*ln(rc/R)*
BesselK(1,k*r0)*BesselI(1,k*rc)-Sias*rc^3*Shyp*ln(r3/R)*Sst*BesselK(1,k*rc)*
BesselI(1,k*r0)*chi*k^2+4*Sias*rc*Shyp*ln(r3/R)*Sst*BesselK(1,k*rc)*BesselI(
1,k*r0)*kappa+Sias*rc^3*Shyp*ln(r3/R)*Sst*BesselK(1,k*r0)*BesselI(1,k*rc)*
chi*k^2+2*r1^2*Sias*chi*Shyp*ln(r3/R)*Sst*k^2*rc*ln(r1/R)*BesselK(1,k*r0)*
BesselI(1,k*rc))/k/(-Sst*Sbl*k*rc*ln(rc/R)*Shyp*BesselK(1,k*rc)*BesselI(1,k*
r0)+Sst*Sbl*k*rc*ln(rc/R)*Shyp*BesselK(1,k*r0)*BesselI(1,k*rc)-Sst*Sbl*k*rc*
Sias*ln(r1/R)*BesselK(1,k*rc)*BesselI(1,k*r0)+Sst*Sbl*k*rc*Sias*ln(r1/R)*
BesselK(1,k*r0)*BesselI(1,k*rc)+Sst*Sbl*k*rc*ln(r1/R)*Shyp*BesselK(1,k*rc)*
BesselI(1,k*r0)-Sst*Sbl*k*rc*ln(r1/R)*Shyp*BesselK(1,k*r0)*BesselI(1,k*rc)-
Sst*Sbl*Shyp*BesselK(0,k*rc)*BesselI(1,k*r0)-Sst*Sbl*Shyp*BesselK(1,k*r0)*
BesselI(0,k*rc)+Sias*rc*k*ln(r2/R)*Sbl*Sst*BesselK(1,k*rc)*BesselI(1,k*r0)-
Sias*rc*k*ln(r2/R)*Sbl*Sst*BesselK(1,k*r0)*BesselI(1,k*rc)-Sias*rc*k*ln(r2/R
)*Sbl*Shyp*BesselK(1,k*rc)*BesselI(1,k*r0)+Sias*rc*k*ln(r2/R)*Sbl*Shyp*
BesselK(1,k*r0)*BesselI(1,k*rc)+Sias*rc*k*Shyp*ln(r3/R)*Sst*BesselK(1,k*rc)*
BesselI(1,k*r0)-Sias*rc*k*Shyp*ln(r3/R)*Sst*BesselK(1,k*r0)*BesselI(1,k*rc))
;
B1 := -1/4/(-Sst*Sbl*k*rc*ln(rc/R)*Shyp*BesselK(1,k*rc)*BesselI(1,k*r0)+Sst*
Sbl*k*rc*ln(rc/R)*Shyp*BesselK(1,k*r0)*BesselI(1,k*rc)-Sst*Sbl*k*rc*Sias*ln(
r1/R)*BesselK(1,k*rc)*BesselI(1,k*r0)+Sst*Sbl*k*rc*Sias*ln(r1/R)*BesselK(1,k
*r0)*BesselI(1,k*rc)+Sst*Sbl*k*rc*ln(r1/R)*Shyp*BesselK(1,k*rc)*BesselI(1,k*
r0)-Sst*Sbl*k*rc*ln(r1/R)*Shyp*BesselK(1,k*r0)*BesselI(1,k*rc)-Sst*Sbl*Shyp*
BesselK(0,k*rc)*BesselI(1,k*r0)-Sst*Sbl*Shyp*BesselK(1,k*r0)*BesselI(0,k*rc)
+Sias*rc*k*ln(r2/R)*Sbl*Sst*BesselK(1,k*rc)*BesselI(1,k*r0)-Sias*rc*k*ln(r2/
R)*Sbl*Sst*BesselK(1,k*r0)*BesselI(1,k*rc)-Sias*rc*k*ln(r2/R)*Sbl*Shyp*
BesselK(1,k*rc)*BesselI(1,k*r0)+Sias*rc*k*ln(r2/R)*Sbl*Shyp*BesselK(1,k*r0)*
BesselI(1,k*rc)+Sias*rc*k*Shyp*ln(r3/R)*Sst*BesselK(1,k*rc)*BesselI(1,k*r0)-
Sias*rc*k*Shyp*ln(r3/R)*Sst*BesselK(1,k*r0)*BesselI(1,k*rc))*BesselI(1,k*r0)
*(2*k^2*Sias*chi*rc^2*ln(r2/R)*Sbl*Sst-2*k^2*Sias*chi*rc^2*ln(r2/R)*Sbl*Shyp
+2*k^2*Sias*chi*rc^2*Shyp*ln(r3/R)*Sst-2*k^2*r1^2*Sias*chi*ln(r2/R)*Sbl*Sst+
2*k^2*r1^2*Sias*chi*ln(r2/R)*Sbl*Shyp-2*k^2*r1^2*Sias*chi*Shyp*ln(r3/R)*Sst+
4*k^2*C_r3*Sst*Sbl*Shyp-2*Sst*Sbl*chi*rc^2*k^2*ln(rc/R)*Shyp-2*Sst*Sbl*chi*
rc^2*k^2*Sias*ln(r1/R)+2*Sst*Sbl*chi*rc^2*k^2*ln(r1/R)*Shyp+2*Sst*Sbl*chi*r1
^2*k^2*Sias*ln(r1/R)-Sst*Sbl*chi*r1^2*k^2*Shyp+Sst*Sbl*Shyp*chi*rc^2*k^2-4*
Sst*Sbl*Shyp*kappa)/k^2;
B2 := -1/4*rc*(2*BesselK(1,k*rc)*BesselI(1,k*r0)*k^2*r1^2*Sias*chi*ln(r2/R)*
Sbl*Sst-2*BesselK(1,k*rc)*BesselI(1,k*r0)*k^2*r1^2*Sias*chi*ln(r2/R)*Sbl*
Shyp+2*BesselK(1,k*rc)*BesselI(1,k*r0)*k^2*r1^2*Sias*chi*Shyp*ln(r3/R)*Sst-4
*BesselK(1,k*rc)*BesselI(1,k*r0)*k^2*C_r3*Sst*Sbl*Shyp-2*BesselK(1,k*rc)*
BesselI(1,k*r0)*Sst*Sbl*chi*r1^2*k^2*Sias*ln(r1/R)+BesselK(1,k*rc)*BesselI(1
,k*r0)*Sst*Sbl*chi*r1^2*k^2*Shyp-BesselK(1,k*rc)*BesselI(1,k*r0)*Sst*Sbl*
Shyp*chi*rc^2*k^2+4*BesselK(1,k*rc)*BesselI(1,k*r0)*Sst*Sbl*Shyp*kappa-2*
```

```
BesselK(1,k*r0)*BesselI(1,k*rc)*k^2*r1^2*Sias*chi*ln(r2/R)*Sbl*Sst+2*BesselK
(1,k*r0)*BesselI(1,k*rc)*k^2*r1^2*Sias*chi*ln(r2/R)*Sbl*Shyp-2*BesselK(1,k*
r0)*BesselI(1,k*rc)*k^2*r1^2*Sias*chi*Shyp*ln(r3/R)*Sst+4*BesselK(1,k*r0)*
BesselI(1,k*rc)*k^2*C_r3*Sst*Sbl*Shyp+2*BesselK(1,k*r0)*BesselI(1,k*rc)*Sst*
Sbl*chi*r1^2*k^2*Sias*ln(r1/R)-BesselK(1,k*r0)*BesselI(1,k*rc)*Sst*Sbl*chi*
r1^2*k^2*Shyp+BesselK(1,k*r0)*BesselI(1,k*rc)*Sst*Sbl*Shyp*chi*rc^2*k^2-4*
BesselK(1,k*r0)*BesselI(1,k*rc)*Sst*Sbl*Shyp*kappa-2*chi*rc*k*Sst*Sbl*Shyp*
BesselK(0,k*rc)*BesselI(1,k*r0)-2*chi*rc*k*Sst*Sbl*Shyp*BesselK(1,k*r0)*
BesselI(0,k*rc))/k/(-Sst*Sbl*k*rc*ln(rc/R)*Shyp*BesselK(1,k*rc)*BesselI(1,k*
r0)+Sst*Sbl*k*rc*ln(rc/R)*Shyp*BesselK(1,k*r0)*BesselI(1,k*rc)-Sst*Sbl*k*rc*
Sias*ln(r1/R)*BesselK(1,k*rc)*BesselI(1,k*r0)+Sst*Sbl*k*rc*Sias*ln(r1/R)*
BesselK(1,k*r0)*BesselI(1,k*rc)+Sst*Sbl*k*rc*ln(r1/R)*Shyp*BesselK(1,k*rc)*
BesselI(1,k*r0)-Sst*Sbl*k*rc*ln(r1/R)*Shyp*BesselK(1,k*r0)*BesselI(1,k*rc)-
Sst*Sbl*Shyp*BesselK(0,k*rc)*BesselI(1,k*r0)-Sst*Sbl*Shyp*BesselK(1,k*r0)*
BesselI(0,k*rc)+Sias*rc*k*ln(r2/R)*Sbl*Sst*BesselK(1,k*rc)*BesselI(1,k*r0)-
Sias*rc*k*ln(r2/R)*Sbl*Sst*BesselK(1,k*r0)*BesselI(1,k*rc)-Sias*rc*k*ln(r2/R
)*Sbl*Shyp*BesselK(1,k*rc)*BesselI(1,k*r0)+Sias*rc*k*ln(r2/R)*Sbl*Shyp*
BesselK(1,k*r0)*BesselI(1,k*rc)+Sias*rc*k*Shyp*ln(r3/R)*Sst*BesselK(1,k*rc)*
BesselI(1,k*r0)-Sias*rc*k*Shyp*ln(r3/R)*Sst*BesselK(1,k*r0)*BesselI(1,k*rc))
;
Bhyp := -1/4*Sias*Sst*Sbl*(4*C_r3*k^2*rc*BesselK(1,k*r0)*BesselI(1,k*rc)-4*
C_r3*k^2*rc*BesselK(1,k*rc)*BesselI(1,k*r0)+2*chi*r1^2*k^2*rc*ln(rc/R)*
BesselK(1,k*rc)*BesselI(1,k*r0)-2*chi*r1^2*k^2*rc*ln(rc/R)*BesselK(1,k*r0)*
BesselI(1,k*rc)+2*chi*r1^2*k*BesselK(0,k*rc)*BesselI(1,k*r0)+2*chi*r1^2*k*
BesselK(1,k*r0)*BesselI(0,k*rc)+chi*r1^2*k^2*rc*BesselK(1,k*rc)*BesselI(1,k*
r0)-chi*r1^2*k^2*rc*BesselK(1,k*r0)*BesselI(1,k*rc)-rc^3*BesselK(1,k*rc)*
BesselI(1,k*r0)*chi*k^2+4*rc*BesselK(1,k*rc)*BesselI(1,k*r0)*kappa+rc^3*
BesselK(1,k*r0)*BesselI(1,k*rc)*chi*k^2-4*rc*BesselK(1,k*r0)*BesselI(1,k*rc)
*kappa-2*rc^2*chi*k*BesselK(1,k*r0)*BesselI(0,k*rc)-2*rc^2*chi*k*BesselK(0,k
*rc)*BesselI(1,k*r0)-2*chi*r1^2*k^2*rc*ln(r1/R)*BesselK(1,k*rc)*BesselI(1,k*
r0)+2*chi*r1^2*k^2*rc*ln(r1/R)*BesselK(1,k*r0)*BesselI(1,k*rc))/k/(-Sst*Sbl*
k*rc*ln(rc/R)*Shyp*BesselK(1,k*rc)*BesselI(1,k*r0)+Sst*Sbl*k*rc*ln(rc/R)*
Shyp*BesselK(1,k*r0)*BesselI(1,k*rc)-Sst*Sbl*k*rc*Sias*ln(r1/R)*BesselK(1,k*
rc)*BesselI(1,k*r0)+Sst*Sbl*k*rc*Sias*ln(r1/R)*BesselK(1,k*r0)*BesselI(1,k*
rc)+Sst*Sbl*k*rc*ln(r1/R)*Shyp*BesselK(1,k*rc)*BesselI(1,k*r0)-Sst*Sbl*k*rc*
ln(r1/R)*Shyp*BesselK(1,k*r0)*BesselI(1,k*rc)-Sst*Sbl*Shyp*BesselK(0,k*rc)*
BesselI(1,k*r0)-Sst*Sbl*Shyp*BesselK(1,k*r0)*BesselI(0,k*rc)+Sias*rc*k*ln(r2
/R)*Sbl*Sst*BesselK(1,k*rc)*BesselI(1,k*r0)-Sias*rc*k*ln(r2/R)*Sbl*Sst*
BesselK(1,k*r0)*BesselI(1,k*rc)-Sias*rc*k*ln(r2/R)*Sbl*Shyp*BesselK(1,k*rc)*
BesselI(1,k*r0)+Sias*rc*k*ln(r2/R)*Sbl*Shyp*BesselK(1,k*r0)*BesselI(1,k*rc)+
Sias*rc*k*Shyp*ln(r3/R)*Sst*BesselK(1,k*rc)*BesselI(1,k*r0)-Sias*rc*k*Shyp*
ln(r3/R)*Sst*BesselK(1,k*r0)*BesselI(1,k*rc));
Bst := -1/4*Shyp*Sias*Sbl*(4*C_r3*k^2*rc*BesselK(1,k*r0)*BesselI(1,k*rc)-4*
C_r3*k^2*rc*BesselK(1,k*rc)*BesselI(1,k*r0)+2*chi*r1^2*k^2*rc*ln(rc/R)*
BesselK(1,k*rc)*BesselI(1,k*r0)-2*chi*r1^2*k^2*rc*ln(rc/R)*BesselK(1,k*r0)*
BesselI(1,k*rc)+2*chi*r1^2*k*BesselK(0,k*rc)*BesselI(1,k*r0)+2*chi*r1^2*k*
BesselK(1,k*r0)*BesselI(0,k*rc)+chi*r1^2*k^2*rc*BesselK(1,k*rc)*BesselI(1,k*
r0)-chi*r1^2*k^2*rc*BesselK(1,k*r0)*BesselI(1,k*rc)-rc^3*BesselK(1,k*rc)*
BesselI(1,k*r0)*chi*k^2+4*rc*BesselK(1,k*rc)*BesselI(1,k*r0)*kappa+rc^3*
BesselK(1,k*r0)*BesselI(1,k*rc)*chi*k^2-4*rc*BesselK(1,k*r0)*BesselI(1,k*rc)
*kappa-2*rc^2*chi*k*BesselK(1,k*r0)*BesselI(0,k*rc)-2*rc^2*chi*k*BesselK(0,k
*rc)*BesselI(1,k*r0)-2*chi*r1^2*k^2*rc*ln(r1/R)*BesselK(1,k*rc)*BesselI(1,k*
r0)+2*chi*r1^2*k^2*rc*ln(r1/R)*BesselK(1,k*r0)*BesselI(1,k*rc))/k/(-Sst*Sbl*
k*rc*ln(rc/R)*Shyp*BesselK(1,k*rc)*BesselI(1,k*r0)+Sst*Sbl*k*rc*ln(rc/R)*
Shyp*BesselK(1,k*r0)*BesselI(1,k*rc)-Sst*Sbl*k*rc*Sias*ln(r1/R)*BesselK(1,k*
rc)*BesselI(1,k*r0)+Sst*Sbl*k*rc*Sias*ln(r1/R)*BesselK(1,k*r0)*BesselI(1,k*
rc)+Sst*Sbl*k*rc*ln(r1/R)*Shyp*BesselK(1,k*rc)*BesselI(1,k*r0)-Sst*Sbl*k*rc*
ln(r1/R)*Shyp*BesselK(1,k*r0)*BesselI(1,k*rc)-Sst*Sbl*Shyp*BesselK(0,k*rc)*
BesselI(1,k*r0)-Sst*Sbl*Shyp*BesselK(1,k*r0)*BesselI(0,k*rc)+Sias*rc*k*ln(r2
/R)*Sbl*Sst*BesselK(1,k*rc)*BesselI(1,k*r0)-Sias*rc*k*ln(r2/R)*Sbl*Sst*
BesselK(1,k*r0)*BesselI(1,k*rc)-Sias*rc*k*ln(r2/R)*Sbl*Shyp*BesselK(1,k*rc)*
BesselI(1,k*r0)+Sias*rc*k*ln(r2/R)*Sbl*Shyp*BesselK(1,k*r0)*BesselI(1,k*rc)+
Sias*rc*k*Shyp*ln(r3/R)*Sst*BesselK(1,k*rc)*BesselI(1,k*r0)-Sias*rc*k*Shyp*
```

```
ln(r3/R)*Sst*BesselK(1,k*r0)*BesselI(1,k*rc));
Bbl := -1/4*Sst*Shyp*Sias*(4*C_r3*k^2*rc*BesselK(1,k*r0)*BesselI(1,k*rc)-4*
C_r3*k^2*rc*BesselK(1,k*rc)*BesselI(1,k*r0)+2*chi*r1^2*k^2*rc*ln(rc/R)*
BesselK(1,k*rc)*BesselI(1,k*r0)-2*chi*r1^2*k^2*rc*ln(rc/R)*BesselK(1,k*r0)*
BesselI(1,k*rc)+2*chi*r1^2*k*BesselK(0,k*rc)*BesselI(1,k*r0)+2*chi*r1^2*k*
BesselK(1,k*r0)*BesselI(0,k*rc)+chi*r1^2*k^2*rc*BesselK(1,k*rc)*BesselI(1,k*
r0)-chi*r1^2*k^2*rc*BesselK(1,k*r0)*BesselI(1,k*rc)-rc^3*BesselK(1,k*rc)*
BesselI(1,k*r0)*chi*k^2+4*rc*BesselK(1,k*rc)*BesselI(1,k*r0)*kappa+rc^3*
BesselK(1,k*r0)*BesselI(1,k*rc)*chi*k^2-4*rc*BesselK(1,k*r0)*BesselI(1,k*rc)
*kappa-2*rc^2*chi*k*BesselK(1,k*r0)*BesselI(0,k*rc)-2*rc^2*chi*k*BesselK(0,k
*rc)*BesselI(1,k*r0)-2*chi*r1^2*k^2*rc*ln(r1/R)*BesselK(1,k*rc)*BesselI(1,k*
r0)+2*chi*r1^2*k^2*rc*ln(r1/R)*BesselK(1,k*r0)*BesselI(1,k*rc))/k/(-Sst*Sbl*
k*rc*ln(rc/R)*Shyp*BesselK(1,k*rc)*BesselI(1,k*r0)+Sst*Sbl*k*rc*ln(rc/R)*
Shyp*BesselK(1,k*r0)*BesselI(1,k*rc)-Sst*Sbl*k*rc*Sias*ln(r1/R)*BesselK(1,k*
rc)*BesselI(1,k*r0)+Sst*Sbl*k*rc*Sias*ln(r1/R)*BesselK(1,k*r0)*BesselI(1,k*
rc)+Sst*Sbl*k*rc*ln(r1/R)*Shyp*BesselK(1,k*rc)*BesselI(1,k*r0)-Sst*Sbl*k*rc*
ln(r1/R)*Shyp*BesselK(1,k*r0)*BesselI(1,k*rc)-Sst*Sbl*Shyp*BesselK(0,k*rc)*
BesselI(1,k*r0)-Sst*Sbl*Shyp*BesselK(1,k*r0)*BesselI(0,k*rc)+Sias*rc*k*ln(r2
/R)*Sbl*Sst*BesselK(1,k*rc)*BesselI(1,k*r0)-Sias*rc*k*ln(r2/R)*Sbl*Sst*
BesselK(1,k*r0)*BesselI(1,k*rc)-Sias*rc*k*ln(r2/R)*Sbl*Shyp*BesselK(1,k*rc)*
BesselI(1,k*r0)+Sias*rc*k*ln(r2/R)*Sbl*Shyp*BesselK(1,k*r0)*BesselI(1,k*rc)+
Sias*rc*k*Shyp*ln(r3/R)*Sst*BesselK(1,k*rc)*BesselI(1,k*r0)-Sias*rc*k*Shyp*
ln(r3/R)*Sst*BesselK(1,k*r0)*BesselI(1,k*rc));
```

10.2 Plant Morphology and Species-specific Parameters

The code in the files `morph` is equivalent to the general calculations of the affective conductance in terms of anatomical parameters given in Section 4. The files `agpar` and `rhypar` contain the (numerical) anatomical information on *Aglaophyton major* and *Rhynia gwynne-vaughanii* given in Section 5, respectively.

File `morph`:

```
read 'diffsol.m';
#
#Digits:=20;
#
#Pa:=1; m:=1; s:=1; mmol:=1; deg:=1;
#
alias(sim=simplify,ev=evalf);
#
# ********************************************************************
# berechnung der CO2-konzentration, des CO2-flusses, der
# wasserdampf-konzentration und des wasserdampf-flusses fuer eine
# axialsymmetrische pflanze aus der stationaeren
# diffusionsgleichung
#
# die CO2-konzentration ausserhalb der pflanze und der CO2-verbrauch
# durch die photosynthese sind vorgegeben  (neumannsche randbedingungen)
#
# die wasserdampf-konzentration ausserhalb der pflanze und die
# wasserdampf-konzentration im mesophyll sind vorgegeben
# (dirichletsche randbedingungen)
# ********************************************************************
#
# (im prinzip) vorgegebene groessen:
# ------------------------------------------------------------------
# aus der pflanzenmorphologie ableitbare groessen:
#
# Ni          porositaeten (dimensionslos)
# T := Le/L   tortuositaeten (dimensionslos)
# Le          effektive laenge einer stromlinie (m)
# L           (gerader) abstand zwischen anfangs- und endpunkt
#             derselben stromlinie (m)
#
# r3          abstand symmetrieachse - aussenkante boundary layer (m)
# R           radius der pflanze (m)
# r2          abstand symmetrieachse - aussenkante hypodermis (m)
# r1          abstand symmetrieachse - aussenkante mesophyll (m)
# r0          abstand symmetrieachse - innenkante mesophyll (m)
#
# AVmes       "spezifische oberflaeche" (d.h. oberflaeche/volumen) einer
#             mesophyllzelle mit radius sigma (1/m)
# fcm         verhaeltnis der (gesamt-)oberflaeche aller chloroplasten zur
#             oberflaeche der mesophyllzelle, in der sie drinnen sind
# ------------------------------------------------------------------
# aus der pflanzenphysiologie (photosynthese) ableitbare groessen:
#
# gliq        leitfaehigkeit fuer waessrig geloestes CO2 zwischen
#             aussenkante mesophyllzelle und chloroplasten im inneren der
#             mesophyllzelle  (mol/m^2/s/Pa)
# Vj          lokale potentielle karboxylationsrate, limitiert durch
#             elektronentransport und photophosphorylation (mol/m^2/s)
# Gamma       CO2 kompensationspunkt (Pa)
#
```

```
# ------------------------------------------------------------------
# sonstige groessen:
#
# Si:=Dco2*Ni/Ti^2;              effektive "leitfaehigkeiten" (m^2/s)
# si:=Dwv*Ni/Ti^2;   # effektive "leitfaehigkeiten" (m^2/s)
#
# C_r3:=14*12*mmol/m^3; # entspricht 340 ppm CO2 * 12
                        # CO2-konzentration ausserhalb der pflanze (mol/m^3)
# c_r3:=0.48*10^3*mmol/m^3;
         # wasserdampf-konzentration ausserhalb der pflanze (mol/m^3)
# c_r1:=1.27*10^3*mmol/m^3; # wasserdampf-konzentration im mesophyll (mol/m^3)
#
# Dwv := 2.42*10^(-5)*m^2/s; # diffusionskonstante von wasserdampf in luft
# bei T = 20 deg C (m^2/s) und p = 1,013*10^5 Pa
# ****************************************************************
# zu berechnende groessen:
#
# C(r)         CO2-konzentration als funktion von r (mol/m^3)
# J(r)         CO2-stromdichte als funktion von r (mol/m^2/s)
#
# c(r)         wasserdampf-konzentration als funktion von r (mol/m^3)
# j(r)         wasserdampf-stromdichte als funktion von r (mol/m^2/s)
#
# ****************************************************************
# sonstige groessen:
#
# Ai,Bi,ai,bi        integrationskonstanten
# BesselI(n,k*r)     modifizierte Besselfunktion der ersten art der ordnung n
# BesselK(n,k*r)     modifizierte Besselfunktion der zweiten art der ordnung n
# ****************************************************************
# um maple nicht unnoetig zu belasten, wurde ihm bislang nur gesagt, es
# koenne die effektiven leitfaehigkeiten si und Si als gegeben betrachten.
# deshalb enthalten c(r),C(r),J(r) und j(r) bislang nur die Parameter si, Si
# sowie r0, r1, r2, R und r3. jetzt erfaehrt maple die details:
#
sbl:=Dwv*Nbl/Tbl^2;
sst:=Dwv*Nst/Tst^2;
shyp:=Dwv*Nhyp/Thyp^2;
#
Sbl:=Dco2*Nbl/Tbl^2;
Sst:=Dco2*Nst/Tst^2;
Shyp:=Dco2*Nhyp/Thyp^2;
Sias:='Dco2*Nias/Tias^2';
#
# ------------------------------------------------------------------
# physikalische "konstanten":
#
#Rgas:=8.3143*10^(-3)*m^3*Pa/mmol/deg; # gaskonstante (J/mol/deg K)
#T:=293.15*deg; # absolute temperatur (deg K), entspricht 20 deg C
#
#Dco2 := 1.51*10^(-5)*m^2/s; # diffusionskonstante von CO2 in luft (m^2/s)
#Dwv := 2.42*10^(-5)*m^2/s; # diffusionskonstante von wasserdampf in luft
# ------------------------------------------------------------------
# aussenrand:
#
# Wasserdampf-konzentration ausserhalb der pflanze (mol/m^3):
#
#c_r3:=480*mmol/m^3;
#
# CO2-konzentration ausserhalb der pflanze (mol/m^3)
#
#C_r3:=14*12*mmol/m^3; # entspricht 340 ppm CO2 * 12, quelle: anita
#C_r3:=14*mmol/m^3; # entspricht 340 ppm CO2 (heute!), quelle: anita
```

```
# ----------------------------------------------------------------
# boundary layer:
#
# fuer die maechtigkeit dbl des boundary layer gilt
# dbl (in mm)=5.8*sqrt(durchmesser (in m)/windgeschwindigkeit (in m/s))
#
dbl:=evalf('5.8*10^(-3)*m*sqrt((2*R)/(vatm*s))');
#vatm:=0.8*m/s;                          # 0.8 m/s typische windgeschwindigkeit
#
#r3:='R'+'dbl';  # abstand symmetrieachse - aussenkante boundary layer (m)
r3:='R+dbl';  # abstand symmetrieachse - aussenkante boundary layer (m)
#
#Nbl:=1; # die porositaet von luft in luft betraegt 100%
#Tbl:=1; # in luft brauchen sich die molekuele nicht zu winden
# ----------------------------------------------------------------
# stomata:
#
asto:=Pi/4*hst*wst; # flaeche eines stoma
#
# wst/2 und hst/2 sind die halbachsen einer ellipsen, hst || symmetrieachse,
# dst radial nach innen, daher
#
Nst:='Pi/4*hst*wst*nust';
Tst:='1+sqrt((Pi/4*hst*wst/(Pi*dst^2)))'; # dst: (radiale) "tiefe" der stomata
                # (quelle: Nobel, p.396)
# ----------------------------------------------------------------
# hypodermis:
#
#r2:='R'-'dst';               # abstand symmetrieachse - aussenkante hypodermis (m)
r2:='R-dst';            # abstand symmetrieachse - aussenkante hypodermis (m)
#
# whyp/2 und hhyp/2 sind die halbachsen einer ellipsen, hhyp || symmetrieachse,
# dhyp radial nach innen, daher
#
# V(hypodermis) = hhyp*Pi*(r2^2/2-r1^2/2)
# V(stomakanal) = Pi*bhyp/2*hhyp/2*dhyp
# anzahldichte der stomata (und der stomakanaele): 1.5*10^6/m^2
# V(alle stomakanaele) = Pi*bhyp/2*hhyp/2*dhyp*1.5*10^6/m^2*hhyp*2*Pi*r2;
# Nhyp:= V(alle stomakanaele)/V(hypodermis)
#
Nhyp:='Pi/4*hhyp*whyp*nust*((2*R-dst)/(2*R-2*dst-dhyp))';
#Thyp:=1; # stomakanaele in der hypodermis sind wie autobahnschneisen
#
# ----------------------------------------------------------------
# innerer "wasserdampf-rand":
#
# Wasserdampf-konzentration an der mesophyll-aussenkante (mol/m^3):
#cc_r1:=1.27*10^3*mmol/m^3;
c_r1:='csat*exp(-(2*Vml*gam)/(Rgas*T*sigma))'; # Kelvin-Gleichung
#
#csat:=1.279*10^3*mmol/m^3; # saettigungskonzentration von wasserdampf bei
                            # T = 25 deg C
#csat:=0.9603*10^3*mmol/m^3; # saettigungskonzentration von wasserdampf bei
                            # T = 20 deg C
#Vml:=1.805*10^(-8)*m^3/mmol; # molvolumen des wassers bei T = 20 deg C
#gam:=0.0728*Pa*m; # oberflaechenspannung des wassers bei T = 20 deg C
# ----------------------------------------------------------------
# mesophyll allgemein
#
r1:='R-(dhyp+dst)';
#r1:=R-(dhyp+dst);  # abstand symmetrieachse - aussenkante mesophyll (m)
#r0:='R'-('dhyp'+'dst'+'dias'); # abstand symmetrieachse - innenkante mesophyll (m)
r0:='R-(dhyp+dst+dias)'; # abstand symmetrieachse - innenkante mesophyll (m)
```

```
#------------------------------------------------------------------
# photosynthese
#
Rd:=0;
#
#
Jph:='alpha*i/sqrt(1+(alpha*i/Jmax)^2)';
# i ist der photonenfluss (mmol/m^2/s) am ort der chloroplasten
#
Wc := q -> Vcmax*q/(q+Kc*(1+pO/Ko));
Wj := q -> Jph*q/(4*(q+pO/tau));
#
Ac := q -> (1-pO/(2*tau*q))*Wc(q); #
Aj := q -> (1-pO/(2*tau*q))*Wj(q); #
#
A := proc(q) global Wj,Wc;
if Wj(q) < Wc(q) then Aj(q) else Ac(q) fi;
end;
# qs: der eine schnittpunkt von Wc und Wj, der andere ist bei q=0.
#
qs := -(4*Vcmax*Ko*pO-Jph*Kc*tau*Ko-Jph*Kc*tau*pO)\
/(4*tau*Ko*Vcmax-Jph*tau*Ko);
#
# Ac(q) und Aj(q) haben dieselbe nullstelle bei q=qn:
qn := 1/2*pO/tau;
#
# funktionswerte von Ac(0) und Aj(0):
Ac0 := -1/2*Vcmax*Ko*pO/tau/Kc/(Ko+pO);
Aj0 := -1/8*Jph;
#
Gamma:=pO/2/tau;
Cgamma:=Gamma/Rgas/T;
#----------------------------------
# wir naehern A durch zwei geradenstuecke: g1c und g1j,
# dann noch die zur q-Achse parallelen geraden g2c und g2j
#
# g1c geht durch (q=0,Ac0) und durch die nullstelle von Ac bei (qn,0):
g1c := q -> 1/2*(-Vcmax*Ko*pO+2*q*tau*Ko*Vcmax)/(Ko+pO)/Kc/tau;
#
# g1j geht durch (q=0,Aj0) und durch die nullstelle von Aj bei (qn,0)
g1j := q -> -1/8*Jph*(1-2*q/pO*tau);
#
# g2c ist die asymptote an Ac fuer q->inf
g2c := q -> Vcmax;
#
# g2j ist die asymptote an Aj fuer q->inf
g2j := q -> Jph/4;
#
g1:=proc(q) global qs,g1c,g1j,Jph,Vcmax;
if qs>0 and Jph>4*Vcmax then g1j(q)
elif qs>0 and Jph<4*Vcmax then g1c(q)
elif qs<=0 and Jph<4*Vcmax then g1j(q)
elif qs<=0 and Jph>4*Vcmax then g1c(q)
fi; end;
#
g2:=proc(q) global qs,g2c,g2j,Jph,Vcmax;
if qs>0 and Jph>4*Vcmax then g2c(q)
elif qs>0 and Jph<4*Vcmax then g2j(q)
elif qs<=0 and Jph>4*Vcmax then g2c(q)
elif qs<=0 and Jph<4*Vcmax then g2j(q)
fi; end;
#
#----------------------------------
```

```
# schnittpunkt von g1c mit g2j:
qc_cj := 1/4*(2*Vcmax*Ko*p0+Jph*Kc*tau*Ko+Jph*Kc*tau*p0)/Vcmax/tau/Ko;
#
# schnittpunkt von g1j mit g2j:
qc_jj := 3/2*p0/tau;
#
# schnittpunkt von g1c mit g2c:
qc_cc := 1/2*(Ko*p0+2*tau*Kc*Ko+2*tau*Kc*p0)/tau/Ko;
#
# schnittpunkt von g1j mit g2c:
qc_jc := 1/2*(Jph+8*Vcmax)*p0/tau/Jph;
#----------------------------------
glue:=proc()  global qs,qc_cj,qc_jj,qc_cc,qc_jc,Jph,Vcmax;
if qs>0 and Jph<4*Vcmax then eval(qc_cj)
elif qs>0 and Jph>4*Vcmax then eval(qc_jc)
elif qs<=0 and Jph>4*Vcmax then eval(qc_cc)
elif qs<=0 and Jph<4*Vcmax then eval(qc_jj)
fi; end;
#
qc:=glue();
#
An:=proc(q) global qc,g1,g2;
if q>=0 and qc>=q then g1(q) elif q>qc then g2(q) fi; end;
#
# schnittpunkte von g1 und g2 von q auf C umgeschrieben
Cc_cj := 1/4*(Ko*Jph*Kc*tau*gliq+2*Ko*Vcmax*p0*gliq+Ko*Jph*tau*Vcmax+Jph*Kc*tau
*gliq*p0)/tau/Rgas/T/gliq/Ko/Vcmax;
Cc_jj := 1/4*(tau*Jph+6*gliq*p0)/T/Rgas/gliq/tau;
Cc_cc := 1/2*(Ko*p0*gliq+2*tau*gliq*Kc*Ko+2*tau*gliq*Kc*p0+2*tau*Ko*Vcmax)/T/
Rgas/tau/gliq/Ko;
Cc_jc := 1/2*(Jph*gliq*p0+8*Vcmax*gliq*p0+2*Vcmax*tau*Jph)/T/Rgas/gliq/tau/
Jph;
#
Glue:=proc()  global qs,Cc_cj,Cc_jj,Cc_cc,Cc_jc,Jph,Vcmax;
if qs>0 and Jph<4*Vcmax then eval(Cc_cj)
elif qs>0 and Jph>4*Vcmax then eval(Cc_jc)
elif qs<=0 and Jph>4*Vcmax then eval(Cc_cc)
elif qs<=0 and Jph<4*Vcmax then eval(Cc_jj)
fi; end;
#
Cqc:=Glue();
#
# g1 und g2 auf von q auf C umgeschrieben:
#
G1c := C -> gliq*Ko*Vcmax/(gliq*Kc*Ko+gliq*Kc*p0+Ko*Vcmax)*C*Rgas*T-\
1/2*gliq*Vcmax*Ko*p0/(gliq*Kc*Ko+gliq*Kc*p0+Ko*Vcmax)/tau;
# G1c=G1c0+G1c1*C:
G1c0 := -1/2*gliq*Vcmax*Ko*p0/(gliq*Kc*Ko+gliq*Kc*p0+Ko*Vcmax)/tau;
G1c1 := gliq*Ko*Vcmax*Rgas*T/(gliq*Kc*Ko+gliq*Kc*p0+Ko*Vcmax);
#
G1j := C -> Jph*tau*gliq/(4*gliq*p0+tau*Jph)*C*Rgas*T-1/2*Jph*gliq*p0/\
(4*gliq*p0+tau*Jph);
# G1j=G1j0+G1j1*C:
G1j0 := -1/2*Jph*gliq*p0/(4*gliq*p0+tau*Jph);
G1j1 := Jph*tau*gliq*Rgas*T/(4*gliq*p0+tau*Jph);
#
G2c := C -> Vcmax;
G2j := C -> Jph/4;
#
G1:=proc(C) global qs,G1c,G1j,Jph,Vcmax;
if qs>0 and Jph>4*Vcmax then G1j(C)
elif qs>0 and Jph<4*Vcmax then G1c(C)
elif qs<=0 and Jph<4*Vcmax then G1j(C)
```

```
elif qs<=0 and Jph>4*Vcmax then G1c(C)
fi; end;
#
G2:=proc(C) global qs,G2c,G2j,Jph,Vcmax;
if qs>0 and Jph>4*Vcmax then G2c(C)
elif qs>0 and Jph<4*Vcmax then G2j(C)
elif qs<=0 and Jph>4*Vcmax then G2c(C)
elif qs<=0 and Jph<4*Vcmax then G2j(C)
fi; end;
#
#
#fQ:=Tias^2/Dco2*fcm*AVmes*(1-Nass)/Nias; # blosse abkuerzung
fQ:='Tias^2/Dco2*fcm*AVmes*(1-Nias)/Nias'; # blosse abkuerzung
#
# ------------------------------------------------------------------
# mesophyll 2
#
fchi:=proc() global qs,fQ,G2c,G2j,Jph,Vcmax;
if qs>0 and Jph>4*Vcmax then fQ*G2c(C)
elif qs>0 and Jph<4*Vcmax then fQ*G2j(C)
elif qs<=0 and Jph>4*Vcmax then fQ*G2c(C)
elif qs<=0 and Jph<4*Vcmax then fQ*G2j(C)
fi; end;
chi:=fchi();
# ------------------------------------------------------------------
# mesophyll 1
#
fkappa:=proc() global qs,fQ,G1c0,G1j0,Jph,Vcmax;
if qs>0 and Jph>4*Vcmax then fQ*G1j0
elif qs>0 and Jph<4*Vcmax then fQ*G1c0
elif qs<=0 and Jph<4*Vcmax then fQ*G1j0
elif qs<=0 and Jph>4*Vcmax then fQ*G1c0
fi; end;
kappa:=-fkappa();
#
fk:=proc() global qs,fQ,G1c1,G1j1,Jph,Vcmax;
if qs>0 and Jph>4*Vcmax then sqrt(fQ*G1j1)
elif qs>0 and Jph<4*Vcmax then sqrt(fQ*G1c1)
elif qs<=0 and Jph<4*Vcmax then sqrt(fQ*G1j1)
elif qs<=0 and Jph>4*Vcmax then sqrt(fQ*G1c1)
fi; end;
k:=fk();
#
#****************************************************************
```

File agpar**:**

```
#
Pa:=1; m:=1; s:=1; mmol:=1; deg:=1;
# ----------------------------------------------------------------
# physikalische "konstanten":
#
Rgas:=8.3143*10^(-3)*m^3*Pa/mmol/deg; # gaskonstante (J/mol/deg K)
T:=293.15*deg; # absolute temperatur (deg K), entspricht 20 deg C
Dco2 := 1.51*10^(-5)*m^2/s; # diffusionskonstante von CO2 in luft (m^2/s)
Dwv := 2.42*10^(-5)*m^2/s; # diffusionskonstante von wasserdampf in luft
# ----------------------------------------------------------------
# aussenrand:
#
# Wasserdampf-konzentration ausserhalb der pflanze (mol/m^3):
#
#c_r3:=720*mmol/m^3;
c_r3:=480*mmol/m^3; # entspricht einer relativen luftfeuchte von 50%
#c_r3:=240*mmol/m^3;
#
# CO2-konzentration ausserhalb der pflanze (mol/m^3)
#
C_r3:=14.0*12*mmol/m^3; # entspricht 340 ppm CO2 * 12 (devon), quelle: anita
#C_r3:=14*mmol/m^3; # entspricht 340 ppm CO2 (heute!), quelle: anita
# ----------------------------------------------------------------
# boundary layer:
#
vatm:=0.8*m/s;        # 0.8 m/s typische windgeschwindigkeit
Nbl:=1; # die porositaet von luft in luft betraegt 100%
Tbl:=1; # in luft brauchen sich die molekuele nicht zu winden
# ----------------------------------------------------------------
# stomata:
#
R:=4500.0/2*10^(-6)*m;      # radius der pflanze (m), quelle: anita
#
# breite, hoehe und tiefe von stomaporen (ellipsenfoermig) in der epidermis:
wst:=10.5*10^(-6)*m; # quelle: anita
hst:=39.0*10^(-6)*m;
dst:=30.0*10^(-6)*m;
nust:=1*10^6/m^2;       # anzahldichte der stomata  quelle: anita
# ----------------------------------------------------------------
# hypodermis:
#
whyp:=30.0*10^(-6)*m; # quelle: anita
hhyp:=40.0*10^(-6)*m;
dhyp:=75.0*10^(-6)*m;
Thyp:=1; # stomakanaele in der hypodermis sind wie autobahnschneisen
# ----------------------------------------------------------------
# innerer "wasserdampf-rand":
#
# Wasserdampf-konzentration an der mesophyll-aussenkante (mol/m^3):
#
#csat:=1.279*10^3*mmol/m^3; # saettigungskonz. von wasserdampf
                            # bei T = 25 deg C
csat:=0.9603*10^3*mmol/m^3; # dito bei T = 20 deg C
Vml:=1.805*10^(-8)*m^3/mmol; # molvolumen des wassers bei T = 20 deg C
gam:=0.0728*Pa*m; # oberflaechenspannung des wassers bei T = 20 deg C
# ----------------------------------------------------------------
# mesophyll allgemein
#
dias:=250.0*10^(-6)*m; # mesophyll-dicke
#
Tias:=evalf(Pi/2); # einfache naeherung: halber kreisumfang/kreisdurchmesser
Nias:=0.35; # quelle: anita
```

```
Nass:=Nias;
#
# "spezifische oberflaeche" einer kugelfoermigen mesophyllzelle (radius sigma):
#AVmes := 3/sigma; # quelle: euklid
sigma:=55.0*10^(-6)*m; # quelle: anita
AVmes:=2/sigma;    # dito fuer eine saeule ohne deckel, quelle: euklid
#
# verhaeltnis der (gesamt-)oberflaeche aller chloroplasten
# zur oberflaeche einer mesophyllzelle, in der sie enthalten sind:
#
fcm:=0.9*2.606; # fuer eta=3/7
#
# leitfaehigkeit fuer waessrig geloestes CO2:
gliq:=0.5*10^(-3)*mmol/m^2/s/Pa; # quelle: parkhurst and mott
#-----------------------------------------------------------------
# photosynthese
# verschiedene groessen aus dem beerling modell der photosynthese:
#
Rd:=0;
T:=293.15*deg;
Rgas:=8.3143*10^(-3)*Pa*m^3/mmol/deg; # gaskonstante (Pa*m^3/mol/deg K)
alpha:=0.2;
#
AmesA:=10; # verhaeltnis mesophyllflaeche zu blatt(ober)flaeche bei fichte
#
amesa:=AVmes*(1-Nias)*(r1^2-r0^2)/2/R;
#
Vcmax:=12.0/AmesA/fcm*10^(-3)*mmol/m^2/s;
Jmax:=32.0/AmesA/fcm*10^(-3)*mmol/m^2/s;
#
Theta:=45/180*Pi; # sonne steht 45 Grad ueber dem horizont
S_0:=1360*4.5*10^(-3)*mmol/m^2/s;
I_0_scattered:=25/55*45/100*S_0;
I_0_direct:=30/55*45/100*S_0;
I_theta:=evalf((I_0_scattered+I_0_direct)*cos(Theta)/Pi);
#
i:=evalf(I_theta/fcm/AVmes/(1-Nias)*2*R/(r1^2-r0^2));
#
p0:=0.2*1.013*10^5*Pa;
#Kc:=exp(35.79-80.47*Pa*m^3/mmol/Rgas/T)*Pa;
#Ko:=exp(9.59-14.51*Pa*m^3/mmol/Rgas/T)*Pa;
Kc:=63.6*Pa;
Ko:=34825*Pa;
tau:=exp(-3.949+28.99*Pa*m^3/mmol/Rgas/T);
#
read morph;
#
```

File rhypar**:**

```
#
#Digits:=20;
#
Pa:=1; m:=1; s:=1; mmol:=1; deg:=1;
# ----------------------------------------------------------------
# physikalische "konstanten":
#
Rgas:=8.3143*10^(-3)*m^3*Pa/mmol/deg; # gaskonstante (J/mol/deg K)
T:=293.15*deg; # absolute temperatur (deg K), entspricht 20 deg C
Dco2 := 1.51*10^(-5)*m^2/s; # diffusionskonstante von CO2 in luft (m^2/s)
Dwv := 2.42*10^(-5)*m^2/s; # diffusionskonstante von wasserdampf in luft
# ----------------------------------------------------------------
# aussenrand:
#
# Wasserdampf-konzentration ausserhalb der pflanze (mol/m^3):
#
#c_r3:=720*mmol/m^3;#
c_r3:=480*mmol/m^3; # entspricht einer relativen luftfeuchte von 50%
#c_r3:=240*mmol/m^3;#
# CO2-konzentration ausserhalb der pflanze (mol/m^3)
#
C_r3:=14.0*12*mmol/m^3; # entspricht 340 ppm CO2 * 12 (devon), quelle: anita
#C_r3:=14*mmol/m^3; # entspricht 340 ppm CO2 (heute!), quelle: anita
# ----------------------------------------------------------------
# boundary layer:
#
vatm:=0.8*m/s;        # 0.8 m/s typische windgeschwindigkeit
Nbl:=1; # die porositaet von luft in luft betraegt 100%
Tbl:=1; # in luft brauchen sich die molekuele nicht zu winden
# ----------------------------------------------------------------
# stomata:
#
R:=1.0*10^(-3)*m;      # radius der pflanze (m), quelle: anita
#
# breite, hoehe und tiefe von stomaporen (ellipsenfoermig) in der epidermis:
wst:=10.0*10^(-6)*m; # quelle: anita
hst:=29.0*10^(-6)*m;
dst:=15.0*10^(-6)*m;
nust:=1.75*10^6/m^2;        # anzahldichte der stomata  quelle: anita
# ----------------------------------------------------------------
# hypodermis:
#
whyp:=20.0*10^(-6)*m; # quelle: anita
hhyp:=30.0*10^(-6)*m;
dhyp:=105.0*10^(-6)*m;
Thyp:=1; # stomakanaele in der hypodermis sind wie autobahnschneisen
# ----------------------------------------------------------------
# innerer "wasserdampf-rand":
#
# Wasserdampf-konzentration an der mesophyll-aussenkante (mol/m^3):
#
#csat:=1.279*10^3*mmol/m^3; # saettigungskonz. von wasserdampf bei T = 25 deg C
csat:=0.9603*10^3*mmol/m^3; # dito bei T = 20 deg C
Vml:=1.805*10^(-8)*m^3/mmol; # molvolumen des wassers bei T = 20 deg C
gam:=0.0728*Pa*m; # oberflaechenspannung des wassers bei T = 20 deg C
# ----------------------------------------------------------------
# mesophyll allgemein
#
dias:=100.0*10^(-6)*m; # mesophyll-dicke
#
Tias:=evalf(Pi/2); # einfache naeherung: halber kreisumfang/kreisdurchmesser
Nias:=0.35; # quelle: anita
```

```
Nass:=Nias;
#
# "spezifische oberflaeche" einer kugelfoermigen mesophyllzelle (radius sigma):
#AVmes := 3/sigma; # quelle: euklid
sigma:=50.0*10^(-6)*m; # quelle: anita
AVmes:=2/sigma; # # dito fuer eine saeule ohne deckel, quelle: euklid
#
# verhaeltnis der (gesamt-)oberflaeche aller chloroplasten
# zur oberflaeche einer mesophyllzelle,
# in der sie enthalten sind:
#
fcm:=0.9*2.606; # fuer eta=3/7
#
# leitfaehigkeit fuer waessrig geloestes CO2:
gliq:=0.5*10^(-3)*mmol/m^2/s/Pa; # quelle: parkhurst and mott
#---------------------------------------------------------------
# photosynthese
# verschiedene groessen aus dem beerling modell der photosynthese:
#
Rd:=0;
T:=293.15*deg;
Rgas:=8.3143*10^(-3)*Pa*m^3/mmol/deg; # gaskonstante (Pa*m^3/mol/deg K)
alpha:=0.2;
#
AmesA:=10; # verhaeltnis mesophyllflaeche zu blatt(ober)flaeche bei fichte
#
amesa:=AVmes*(1-Nias)*(r1^2-r0^2)/2/R;
#
Vcmax:=12.0/AmesA/fcm*10^(-3)*mmol/m^2/s;
Jmax:=32.0/AmesA/fcm*10^(-3)*mmol/m^2/s;
#
Theta:=45/180*Pi; # sonne steht 45 Grad ueber dem horizont
S_0:=1360*4.5*10^(-3)*mmol/m^2/s;
I_0_scattered:=25/55*45/100*S_0;
I_0_direct:=30/55*45/100*S_0;
I_theta:=evalf((I_0_scattered+I_0_direct)*cos(Theta)/Pi);
#
i:=evalf(I_theta/fcm/AVmes/(1-Nias)*2*R/(r1^2-r0^2));
#
p0:=0.2*1.013*10^5*Pa;
#Kc:=exp(35.79-80.47*Pa*m^3/mmol/Rgas/T)*Pa;
#Ko:=exp(9.59-14.51*Pa*m^3/mmol/Rgas/T)*Pa;
Kc:=63.6*Pa;
Ko:=34825*Pa;
tau:=exp(-3.949+28.99*Pa*m^3/mmol/Rgas/T);
#
read morph;
#
```

10.3 Determination of r_c

In the file **a_rc** tests are performed, whether r_c (as defined in Section 3.4.3 and explained in Section 3.5) takes on one of the values r_0 or r_1, or whether it must be calculated (by floating point arithmetics) explicitly from equation (3.70). **a_rc** employs data for *Aglaophyton major* (as can be seen from the **read agpar** statement in the first line). Similar calculations in the case of *Rhynia gwynne-vaughanii* should use the statement **read rhypar** instead.

File a_rc:

```
#
Pa:=1; m:=1; s:=1; mmol:=1; deg:=1;
#
read agpar;
read morph;
#
unassign('rc');
read morph;
#
C2t:=unapply(evalf(C2(r)),r,rc);
C1t:=unapply(evalf(C1(r)),r,rc);
#--------------------------------------
bed1:=proc() # rc=r0
evalf(C2t(r0,r0)) > Cqc and evalf(C2t(r1,r0)) > Cqc;
end;

act1:=proc() global rc;
rc:=r0; print(evaln(rc)=rc);
end;
#--------------------------------------
bed2:=proc() # rc=r1
evalf(C1t(r0,r1)) < Cqc and evalf(C1t(r1,r1)) < Cqc ;
end;

act2:=proc() global rc;
rc:=r1; print(evaln(rc)=rc);
end;
#--------------------------------------
act3:=proc() global rc; local ec;
unassign('rc');
ec:=evalf(C2t(rc,rc))-Cqc;
rc:=fsolve(ec,rc,r0..r1);
print(evaln(rc)=rc);
end;
#--------------------------------------
rrr:=proc()
if bed1() then act1() \
elif bed2() then act2() \
else act3() \
fi;
end;
#--------------------------------------
rrr();
#
#read a_plcj;
#
```

10.4 Generation of Plots for $C(r)$ and $j(r)$

The file a_plcj generates plots for $C^{CO_2}(r)$, $j^{CO_2}(r)$, $C^{H_2O}(r)$ and $j^{H_2O}(r)$.

File a_plcj:
```
#
# nun programmiertechnische vorbereitungen zur graphischen darstellung:
#
dr0:=simplify(evalf(r0/m));
drc:=simplify(evalf(rc/m));
dr1:=simplify(evalf(r1/m));
dr2:=simplify(evalf(r2/m));
dR:=simplify(evalf(R/m));
dr3:=simplify(evalf(r3/m));
#
#
paC:=plot(subs(m=1,m^3/mmol*Cn(r)),r=0.95*dr0..1.05*dr3,\
title='Carbon dioxide concentration',labels=['r in m','mmol/m^3'],\
axes=boxed,resolution=500,xtickmarks=7,ytickmarks=7,numpoints=500,thickness=3);
paC;
#
paJ:=plot(subs(m=1,m^2*s/mmol*Jn(r)),r=0.95*dr0..1.05*dr3,\
title='Carbon dioxide flux',labels=['r in m','mmol/m^2/s'],\
axes=boxed,resolution=500,xtickmarks=7,ytickmarks=7,numpoints=500,thickness=3);
paJ;
#
pac:=plot(subs(m=1,m^3/mmol*cn(r)),r=0.95*dr0..1.05*dr3,\
title='Water vapour concentration',labels=['r in m','mmol/m^3'],\
axes=boxed,resolution=500,xtickmarks=7,ytickmarks=7,numpoints=500,thickness=3);
pac;
#
paj:=plot(subs(m=1,m^2*s/mmol*jn(r)),r=0.95*dr0..1.05*dr3,\
title='Water vapour flux',labels=['r in m','mmol/m^2/s'],\
axes=boxed,resolution=500,xtickmarks=7,ytickmarks=7,numpoints=500,thickness=3);
paj;
#
save paJ,paj,paC,pac,'pa_cj.m';
#
```

10.5 Calculation of the Water Use Efficiency (WUE)

In the file wuf the water use efficiency (WUE) is calculated and compared with typical present day values.

File wuf:

```
print('----------------------------------------------------------------');
print('diverse radien: ');
print(evaln(r0)=r0,'  ',evaln(rc)=rc,'  ',evaln(r1)=r1);
print(evaln(r2)=r2,'  ',evaln(R)=R,'  ',evaln(r3)=r3);
#Digits:=10;
#
print('----------------------------------------------------------------');
print('CO2-konzentration ausserhalb der pflanze: ',evaln(C_r3)=C_r3);
print('14 mmol/m^3 entspricht 340 ppm CO2 ,dem heutigen wert,');
print('168 mmol/m^3 entspricht 4080 ppm CO2, dem wert im devon');
#
print('----------------------------------------------------------------');
print('wasserdampf-konzentration ausserhalb der pflanze: ',evaln(c_r3)=c_r3);
print('480 mmol/m^3 entspricht 50% luftfeuchte');
#
print('----------------------------------------------------------------');
print('absolute temperatur (deg K): ',evaln(T)=T);
print('celsius temperatur (deg C): ',theta=T-273.15*deg);
#
print('----------------------------------------------------------------');
print(evaln(Ko)=Ko,'    ',evaln(Kc)=Kc,'    ',evaln(Gamma)=Gamma);
print(evaln(gliq)=gliq,'  ',evaln(Vcmax)=Vcmax,'  ',evaln(Jmax)=Jmax);
print(evaln(p0)=p0,'  ',evaln(tau)=tau,'  ',evaln(i)=i);
print(evaln(alpha)=alpha,'  ',evaln(sigma)=sigma,'  ',evaln(fcm)=fcm);
#
print('');
print('----------------------------------------------------------------');
print('transpirations- und assimilationsrate pro volumen');
print(evaln(T)=2/R*jn(R),'   ',evaln(A)=2/R*abs(Jn(R)));
#
print('');
print('----------------------------------------------------------------');
print('wasserdampf und co2-stroeme bei ',evaln(R)=R);
print(evaln(jwv(evaln(R)))=jn(R),'   ',evaln(jco2(evaln(R)))=Jn(R));
#
print('');
print('----------------------------------------------------------------');
print('co2-verhaeltnis assimilationsgewebe/atmosphaere ');
print('_C(_r0)/_C(_R)'=Cn(r0)/Cn(R));
#
print('----------------------------------------------------------------');
print('water use efficiency:  WUE = |Jco2(R)/jwv(R)|');
#
WUE:=abs(simplify(evalf(Jbl(R)/jbl(R))));
#
WUEheute:=0.0020; # quelle: anita
#WUEheute := .4720174327e-4; # psilotum
#
print('----------------------------------------------------------------');
print('dev_rez := (WUE im devon)/(WUE heute)');
#
dev_rez:=WUE/WUEheute;
#
print('----------------------------------------------------------------');
```

10.6 Generation of Plots for the Assimilation Rate as a Function of V_{max} and J_{max}

The dependance of the assimilation rate of *Aglaophyton* on the variables V_{max} and J_{max} is calculated and displayed as a three-dimensional and a contour line plot in the file `a_jmavma`. Similar calculations in the case of *Rhynia* are performed in the file `r_jmavma`.

File `a_jmavma`:

```
#Digits:=20;
#
read agpar;
alias(sim=simplify);
jmax:=Jmax;
vcmax:=Vcmax;
#
unassign('rc','Jmax','chi','kappa','k','Vcmax');
read morph;
unassign('rc','Jmax','chi','kappa','k','Vcmax');
#
JJ:=unapply(evalf(J(R)),rc,Jmax,chi,kappa,k,Vcmax);
#
CC2 := unapply(evalf(C2(r)),r,rc,Jmax,chi,kappa,k,Vcmax);
CC1 := unapply(evalf(C1(r)),r,rc,Jmax,chi,kappa,k,Vcmax);
#
qqs:=unapply(qs,Jmax,Vcmax);
#
JJph:=unapply(Jph,Jmax);
#
chic:=unapply(fQ*Vcmax,Jmax,Vcmax);
chij:=unapply(fQ*Jph/4,Jmax,Vcmax);
cchi:=proc(Jmax,Vcmax) global qqs,chic,chij;
if qqs(Jmax,Vcmax)>0 and JJph(Jmax)>4*Vcmax then eval(chic(Jmax,Vcmax))
elif qqs(Jmax,Vcmax)>0 and JJph(Jmax)<4*Vcmax then  eval(chij(Jmax,Vcmax))
elif qqs(Jmax,Vcmax)<=0 and JJph(Jmax)>4*Vcmax then  eval(chic(Jmax,Vcmax))
elif qqs(Jmax,Vcmax)<=0 and JJph(Jmax)<4*Vcmax then  eval(chij(Jmax,Vcmax))
fi; end;
#
kappac:=unapply(fQ*G1c0,Jmax,Vcmax);
kappaj:=unapply(fQ*G1j0,Jmax,Vcmax);
kkappa:=-proc(Jmax,Vcmax) global qqs,kappac,kappaj;
if qqs(Jmax,Vcmax)>0 and JJph(Jmax)>4*Vcmax then eval(kappaj(Jmax,Vcmax))
elif qqs(Jmax,Vcmax)>0 and JJph(Jmax)<4*Vcmax then eval(kappac(Jmax,Vcmax))
elif qqs(Jmax,Vcmax)<=0 and JJph(Jmax)>4*Vcmax then eval(kappac(Jmax,Vcmax))
elif qqs(Jmax,Vcmax)<=0 and JJph(Jmax)<4*Vcmax then eval(kappaj(Jmax,Vcmax))
fi; end;
#
kc:=unapply(sqrt(fQ*G1c1),Jmax,Vcmax);
kj:=unapply(sqrt(fQ*G1j1),Jmax,Vcmax);
kk:=proc(Jmax,Vcmax) global qqs,kc,kj;
if qqs(Jmax,Vcmax)>0 and JJph(Jmax)>4*Vcmax then eval(kj(Jmax,Vcmax))
elif qqs(Jmax,Vcmax)>0 and JJph(Jmax)<4*Vcmax then  eval(kc(Jmax,Vcmax))
elif qqs(Jmax,Vcmax)<=0 and JJph(Jmax)>4*Vcmax then  eval(kc(Jmax,Vcmax))
elif qqs(Jmax,Vcmax)<=0 and JJph(Jmax)<4*Vcmax then  eval(kj(Jmax,Vcmax))
fi; end;
#
#
CCc_cj:=unapply(Cc_cj,Jmax,Vcmax);
CCc_jj:=unapply(Cc_jj,Jmax,Vcmax);
CCc_cc:=unapply(Cc_cc,Jmax,Vcmax);
CCc_jc:=unapply(Cc_jc,Jmax,Vcmax);
```

```
#
CCqc:=proc(Jmax,Vcmax)  global qqs,CCc_cj,CCc_jj,CCc_cc,CCc_jc;
if qqs(Jmax,Vcmax)>0 and JJph(Jmax)<4*Vcmax then eval(CCc_cj(Jmax,Vcmax))
elif qqs(Jmax,Vcmax)>0 and JJph(Jmax)>4*Vcmax then  eval(CCc_jc(Jmax,Vcmax))
elif qqs(Jmax,Vcmax)<=0 and JJph(Jmax)>4*Vcmax then eval(CCc_cc(Jmax,Vcmax))
elif qqs(Jmax,Vcmax)<=0 and JJph(Jmax)<4*Vcmax then eval(CCc_jj(Jmax,Vcmax))
fi; end;
#
Pa:=1; m:=1; s:=1; mmol:=1; deg:=1;
#-----------------------------------------------------------------------------
bed1:=proc(Jmax,Vcmax) # rc=r0
evalf(CC2(r0,r0,Jmax,cchi(Jmax,Vcmax),kkappa(Jmax,Vcmax),\
kk(Jmax,Vcmax),Vcmax)) > CCqc(Jmax,Vcmax) and \
evalf(CC2(r1,r0,Jmax,cchi(Jmax,Vcmax),kkappa(Jmax,Vcmax),\
kk(Jmax,Vcmax),Vcmax)) > CCqc(Jmax,Vcmax) end;

act1:=proc(Jmax,Vcmax) global rc;
rc:=r0; end;
#-----------------------------------------------------------------------------
bed2:=proc(Jmax,Vcmax) # rc=r1
evalf(CC1(r0,r1,Jmax,cchi(Jmax,Vcmax),kkappa(Jmax,Vcmax),\
kk(Jmax,Vcmax),Vcmax)) < CCqc(Jmax,Vcmax) and \
evalf(CC1(r1,r1,Jmax,cchi(Jmax,Vcmax),kkappa(Jmax,Vcmax),\
kk(Jmax,Vcmax),Vcmax)) < CCqc(Jmax,Vcmax) end;

act2:=proc(Jmax,Vcmax) global rc;
rc:=r1; end;
#-----------------------------------------------------------------------------
act3:=proc(Jmax,Vcmax) global rc; local ec;
unassign('rc');
ec:=evalf(CC2(rc,rc,Jmax,cchi(Jmax,Vcmax),kkappa(Jmax,Vcmax),\
kk(Jmax,Vcmax),Vcmax))- CCqc(Jmax,Vcmax);
rc:=fsolve(ec,rc,r0..r1);
end;
#
#-----------------------------------------------------------------------------
#
p:=proc(Jmax,Vcmax) global rc;
if bed1(Jmax,Vcmax) then act1(Jmax,Vcmax) \
elif bed2(Jmax,Vcmax) then act2(Jmax,Vcmax) \
else act3(Jmax,Vcmax) \
fi;
rc;
end;
#-----------------------------------------------------------------------------
J_Jmax_Vcmax:=proc(Jmax,Vcmax) global p,cchi,kkappa,kk;
evalf(JJ(p(Jmax,Vcmax),Jmax,cchi(Jmax,Vcmax),kkappa(Jmax,Vcmax),\
kk(Jmax,Vcmax),Vcmax));\
end;
#-----------------------------------------------------------------------------
J_JV:=proc(Jmax,Vcmax) global p,cchi,kkappa,kk;
if  (JJph(Jmax) - 4*Vcmax)^2 < 0.00000001 then -0.01 else  0.5 fi; end;
#-----------------------------------------------------------------------------
#
pa:=plot3d('evalf(J_Jmax_Vcmax(Jmax,Vcmax))','Jmax'=0..10*jmax,\
'Vcmax'=0..10*vcmax,axes=boxed,labels=['Jmax','Vcmax','J'],numpoints=1600,\
shading=none,orientation=[25,50]);
#
pa;
#
#
with(plots);
#
```

```
ta:=textplot3d([jmax,vcmax,1.001*J_Jmax_Vcmax(jmax,vcmax),'Ag'],\
color=black);
#
sa:=display([pa,ta]);
sa;
#
pajv:=plot3d('evalf(J_JV(Jmax,Vcmax))','Jmax'=0..10*jmax,\
'Vcmax'=0..10*vcmax,axes=boxed,labels=['Jmax','Vcmax','J/V'],numpoints=16000,\
shading=none,orientation=[0,0.1],style=point);
#
pajv;
#
parc:=plot3d('-p(Jmax,Vcmax)','Jmax'=0..10*jmax,\
'Vcmax'=0..10*vcmax,axes=boxed,labels=['Jmax','Vcmax','_rc'],numpoints=1600,\
shading=none,orientation=[25,50]);
#
parc;
#
save pa,ta,sa,pajv,parc,'pa_jmavma.m';
#
```

11. Epilogue

11.1 Danksagungen

Einige Danksagungen liegen mir am Herzen:

— Manchmal nehmen gute Feen die Gestalt von Lehrstuhlinhabern an: Volker Mosbrugger hat mir als Diplomarbeit ein Thema gestellt, welches mir erlaubte, die mir noch einigermaßen neuen Felder der Paläontologie und der Geologie auf dem Rücken meines liebsten Steckenpferdes, der Theoretischen Physik, zu erforschen und darin nach Herzenslust herumzugaloppieren.

— Anita Roth-Nebelsick, gelernte Biologin und für die Betreuung meiner Arbeit zuständig, hat sich an meinem Steckenpferd überhaupt nicht gestört (was wiederum mich sehr gefreut hat). Sie hat immer Zeit für mich gehabt, und war insgesamt eine sehr angenehme, quasi nicht-lineare Chefin, denn die vorliegende Arbeit ist ein schöner Beleg für die alte Weisheit, daß das Ganze mehr sein kann als die Summe seiner Teile: Rührt man Biologie und Theoretische Physik im richtigen Mischungsverhältnis zusammen und murmelt dabei die passenden Beschwörungsformeln, so entsteht Paläontologie.

— Im Institutsgebäude in der Herrenberger Straße herrscht eine sehr freundliche Atmosphäre: Zum einen sind die Räumlichkeiten sehr schön — lange Jahre relativistischer Einzelhaft in der Zelle D 8 A 02 im wissenschaftlichen Bollwerk auf der Morgenstelle haben mich gelehrt das Zimmer im dritten Stockwerk der Herrenberger Straße mit Jimmy, den vielen toten Tieren, den Unmengen Papier und dem generellen Durcheinander zu lieben, auch wenn meine Anwesenheitsfrequenz anderes anzudeuten scheint. Zum zweiten ist die im Hause herrschende Paläontologenmentalität — (vergangene) Wirklichkeiten werden nicht nur beschrieben sondern auch offensiv konstruiert — sehr nach meinem Geschmack, auch wenn Angehörige anderer Naturwissenschaften — speziell Mathematiker und Theoretische Physiker — ob derartiger Unbefangenheit gern ins Grübeln geraten. Schließlich bin auch ich nie den Verdacht los geworden, am Ende könnten die Solipsisten recht behalten mit ihrer Ansicht, die Welt sei lediglich der böse Traum eines von Verdauungsbeschwerden geplagten schlafenden Hundes. Zum dritten sitzen dort sehr angenehme (siehe zweitens) ZeitgenossInnen, deren Gesellschaft ich immer wieder gerne suche: Anita, Anke, Christopher, Dieter, Hanna, James, Luci, Sonja, Stefan, Ute und Volker.

— Es ist mir ein tiefinnerstes Bedürfnis auch den Kolleginnen und Kollegen im Gemeinderat — ich habe diesem Gremium während der Wahlperiode 1994 – 1999 angehört — und der Verwaltung der Universitätsstadt Tübingen zu danken, denn ihr Beitrag zum Gelingen dieser Arbeit ist kein geringer: Da Arbeits- und Umgangsstil dieser Institutionen bestens geeignet sind, einen Menschen, der inhaltliche Arbeit liebt und taktischer Spielchen abhold ist, in abgrundtiefe Trostlosigkeit zu stürzen, stand ich nach anderthalb Jahren Zugehörigkeit zum Gemeinderat vor der Wahl, entweder meinen beginnenden geistigen Verfall als den Preis anzusehen, den

der mündige Bürger der real existierenden Demokratie schuldet, oder aber ein Zweit- (bzw. Dritt-)studium an der Universität eben dieser Universitätsstadt aufzunehmen. Es spricht für Weisheit und Weitsicht von Gemeinderat und Stadverwaltung, daß sie meinen Leidensdruck mittels der "Pfrondorfer Beschlüsse" so zu steigern vermochten, dass mir nur die zweite Möglichkeit blieb.

Ab Oktober 1996 — dem Beginn des Studiums — gerieten die endlosen Sitzungen dann zu interessanten Lesestunden in Mineralogie, Geologie und Paläontologie, die mich für mancherlei im Rathaus erlittene Unbill entschädigten.

In angenehmer und wirklich dankbarer Erinnerung bleiben mir aus dieser Zeit meine FraktionskollegInnen Bruno, Claudia, Evi, Gitta und Ina, die mir das Studieren gönnten und mich während studienbedingter Abwesenheiten oft und bereitwillig in diversen Sitzungen vertraten.

— Manchmal nehmen gute Feen auch die Gestalt von
Lebensgefährtinnen an. Ich jedenfalls hatte das Glück,
vor einigen Jahren an Birgit Binder und ihren Hund
Gruyère zu geraten.

Mit dem Bergeinsiedel zechend

Selbander sitzen wir beim Trunk;
 im Berge blüht der Hain.
Ein Becher und ein Becher und
 noch einmal ein Becher Wein.

Ich bin berauscht und möchte schlafen.
 Hochwürden, geht auch Ihr!
Seid morgen früh, wenn's Euch gefällt,
 mit eurer Zimbel hier.

Li Tai-Bo